LYSOSOMAL ABNORMALITIES IN OLIGODENDROCYTES IN MURINE MODELS OF KRABBE DISEASE

By

Marie Xun Wang

A DISSERTATION

Presented to the Neuroscience Graduate Program

and the Oregon Health & Science University

School of Medicine

in partial fulfillment of

the requirements for the degree of

Doctor of Philosophy

August 2016

School of Medicine
Oregon Health & Science University

_____

CERTIFICATE OF APPROVAL

_____

This is to certify that the Ph.D. dissertation of
MARIE XUN WANG
has been approved on June 30, 2016

_____
Advisor, Magdalena Petryniak, M.D.

_____
Member and Chair, Fred Robinson, Ph.D.

_____
Member, Lawrence Sherman, Ph.D.

_____
Member, Gary Westbrook, M.D.

TABLE OF CONTENTS

ABREVIATIONS

anterior entopeduncular area (AEP)

arachidonic acid (AA)

arylsulfatase A (ASA)

autophagic lysosome reformation (ALR)

autophagy-related (Atg)

bone marrow transplant (BMT)

cation-independent mannose 6-phosphate receptor (CI-MPR)

ceramide galactosyltransferase (CGT)

galactocerebrosidase (GALC)

galactosylceramide (GalCer)

galactosylsphingosine (psychosine)

globoid cell leukodystrophy (GLD)

human GALC (h-GALC)

human $GALC^{E130K}$ (h-$GALC^{E130K}$)

Human Gene Mutation Database (HGMD)

immunofluorescence (IF)

immunohistochemistry (IHC)

lateral ganglionic eminence (LGE)

lysophosphatidylcholine (LPC)

mannose 6-phosphate receptor (MPR)

medial ganglionic eminence (MGE)

newborn screening (NBS)

nitric oxide synthases (iNOS)

oligodendrocyte precursor cell (OPC)

periodic acid-Schiff (PAS)

phosphatidylinositol-3,5-bisphosphate (PtdIns(3,5)P_2)

phosphatidylinositol-4,5-bisphosphate (Ptdlns(4,5)P_2)

secretory phospholipase A_2 (sPLA_2)

selected reaction monitoring (SRM)

structured illumination (SIM)

sulphatide (SO_3H-GalCer)

Triiodothyronine (T_3)

trans-Golgi network (TGN)

hematopoietic stem cell transplant (HSCT)

twitcher (*Twi*)

twitcher-5J (*Twi-5J*)

β-N-Acetylglucosaminidase (β-NAG)

LIST OF FIGURES

ACKNOWLEGEMENTS

It has been an amazing five years of PhD training at OHSU Neuroscience Graduate Program. I have experienced a great deal of personal and professional growth, and I owe all my success to the support I received from my program, colleagues, friends and family.

I want to say thank you very much to my lab for offering me an opportunity to achieve my thesis research project. Thanks to Dr. Magdalena Petryniak for being my mentor and supporting my research. Thanks to Dr. Gregory Potter for teaching me experimental techniques and discussing scientific questions. Thanks to Elise Dent for assisting with research projects and offering feedbacks for my writings in English. Thanks to Katie Murphy and Erin Bidman for taking care of animals and being great lab partners. In the past two years, there were exiting moments of discovery in science, stressful moments of meeting deadlines, and cheerful moments of seeing lab members making progress on their careers. I cherish every single moment I shared with all of you.

I deeply appreciate all the support I received from my thesis advisory committee: Dr. Gary Westbrook, Dr. Fred Robinson, Dr Larry. Sherman, and Dr Ines. Koerner. I remember every meeting and discussion we had, as well as all the feedback and encouragement you gave to me. You have been guiding my research and career development. I just can't thank you enough for taking care of me.

I am eternally grateful for the positive learning environment the Neuroscience Graduate Program provided me. I have learned so much from the classes, the first year rotations in the labs of Dr. Gary Westbrook, Dr. Gail Mandel and Dr. Laurence Trussell labs. I want to say thank you to my colleagues in Dr. Trussell's lab: Dr. Laurence Trussell, Dr. Hsin-Wei Lu, Dr. Hai Huang, Dr. Pierre Apostolides, Dr. Jeffery Zheng, Dr. Daniel Yaeger, and Dr. Carolina Glogowski with whom I spent the first half of my Ph.D. training. By seeing how everyone worked in the lab, I learned what makes a researcher successful. I appreciate the support and feedback I received from my oral examination committees: Dr. John Williams, Dr. Eric Schnell, Dr. Steven Smith, and Dr. John Adelman. And I also want to say thanks to Liz Lawson-Weber for taking care of my student status and arranging my Ph.D. defense.

I wholeheartedly appreciate the support I received from Dr. Stefanie Petrie and Dr. Aurelie Snyder for teaching me microscopic techniques and offering suggestions for my career development. I want to say thank you very much to Dr. Sue Aicher, Dr. Maria Borisovska and Sam Hermes for generating the electronmicrographic data for my thesis project. I am very thankful for the encouragement and guidance from Dr. Tianyi Mao and Dr. Haining Zhong in the past five years. You helped me get through all the tough moments and asked me to never give up. I want to say thank you to Dr. Ben Emery and Dr. Tassin Srivastava for wonderful scientific discussions, Dr. Yoanne Clovis for suggestions for my career development, Dieter Brandner and Daniel Shaver for helping me with my experiments and English. And I also want to

say thank you to my classmates: Daniel Robinson, Lilly Winfree, Ben Murphy-Baum, Paul Kramer, and Chris Vaaga. You guys are always very supportive and united, and I am so glad to be a part of this team!

Last but not least, I want to say thank you so much to my family and friends. The family spirit of determination and fearlessness is the best gift I ever had. Seeing how everyone is achieving their life goals motivates me to do the same. I particularly want to say thank you to my mom. You are a role model to me and have always been supportive of my career development and personal growth. I want to say thank you to Huanyu He for your patience, support and encouragement. I also want to thank my friends for all your care, help and kindness. I love you all.

Chapter 1 Thesis Introduction

100 years of Krabbe disease

In 1916, Danish neurologist Knud H. Krabbe reported a case in which a 50-day-old patient exhibited a variety of symptoms, including frequent crying and gasping, muscle spasms, weight loss, optic atrophy, and, eventually, death at 13 months of age. The patient was diagnosed as "sclerosis cerebri diffuse"[1]. During the autopsy, K. Krabbe found an unusual manifestation in the brain sections. He wrote: *the white substance is replaced by abnormal neuroglia, gigantic polynuclear glia-cells with big fibers and degenerated nuclei*[1]. The polynuclear cells were later named globoid cells and the disease was named Krabbe disease, or globoid cell leukodystrophy (GLD). In 1970, half of a century after the first diagnosis of Krabbe disease, K. Suzuki and Y. Suzuki made their breakthrough discovery of a galactocerebroside β-galactosidase, also called galactosylceramidase or galactocerebrosidase (GALC), deficiency in Krabbe disease patient's specimens of grey matter, white matter, liver, spleen, serum, leukocytes, and cultured fibroblasts[2,3]. In the following 10 years, many experiments focused on identifying the natural substrates hydrolyzed by GALC, including galactosylceramide (GalCer), lactosylceramide, monogalatosyl diglyceride, and galactosylsphingosine (psychosine) [2,4-6]. It was during this time that K. Suzuki developed the psychosine hypothesis, which suggested that psychosine, unlike other GALC substrates, accumulated in toxic levels in brain tissues as a result of GALC deficiency[7,8]. In 1980, the first murine model of Krabbe Disease, the twitcher mouse, was identified at the Jackson Laboratory, offering a great tool for investigating the molecular and cellular mechanism underlying the disease[9], but it wasn't until the

early 1990s that two other milestones were established in the history of Krabbe disease: the GALC protein was isolated and purified by David Wenger's group and the full-length cDNA of GALC was cloned and characterized by David Wenger's and Shintaro Okada's groups[10-12]. Since then, researchers have made significant progress in understanding Krabbe disease symptoms, causes, pathophysiology, epidemiology and treatments. Over the years, the psychosine hypothesis has survived and been refined, but additional molecular and cellular mechanisms have been proposed to explain Krabbe disease pathologies. However, our knowledge of the mechanisms and treatments for Krabbe disease is still limited, yet significantly more advanced than in the 20th century.

Krabbe disease epidemiology, symptoms, and pathology

Krabbe disease is rare, occurring in 1 of 100,000 infants in the United States, 0.74 of 100,000 infants in Australia, 1.35 of 100,000 infants in Netherlands[13-15], but it occurs in high incidence in some communities. For example, 6 in 1000 infants in a highly insular community in a large Druze kindred in Israel are born with the disease[16]. Approximately 95% of the patients have the infantile-onset form of Krabbe disease in which patients exhibit signs and symptoms in the first few months of life and die around 2 years of age[17,18]. The clinical signs of early-onset Krabbe disease are roughly divided into three states[18,19]. The first stage begins around 3 to 6 months of age and is characterized by frequent crying, fever without

apparent cause, muscle spasms, extreme irritability, regression of psychological and physiological development, and vomiting with feeding difficulties. Seizures may also occur at this stage[18,19]. In the second stage, patients rapidly develop optic atrophy, as well as progression of motor and mental deterioration[18,19]. During the final stage, patients are blind and their cognitive development severely deteriorates until the patient's death[18-20]. The other 5% of the patients express the juvenile or adult onset form[17,19,21]. Patients with late-onset Krabbe disease exhibit a diversity of phenotypes, and clinical examination must be carefully performed to detect these cases[19,21]. Patients general experience a slow progression of the disease and show some, but not all of the early-onset symptoms[17,19,21]. Histopathology of brain tissue from human patients reveals severe demyelination, loss of oligodendrocytes via apoptosis, macrophage and microglia recruitment, and astrocyte activation in both the CNS and PNS, with the phenotype being particularly apparent in the cerebellum[17,19,22]. In addition, brain specimens of Krabbe disease often show multi-nuclear globoid cells that are periodic acid-Schiff (PAS)-positive and often cluster around blood vessels [17,19,23,24].

Krabbe disease genetic cause and GALC essential properties

Krabbe disease is caused by the lack of GALC enzymatic activity. GALC is a soluble lysosomal hydrolase that removes the galactosyl moiety from substrates. It has the highest enzymatic aciivity at pH 4.5~5.0, consistent with the acidic lysosomal

environment[25]. GALC is encoded by the GALC gene, which is highly conserved among humans, rhesus monkeys, dogs, and mice, [26,27]. The human GALC gene is located at 14q31 and contains 17 exons, spanning nearly 60kb genomic DNA[28,29]. The GALC protein has a molecular mass of about 73 kD and contains 669 amino acids[10,12]. Once translated, GALC trafficks through the ER and Golgi complex before being processed into a ~30 kD and a ~50 kD fragment within lysosomes[30]. Both fragments are required for GALC enzymatic activities[30]. GALC is also a secretory protein which is taken up via an endocytosis process mediated by the mannose 6-phosphate receptors (MPRs)[30]. The crystal structure of murine GALC protein, which has 83% identity with human GALC, was reported and further characterized in different mutant forms by Randy J. Read's and Janet E. Deane's groups in 2011 and 2013, respectively[25,31]. These results indicate that the first 24 amino acids of the N-terminus of GALC, which encodes the ER targeting signal, are cleaved during secretion. The mature GALC without the first 24 amino acids consists of three parts: A β-sandwich domain (residues 25-40, 338-452), a central triosephosphate isomerase (TIM) barrel (residuals 41-337), and a lectin domain (residuals 472-668). All three domains contribute to form the substrate-binding pocket. The crystal structure also suggests that the very large buried surface area between the two GALC fragments makes them tightly associated and function as a whole.

Fig 1.1 GALC structures

Deane et al., 2011, PNAS

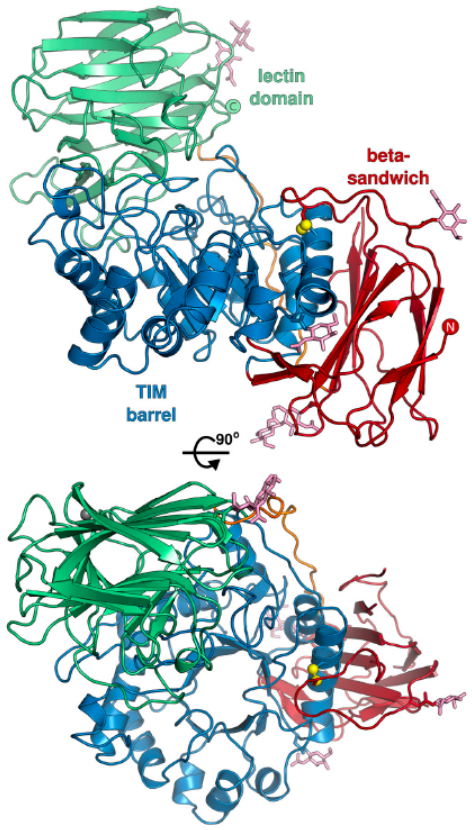

The structure of GALC is shown in two orthogonal views. The C- and N- terminals are marked by labeled circles in green and red, respectively. The first 24 amino acids of the N-terminus of GALC, which encodes the targeting signal to the ER, are cleaved during secretion. The mature GALC without the first 24 amino acids consists of three parts: A β-sandwich domain (residues 25-40, 338-452) shown in red, a central triosephosphate isomerase (TIM) barrel (residuals 41-337) shown in blue, and a lectin domain (residuals 472-668) in green.

So far, 138 mutations of GALC have been reported in the Human Gene Mutation Database (HGMD), including nonsense mutations, missense mutations, deletions, and insertions. Mutations in the GALC gene often cause reduced GALC expression, decreased enzymatic activity, misfolding, and mistrafficking. For example, two common mutations, T513M (alternative numbering T529M) and Y551S (alternative numbering Y567S), trap GALC in the ER, preventing the enzyme from reaching the lysosome and, therefore, reducing its enzymatic activity[32,33]. GALC's metabolic function also requires a co-enzyme, saposin A[34-36]. Saposin A belongs to a family of

sphingolipid activator proteins that are often required for lysosomal degradation of hydrophobic sphingolipids with short carbohydrate chains[37]. Saponsin A mutations have also been found in human patients with the infantile onset Krabbe disease phenotype[38]. Saposin A knockout mice mimic the late-onset Krabbe disease characteristics, indicating the importance of Saposin A in GALC activity[38].

Fig 1.2 GALC genetic mutations

D. Wenger et al., 2000, *Molecular Genetics and Metabolism*, review

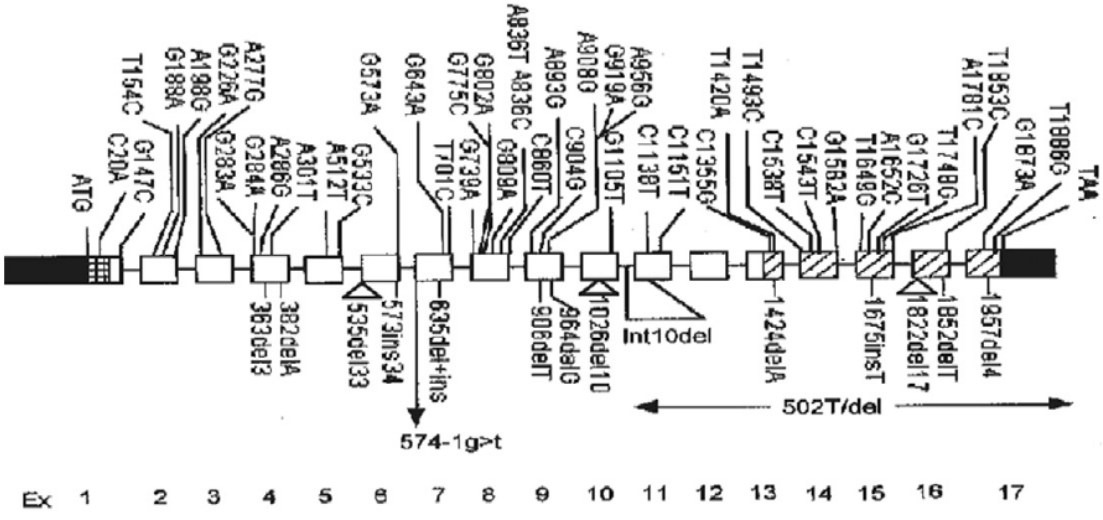

The untranslated regions at both sides are shown in black. Once transported to the lysosomes, GLAC is processed into two fragments that tightly bind to each other and function as a whole. One of the two fragments, the ~50 kDa piece, is coded by the regions marked by the open boxes. The other fragments, the 30 kDa piece, is coded by the regions marked by the cross-hatched boxes. Representative mutations are labeled in the exons. Missense mutations are shown on the top and deletions and insertions are shown at the bottom. The numbers of the mutations indicate the locations in the cDNA sequence that counts from the A of the initiation codon.

Roles of GALC in the sphingolipid pathway and myelin formation

GALC is ubiquitously expressed in all cells, but the main substrate of GALC, GalCer, is the most abundant lipid component of myelin, making up for 2% of the dry weight of gray matter and 12% of the dry weight of white matter[17]. In the sphingolipid pathway, GalCer is the intermediate product between sulphatide (SO_3H-GalCer) and ceramide (Fig. 1.3). Four different enzymes catalyze these bi-directional reactions[39]. Mutations in one of these enzymes, arylsulfatase A (ASA), which catalyzes the SO_3H-GalCer to GalCer reaction, results in an accumulation of SO_3H-GalCer, a toxin that leads to a demyelinating disorder called metachromatic leukodystrophy[40]. In contrast to metachromatic leukodystrophy, Krabbe disease does not include a significant accumulation of GalCer[7,41]. The original work that addressed this issue was publish in 1975 by Vanier MT, Svennerholm L, and was further characterized by Jan-Eric Mansson's group[7,41]. The latter study measured the quantitative distribution of the neutral glycospingolipids in the cerebral white matter of Krabbe disease patients and found that GalCer was actually reduced to about 20% of the control level in cerebral white matter. Because they also found the reduction of other white matter lipids, including sulfatide, glucosylceramide, and lactosylceramide , they suggested that the decrease of GalCer likely resulted from the death of oligodendrocytes and loss of myelin. In 1985, Yoshigoro Ku's group provided a different explanation for the decrease in GalCer. They reported that GM1 ganglioside beta-galactosidase, another β-galactosidase that was genetically distinct from GALC, was also capable of hydrolyzing GalCer[42]. Moreover, GM1 ganglioside

beta-galactosidase had very low enzymatic affinity for psychosine, which explains why psychosine accumulated whereas GalCer did not in GALC-deficient white matter[42]. These two theories are not mutually exclusive and both are commonly accepted today.

Fig 1.3 Sphingolipid pathway and Krabbe disease

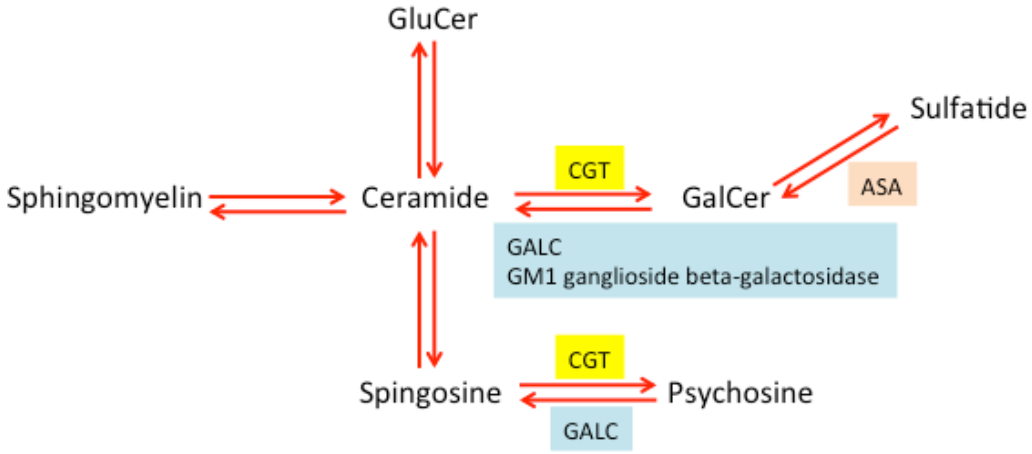

In the sphingolipid pathway, GALC catalyzes GalCer, the most abundant lipid component in myelin. Besides GALC, GM1 ganglioside beta-galatosidase can also catalyze GalCer. Unlike metachromatic leukodystrophy by which sulfatide is accumulated due to the ASA deficiency, Krabbe disease doesn't lead to GalCer accumulation. Instead, psychosine, a toxin to the nervous system, is accumulated about 100-fold. Psychosine is a byproduct of myelin generation. The same enzyme, CGT that catalyzes ceramide to GalCer, also catalyzes sphingosine to psychosine. In Krabbe disease, ceramide is also reduced. But the level of the reduction of ceramide is not as robust as the level of the accumulation of psychosine. Ceramide is an intermediate product in the sphingolipid pathway and can be generated from many molecules, e.g. sphingomyelin and GluCer, etc, which explains why the ceramide level is less affected than the psychosine level as a result of GALC deficiency.

Krabbe disease pathogenesis and the psychosine hypothesis

Psychosine accumulation, which is undetectable in control white matter and increases to 6-10 nmol/g in affected patients, has been considered the primary cause of Krabbe disease pathology[17]. Psychosine is theorized to be a byproduct of myelin generation[17,19]. The same enzyme, that generates GalCer from ceramide, ceramide galactosyltransferase (CGT), can concurrently generate psychosine from sphingosine[43]. In 1976, Kunihiko Suzuki's group demonstrated the toxicity of psychosine *in vivo* and hypothesized that among the four substrates of GALC, psychosine was the cause of non-selective tissue damage[8]. These authors administrated psychosine into rat brains in two ways, either by implanting a 1 mg psychosine pellet or injecting 0.1 to 0.2 mg psychosine dissolved in physiological saline. Fifteen days later, they found that both psychosine implantation and injection resulted in severe tissue degeneration, diffuse cellular necrosis and hemorrhage. When they administered the other three GALC substrates, GalCer, lactosylceramide, and monogalatosyl diglyceride, they observed activation of globoid cells, a loose aggregation of electron dense materials, and an appearance of lamellae, respectively, but without the destructive effects observed with psychosine. There is also a correlation between the level of brain psychosine accumulation and the severity of the disease[19]. And several molecular studies[24,44-50], particularly over the last 20 years, support the psychosine hypothesis.

Due to the technical difficulties in manipulating endogenous psychosine, the psychosine hypothesis has often been tested by exogenous application of psychosine *in vitro*. Exogenous psychosine has been reported to induce cell death in cultured Schwann cells, MO3.13 human oligodendrocyte-like cell lines, mouse-derived oligodendrocyte progenitor cell lines (OLP-II), G_6 glial cells, human natural killer cells, and immune peripheral cells of Krabbe patients[45,46,48-51]. Exogenous psychosine-induced cell death *in vitro* is often via caspase-dependent apoptosis[46,50]. In MO3.13 human oligodendrocyte-like cell lines, exogenous psychosine up regulates the JNK/*c-jun* pathway and AP-1 induction, a pro-apoptotic signal cascade, and down regulates the NF-κB transactivation, a likely anti-apoptotic pathway[50]. In addition, exogenous psychosine activates secretory phospholipase A_2 ($sPLA_2$), inducing the generation of arachidonic acid (AA) and lysophosphatidylcholine (LPC). The later is a toxin that induces demyelination [52,53]. Psychosine is also linked to inflammation responses. For example, in G_6 glial cells and rat primary astrocytes, exogenous psychosine induces iNOS expression and NO production, seemingly consistent with the increased iNOS expression in Krabbe brain tissue[49]. Furthermore, exogenous psychosine can induce peroxisomal dysfunction, e.g. reduced expression of alkyl-DHAP-synthase and inhibit peroxisomal β-oxidation activity, suggesting a possible explanation for the dysfunction of peroxisomes in GALC deficient mouse brains[54,55]. In addition, exogenous psychsoine also inhibit fast axonal transport in cultured cortical neurons through deactivating GSK3β[56]. Last but not least, exogenous psychosine accumulates in the plasma membrane lipid rafts and alters membrane architecture through a lipid-lipid interaction, thus affecting

cholesterol distribution, membrane dynamics, and PKC activity[44,47,57]. In Summary, psychosine that accumulates in the Krabbe disease patients has been reported to cause to cell death, neuroinflammation, peroxisomal dysfunction, and disrupted membrane architecture, etc.

Accessing Krabbe disease: animal models are the key

Our understanding of Krabbe disease has benefitted from the discovery of Krabbe disease animal models. The first animal model, the *twitcher* mouse, is a pontaneous mutations discovered at Jackson Laboratory[9,58]. *Twitcher* mice were discovered prior to the cloning of full length GALC cDNA, so the identification was based on the behavioral phenotype, histopathology and the deficiency of GALC enzymatic activity[9,58]. The original *twitcher* mice were on a mixed C57BL/6J and CE/J background and showed initial clinical signs of the disease around 30 days of age, including weight loss and tremor. Affected mice then developed muscular weakness, especially in the hindlimbs, and lived no longer than three months[9,58]. Later, the original *twitcher* mice were backcrossed to a C57BL/6J background. This full congenic stain shows the onset of the symptom at about 3 weeks and lives no longer than 6 weeks[59]. After the murine GALC cDNA was cloned in 1996, it was discovered that the genetic deficiency in *twitcher* mice was a nonsense mutation that resulted in degradation of mRNA and lack of GALC protein expression[60]. Histopathology of *twitcher* mice revealed a lack of myelin, astrocytic gliosis, microglia recruitment, and

globoid cell appearances in both CNS and PNS[9,58,61]. However, myelin generation in twitcher mice is normal in early stages of oligodendrocyte development[62,63]. Axonopathy of sciatic nerves and spinal cords, e.g. swelling and varicosities, occurs at the first week or two of age prior to myelin degeneration[62,64]. Myelin degeneration in peripheral nerve and spinal cord becomes apparent at around 2 and 3 weeks of age, respectively[62,63,65]. Myelin degeneration in brains first appears in the brain stems of *twitcher* mice at about 3 weeks of age and occurs in cerebellar cortexes at about 4 weeks of age, corresponding to the time course of myelination during development from posterior to anterior[66,67]. Astrocyte activation, as well as microglia and microphage recruitment, is generally concomitant with myelin degeneration, but does not necessarily require apparent myelin pathology[66,67]. Both the PNS and CNS of *twitcher* mice accumulate significant amounts of psychosine[67-69].

Another murine model of Krabbe disease, *twitcher-5J*, appeared in recent years and was systematically characterized in 2013[61]. These mice carry a missense mutation, E130K, and express a mutant version of the GalC enzyme known as $GALC^{E130K}$ [61]. $GALC^{E130K}$ lacks enzymatic activity and is predicted to be misfolded[25,61]. The original *twitcher-5J* mice on the BXD32/TyJ background live for about 25 days and show clinical signs of the disease, e.g. tremor and weight loss, at about 2 weeks of age[61]. Robust astrocyte and microglia activation of twitcher-5J mice occur prior to axonal degeneration and demyelination, both of which are more severe in the PNS than in the CNS[61]. Psychosine also accumulates in both the CNS and PNS of *twitcher-5J* mice[61]. Besides these murine models of Krabbe disease, there are also other species

carrying mutations of GALC gene used for studying Krabbe disease, including dog and rhesus monkey, etc[70,71]. Canine and non-human primate models, given the cost, are difficult to maintain, but can be useful for testing clinical treatments in addition to murine models.

Fig 1.4 WT (top) and Twitcher mice (bottom) at 6 weeks of age

De Gasperi et al., 2004, *Gene Therapy*

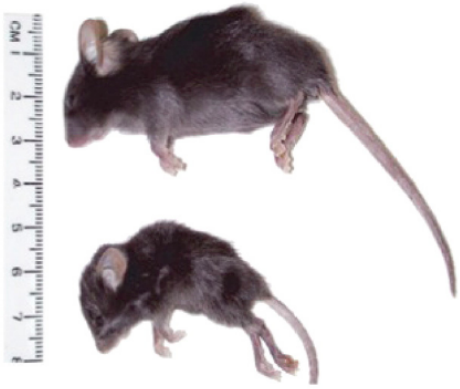

Twitcher mice in C57/Bl6 background (bottom) show initial clinical signs of the disease at about 3 weeks of age, including weight loss and tremor. Affected mice then developed muscular weakness, especially in the hindlimbs, and lived no longer than 6 weeks.

Clinical treatments

The clinical treatments of Krabbe disease have been advanced but still lack efficiency and certainty. Because Krabbe disease is caused by a lack of GALC enzymatic activity, transplantation of hematopoietic stem cells (HSCT) or bone marrow cells (BMT) has been used to enhance GALC secretion [17]. The idea of both HSCT and BMT is that the donor cells, e.g. bone-marrow derived macrophages in BMT treatment, will secrete GALC that is then taken up by the neighboring

oligodendrocytes where it can rescue physiological function[17,72]. Cell transplantation therapies have resulted in some improvement of clinical symptoms in twitcher murine model, canine model and patients, specifically slightly prolonged life, elevated GALC activities, and reduced psychosine accumulation , but have not resulted in full restoration of myelin and complete recovery of cognitive symptoms[17,20,73-77]. Furthermore, cell transplantation therapies have been more efficient on pre-symptomatic patients[17,19], perhaps indicating a need for early intervention. The delivery of the GALC enzyme by direct intracerebroventricular administration and by injection of retrovirus, AAV and lentivirus has been shown to enhance performances of *twitcher* mice to a limited degree[17,78-87]. In other approaches, substrate reduction using L-cycloserine, an inhibitor of sphingolipid production, as well as neuroinflammation inhibition therapy using HQL-79, an inhibitor of HPGDS/PGD_2/DP signaling pathway, have also been investigated in *twitcher* mice, reducing psychosine level by 45% and suppressed gliosis and demyelination, respectively[88-91]. Finally, chemical chaperone therapies have drawn more attention in recent years as several research groups have made progress in identifying molecules that could correct misfolding of GALC and thus improve GALC trafficking to lysosomes[92-94]. Overall, Krabbe disease therapies are broadly under investigation using GALC-deficient animal models and are exploring a variety of methods to enhance GALC enzymatic activitiy.

Early screening and intervention

As cell transplantation therapies must be performed when a patient is pre-symptomatic to achieve clinical efficiency, early diagnosis through genetic strategies is the ideal[17-19,95,96]. However, because of the complicated genetics of the disease and our limited knowledge of the natural history of the disorder, current newborn screening (NBS) activities are very costly and have very low positive predictive value (less than 1.5%)[95-98]. New York State implemented NBS for Krabbe disease in 2006. In 2016, two research papers were published and provided a full evaluation of the outcome of the screening during the eight years between 2006 and 2014[97,98]. Based on those results, over 1.9 million newborn babies in New York State were screened using mass spectrometry to test blood GALC protein levels[95,97,98]. If GALC protein levels were low, DNA testing and enzymatic activity assays were performed to predict the risks of developing symptoms later on[95,97,98]. High risk infants were referred to follow-up diagnostic testing and neurological examination to determine the need of the cell transplantation therapies[95,97,98]. By 2014, five infants were diagnosed for Krabbe disease by their deficient enzymatic activity, genetic mutations, and neurological abnormities[97]. Four of five received HSCT therapies. Two died from transplantation-related complications and two survived but suffered from moderate to severe developmental delay[97,98]. There were also 46 asymptomatic infants who were suggested to have moderate to high risks of developing late-onset Krabbe disease[97].

The clinical outcome of the NBS for Krabbe disease in New York State was undesirable because of the low cost-effectiveness[95]. This outcome led to debate on whether the screening should continue. The major issues raised in this debate are summarized here. First, the incidence of infantile Krabbe disease was 1 in 394,000 in the NY study, which was lower than 1 in 100,000 as expected[95,97]. Second, the screening and all the follow-up diagnostic testing for Krabbe disease were costly compared to other disease screening programs[95]. Third, even though Krabbe disease could be predicted by using genetic approaches combined with neurological testing, the current clinical therapies were unable to achieve a satisfactory outcome of rescuing patients' lives and disabilities[95,96,98]. Lastly, but most importantly, the prediction value of NBS for Krabbe disease was low. In New York State, there were 620 infants subjected to the genetic and enzymatic analysis and 348 of them were referred for the neurological testing. Only five of them were diagnosed to have infantile-onset Krabbe disease after the neurological examination, which brought the positive predictive value as low as 1.4% (5/436)[97]. Such a low ratio results from the genetic complication of Krabbe disease[17,95,97,98]. More than a hundred of genetic mutations have been identified in previous studies, but no genotype-phenotype correlation was found in Krabbe disease[17,95,99]. Few mutations have been shown to be strongly associated with infantile-onset Krabbe disease. For example, a large deletion of exons 11-17 combined with a polymorphism at position 502 of cDNA was a common cause for patients of European ancestry[100]. However, most of the mutations do not consistently correlate with the disease development and many of them relied on a founder effect[17,95]. Therefore, the positive results from the

molecular test currently leaves a clinician uncertain about the final diagnosis until significant neurological examination is performed[95]. In summary, whether NBS is an effective way for Krabbe disease prevention is under discussion, more advanced knowledge and techniques are needed to improve prediction and develop robust clinically relevant tests.

Oligodendrocytes used for studying Krabbe disease

Oligodendrocyte is the most vulnerable cell type in the central nervous system to Krabbe disease pathology due to the accumulation of psychosine, a byproduct of myelin generation. Oligodendrocytes form myelin sheaths, which wrap around axons and serve essential roles in enhancing axonal electrical signal transmission, supporting neuronal metabolism, and regulating neuronal plasticity [101-104]. Oligodendrocytes in the mouse telencephalon are derived from oligodendrocyte precursor cells (OPCs) [104-106]. OPCs originate at around embryonic day 12.5 (E12.5) in the medial ganglionic eminence (MGE) and anterior entopeduncular area (AEP), then migrate laterally and dorsally throughout cerebral cortex[104-106]. At E15.5, the second wave of OPC generation occurs in the lateral ganglionic eminence (LGE) area[104-106]. OPCs express Olig2, Sox10, PDGFα, and NG2, and later differentiate into mature oligodendrocytes, which express Olig2, Sox10, and myelin-specific proteins, including APC/CC-1, CNPase, PLP, MAG, and MBP[104-108]. Myelin formation is ongoing at birth and reaches a peak at around P20 in rodents[109]. MBP labeling of mouse

whole brain sagittal sections has been used to examine the chronological course of myelin generation, which initiates in the brain stem and later occurs in the cerebral cortex[110]. The chronology of myelin generation is important in the pathology of *twitcher* mice. Because demyelination in *twitcher* mice occurs subsequent to the normal myelination at early stages, the chronological course of myelin generation also represents the order of demyelination[66,67]. Studies of oligodendrocytes *in vivo* is appropriate for studying Krabbe disease progression, but it is difficult to access the subcellular structures or molecular and cellular mechanisms. Therefore, cultured oligodendrocyte have been developed and used for investigating signal pathways and for drug screening. There are a few oligodendrocyte-like immortal cell lines, including Oli-neu and N20.1 cells lines, both of which were generated by immortalizing mouse primary oligodendrocytes with oncogenes[111]. However, the most commonly used oligodendrocyte-like cell line in Krabbe disease research is the MO3.13 cell line, which was generated by fusing adult human oligodendrocytes with human rhabdomyosarcoma RD, skeletal muscle cancer cells[112]. MO3.13 cells are polygonal with few short membrane extensions that express MBP, PLP, MAG, CNPase, GFAP and GalCer[112,113]. MO3.13 cells are easy to maintain, this cell line has been used to study molecular cascades triggered by exogenous psychosine[50,71]. To better mimic endogenous psychosine accumulation, GALC knockdown MO3.13 cells and GALC knockdown primary rat oligodendrocytes have been generated using lentivirus-delivered GALC RNA interference[114]. Knockdown of GALC expression in MO3.13 and primary rat oligodendrocytes blocks cell differentiation as determined by MBP and PLP expression, results that oppose the *in vivo* studies in which GALC-

deficient oligodendrocytes normally generate myelin at early stages[62,63,114]. Thus the cellular pathologies resulting from endogenous psychosine accumulation and GALC deficiency may be better studied using primary oligodendrocytes from GALC mutant murine models, e.g. *twitcher* and *twitcher-5J* mice. One recent study obtained primary OPC cultures from *twitcher* mice using a "shaking" method, which assumes that OPCs are less tightly attached to the bottom of the culture dish than astrocytes, and can therefore be isolated by shaking them off from a mixed glial culture[115,116]. However, the *twitcher* primary OPCs in this study were not induced to differentiate and retained their precursor status[115]. An immunopanning method published by Ben Emery and Jason C. Dugas in 2013 provides another tool to isolate and purify oligodendrocytes in a specific differentiating status[117]. In this protocol, OPCs are positively selected by expression of the PDGFα receptor and differentiated synchronously by replacement of PDGFα and NT3 with T3. Oligodendrocytes generated by this method have been used to study oligodendrocyte differentiation during development, but have not yet been applied to *twitcher* and *twitcher-5J* murine models to investigate Krabbe disease molecular and cellular pathologies[118].

Lysosomes in Krabbe disease

Since the first reported case of Krabbe disease, our knowledge of the genetic pathology and psychosine-induced molecular cascades has become remarkably advanced. However, the pathophysiology of lysosomes has received little attention.

Steven M. LeVine and Maria V. Torres, in describing the morphological changes in degenerating oligodendrocytes in twitcher mice, wrote: *In addition to having abnormal cellular processes oligodecndrocytes in twitcher mice also contained darkly stained, oval structures within their cytoplasm, these oval structures appeared more numerous and often larger in oligodendrocytes from twitcher mice than normal mice, this finding suggests that the iron-rich structures arc iysosomes since the twitcher mutation affects a lysosomal enzyme, and lysosomes appear to accumulate in twitcher mice*[119]. A few years later, Kinuko Suzuki's group, in describing the apoptotic depletion of oliogodendrocytes in *twitcher* mice, noted: *The varicose swelling of the processes was attributable to the multiple membrane-bound vacuoles frequently containing fine tubular inclusions of GLD, these vacuoles most likely correspond to "iron-rich, oval structures" indicating possible lysosomes as previously described*[120]. There was no follow-up, most likely because the overwhelming focus on the psychosine hypothesis pushed the question of lysosome pathology to the side.

Lysosomes, as vesicular organelles, serve important roles in many cellular processes, including degrading macromolecules and pathogens, recycling and repairing membrane structures, apoptosis and authophagy[121-123]. Lysosomes are highly regulated and dynamic systems. More than 60 lysosomal hydrolases actively degrade substrates within the acidic, (pH 4.5~5.0) lumens, whereas highly glycosylated lysosomal membrane proteins, LAMP1 and LAMP2, form a glycoprotein wall at the luminal side of protect lysosomes from self-digestion[124-126]. Lipid regulation of lysosomes involves the expression of phosphatidylinositol-3,5-

bisphosphate (PtdIns(3,5)P_2), which guarantees the accuracy of trafficking in the endomembrane system[127,128]. Because of the essential role of lysosomes, mutations of lysosomal genes often cause human disorders. Approximately 50 lysosomal disorders including Krabbe disease have been discovered, and many are lethal[122,129]. The genetic mechanisms of each lysosomal disorder are distinct, but the pathological causes in many cases are comparable. For example, in metachromatic leukodystrophy, caused by the deficiency of arylsulfatase A, SO_3H-GalCer accumulation in oligodendrocytes causes demyelination[40]. In Gaucher disease, caused by the deficiency of β-glucocerebrosidase, GluCer accumulation results in liver and spleen enlargement, neurodegeneration, and skeleton muscle malfunction[130,131]. Therefore, understanding the lysosomal pathology associated with GALC deficiency may not only extends our knowledge of Krabbe disease, but also provide insights into the general cellular pathology and mechanisms of lysosomal disorders.

Purpose of the thesis project

This thesis project was designed to answer the question: what is the lysosomal pathology in Krabbe disease? In the data chapters to follow, I used both *in vitro* and *in vivo* approaches in *Twitcher* and *Twitcher-5J* murine models. The results offer a characterization of the lysosomal changes directly caused by GALC genetic deficiency. By applying two murine models of Krabbe disease carrying different

mutations in the same gene, I was able to investigate the common mechanisms resulting from GALC deficiency. Using both neurosphere mixed culture as well as primary mouse oligodendrocytes generated by the immunopanning methods, I was able to characterize lysosomes in individual cells and determine the cell autonomous effects. Modern imaging approaches provided an important tool to observe lysosomal at an improved level of resolution.

Chapter 2 Thesis Results

GALC Deficient Oligodendrocytes develop Enlarged Lysosomes in *Twitcher-5J* and *Twitcher* Murine Models of Krabbe Disease

Marie X. Wang[1], Greg B. Potter[1], Sydney E. Dent[1], Maria Borisovska[2], Sue A. Aicher[2], Ernesto R. Bongarzone[3], Magdalena A. Petryniak[1]

[1]Oregon Health & Science University, Pediatric Department, Portland, OR, USA.

[2]Oregon Health & Science University, Physiology & Pharmacology Department, Portland, OR, USA.

[3]University of Illinois at Urbana–Champaign, Anatomy and Cell Biology, Champaign, IL, USA.

ABSTRACT

Krabbe disease, also known as globoid cell leukodystrophy, is caused by loss of function of the lysosomal enzyme galactosylceramidase (GALC). The disorder is characterized by neuroinflammation, demyelination, and axonal degeneration. The mechanisms by which GALC causes disease pathology includes psychosine accumulation and peroxisomal dysfunction. However, little is known about how lysosomes are affected by GALC enzymatic deficiency. To investigate the lysosomal defects of Krabbe disease, we performed experiments using two murine models, *twitcher* (*Twi*) and *twitcher-5J* (*Twi-5J*). Both of these mice lack GALC activity, but unlike *Twi*, *Twi-5J* expresses a mutant GALC ($GALC^{E130K}$) that has been predicted to be misfolded[31]. We find that *Twi-5J* primary oligodendrocytes differentiated comparably to WT and accumulated significant amounts of psychosine. Both *Twi-5J* and *Twi* primary oligodendrocytes developed enlarged and tubular lysosomes determined by LAMP1 and LAMP2 immunostaining, indicating a common phenotype of disrupted lysosomal dynamics. Enlarged lysosomes also occurred *in vivo* in *Twi-5J* and *Twi* white matter as early as two weeks of age, suggesting that lysosomal enlargement was an early-onset phenotype alongside the myelin development. Abnormal lysosomes retained an acidic pH, electron-micrographic heterogeneities, unchanged β-N-Acetylglucosaminidase (β-NAG) activities, and an expression of Cathepsin D and $GALC^{E130K}$, suggesting partially preserved lysosomal functions. Finally, enlarged lysosomes primarily occurred in oligodendrocytes in both white matter and neurosphere mixed culture, corresponding to the disruption

of sphingolipid metabolism, e.g. psychosine accumulation, in myelin caused by the GALC enzymatic deficiency.

In conclusion, our results provide the first evidence for lysosomal pathophysiologies of Krabbe disease. The lysosomal phenotype could be due to enhanced lysosomal fusion or reduced lysosomal fission and resulted in cellular damage. Therefore, our findings not only advanced our knowledge of the cellular mechanisms of the disease progression, but also enabled the phenotype of early onset abnormality to become a potential target for developing clinical treatments.

INTRODUCTION

Krabbe disease, also called globoid cell leukodystrophy, was first identified by Danish neurologist Knud Haraldsen Krabbe in 1916 and is a lysosomal storage disorder[1]. Though it is a rare disease, occurring in about 1 of 100,000 infants in USA, it is often fatal, and currently lacks effective clinical therapies[15,132]. Except in about 5% of patients who show symptoms as juveniles or adults, affected infants generally begin exhibiting symptoms during their first few months of life and die around two years of age[17,18]. Typical symptoms of Krabbe disease include fever, seizures, decline of alertness, impaired mental development, extreme irritability, limb stiffness, progressive loss of hearing and sight, and life threatening dysphagia and dyspnea[19,20,133]. The major histopathologies of human patients are extreme demyelination, gliosis, and globoid cell infiltration[19].

Krabbe disease is caused by recessive mutations of the galactosylceramidase (GALC) gene and over 100 mutations have been identified among human patients[2,32,134]. GALC is a lysosomal hydrolase ubiquitously expressed in all cells, but its main substrate, galatosylceramide (GalCer), is the most abundant lipid component of myelin[17]. In the sphingolipid metabolic pathway of oligodendoryctes, GALC removes the galactose from GalCer. Other substrates of GALC include lactosylceramide, monogalatosyl diglyceride, and galactosylsphingosine (psychosine) [5,6,8,135]. Psychosine is a known cytotoxin, and its accumulation has been proposed as a possible cause of cell death in Krabbe disease[8,24,45,46,48,50,114]. Recent studies have

focused on pathophysiologic cascades induced by psychosine, such as interruption of lipid raft architectures[44,47], activation of inducible nitric oxide synthases (iNOS) and phospholipase A2 (PLA2)[49,71], and inhibition of fast axonal transport[56]. However, less is known about lysosomal pathologies that may result from the GALC deficiency.

Lysosomes, first discovered by Dr. Christian De Duve in 1955, are known to serve important roles in many cellular processes including degrading macromolecules and pathogens, recycling and repairing membrane structures, apoptosis, and authophagy[121-123]. Due to the crucial functions of lysosomes, mutations of lysosomal genes often result in human disorders[39,122]. Approximately 50 lysosomal disorders have been discovered and many of them are lethal[122,129]. Current research has been advancing our understanding of the pathophysiology of lysosomal disorders by investigating perturbations of lysosomal morphology and physiology. Lysosomes are a heterogeneous group of vesicles often having the size of 0.1~1.2 μm and containing vacuoles or electron-light or -dense deposit under electron microscopy[125,136]. Unlike cytosol which has a pH of 7.2, lysosomes maintain an acidic luminal pH of 4.6~5.0[125,137]. This acidic environment is generated by H^+-ATPase and supports to their function as the terminal digestive compartment[125,137]. To protect lysosomal membranes from digestion by their low pH, two lysosomal membrane glycoproteins known as LAMP1 and LAMP2, comprise 50% of all lysosomal membrane proteins to maintain integrity and metabolism[124,138-140]. Furthermore, lipid components of lysosomal membrane, e.g. sphingolipids and glycosphingolipids,

are crucial for regulating lysosome trafficking and biogenesis[125,141,142]. To better understand the cellular pathophysiology of Krabbe disease, we investigated how lysosomes in the murine central nervous system are affected by GALC mutations.

Two different murine models were used in this study: *Twitcher-5J* (*Twi-5J*) and *Twitcher* (*Twi*). Both *Twi-5J* and *Twi* animals have mutations in the GALC gene. *Twi* animals contain a nonsense mutation that causes nonsense-mediated decay of GALC mRNA, and therefore do not express GALC protein[9,60,143]. *Twi-5J* animals have an G388A mutation in *Galc* gene, the same mutation that has been identified in human patients, and express $GALC^{E130K}$ [144]. $GALC^{E130K}$ from *Twi-5J* lacks enzymatic activity[61] and is thought to be misfolded[31] (Fig. 2.1). Both *Twi-5J* and *Twi* mice showed similar phenotypes including progressive loss of body weight, muscle weakness, twitching phenotypes in the hindlimbs, and premature death[58,59,61]. Using both models gave us the advantages of understanding the common mechanisms caused by the GALC enzymatic deficiency. In this study, we applied primary oligodendrocytes generated from Krabbe disease murine models using immunopaning methods, which better mimicked the oligodendrocytes' behaviors than using oligodendrocyte-like cell lines. Our findings identified that $GALC^{mutant}$ oligodendrocytes of *Twi-5J* and *Twi* models develop enlarged lysosomes both *in vitro* and *in vivo*, thus providing insight into the progression of Krabbe disease pathophysiology.

MATERIALS AND METHODS

Mice

All procedures at OHSU were approved by the Institutional Animal Care and Use Committee (OHSU protocol number IS00003433). Two mutant strains BXD32/TyJ-*Galc*$^{twi\text{-}5J}$/J (referred as *Twi-5J*) and B6.CE-*Galc*^{twi}/J (referred as *Twi*) are available at the Jackson Laboratory (stock number are 003613 and 000845, respectively). To generate *Twi-5J* strain on B6 background, we backcrossed the original Jackson Lab *Twi-5J* females to C57BL/6J males (stock number 000664) for at least six generations.

Genotyping

DNA was extracted from tail or toe samples of *Twi* and *Twi-5J* mice. *Twi* allele was identified as following steps: (1) PCR reaction with primer pair: *ATGGCCCACTGTCTTCAGGTGATA* (forward) and *ATCAGACTGAAATTGGTAGACAGC* (reverse); (2) EcoRV-HF (NEB Cat# R3195) enzymatic digestion at 37^{o}C for 2 hours; (3) DNA electrophoresis, expected WT band size a.a. 133 base pairs and *Twi* band size a.a. 110 base pairs. *Twi-5J* allele was identified using TagMan SNP genotyping methods described in the previous study[61].

Oligodendrocyte primary culture

Mice primary oligodendrocytes were generated following the CSHL protocol (Ben Emery and Jason C. Dugas, 2014)[145] but only oligodendrocyte precursor cells (OPCs) were collected. For each geneotype, we combined the cortexes of 3 to 6 animals together to generate one initial OPC plate. Once OPCs proliferated, we passaged them 2 to 3 times. At the last passage, cells were placed in the 24-well plates with glass cover slices in wells for immunostaining, 35 mm glass bottom culture dish for live cell imaging, or 10 cm dish for collecting cell pellets for WB and psychosine measurements. At the last passage, growth factors were removed and thyroid hormone added to trigger the differentiation. Primary olidendrocytes of *Twi*, *Twi-5J* (BXD32) as well as *Twi-5J* (Bl6) were generated as separated batches.

Neurosphere culture

Neurospheres were generated from mice at P3. One animal is enough for each batch, and experiments were repeated in three independent batches. Areas around the later ventricles were collected and trypsinized by 0.05% Trpsin-EDTA at 37 ^{o}C for 5 minutes. Neurospheres were proliferated in the 6-well suspension plate in the NSC medium containing βFGF 20 ng/ml, EGF 20 ng/ml and PDGF 10 ng/ml. Adding PDGF was to boost up the proliferation of oligodendrocytes that generally were a very low percentage among all cells. After the first passage, cells were placed in 24-well plates with glass cover slips in wells, and growth factors were replaced by 1% FBS to induce differentiation.

Immunofluorescence

For cell cultures, glass cover slips were collected and fixed by 4% paraformaldehyde at RT for 1 hour and stored in PBS at 4^{o}C. For animals, mice at 2, 3, and 6 weeks of age were perfused with 4% paraformaldehyde followed by overnight post-fixation at 4^{o}C in the same perfusion solution. Brains were sectioned on the vibrotome (Leica VT1000S), and coronal sections of 50 μm thickness were collected and stored in anti-frozen solution at -20 ^{o}C. Sections were washed in PBS for 5 times and 5 minutes at each time to wash off the anti-freeze solution before immunostaining. For both culture slices and brain sections, immunostaining was applied with 1st antibody overnight at 4 ^{o}C and 2nd antibody for 2 hours at room temperature, and mounted in the ProLong® Gold Antifade Reagent with DAPI (ThermoFisher P36931). Primary antibodies are shown in the table, and all 2nd antibodies were purchased from Molecular Probes.

Primary Antibodies	**Labeling structures**	**Inc.**	**Cat. #**	**Applied on Cells**	**Applied on Tissues**
Cathepsin D	lysosome	Abcam	ab6313	1:400	1:400
LAMP1 (1D4B clone)	lysosome	Abcam	ab25245	1:500	1:500
LAMP2	lysosome	DSHB	GL2A7	1:200	1:200
Calreticulin	ER	BD	612137	1:300	-
GM130	Golgi	BD	610822	1:300	-
GALC	GALC	Eckman's lab	CL1021AP	1:800	-
APC/CC-1	Oligo lineage	Millipore	OP80	-	1:100
MBP	Oligo lineage	Millipore	MAB386	1:250	1:250
MAG	Oligo lineage	Abcam	ab89780	-	1:400
Olig2	Oligo lineage	Millipore	AB9610	-	1:250
PLP	Oligo lineage	Millipore	AB15454	1:100	
Neurofilament-H	Axon	Biolegend	837904	-	1:500
Tubulin belta 3 (Tuj1 clone)	Neuron Axon	Covance	MMS-435P	1:2000	-
GFAP	Astrocyte	Millipore	AB5804	1:5000	1:5000
Iba1	Microglia	Wako	019-19741	-	1:1000

Image quantification

For MBP quantification of oligodendrocyte primary culture, images were taken at 10X. DAPI counting was done by Fiji automatically-detecting-particles function and MBP counting was done manually. For LAMP1 quantification of primary oligodendrocytes, images were taken at 60X, and LAMP1 diameters were measured manually. For LAMP1 quantification of astrocytes in the neurosphere culture, images were taken at 60X, and lysosome diameters were measured by IMARIS spot function. For LAMP1 quantification of brain images, images were taken at 60X along the corpus callosum, and lysosomal areas were measured by IMARIS surface function, then equivalent diameters were calculated from the areas of the spots.

Lysosome pH detection

To detect the pH of lysosomes of primary oligodendrocytes, pH sensitive dye, LysoTracker Red DND-99 (ThermoFisher L7528) was applied to the live cells at 50 nM concentration. Cells were incubated at 37^{o}C for 30 minutes then washed by PBS twice. After the final wash, live cell imaging solution (ThermoFisher A14281DJ) was added to the dish, and images were taken under confocal microscopy.

β-NAG enzymatic activity assay

OPCs were cultured in 10 cm dishes and induced differentiation. Cells were collected 11 days after differentiation using M-PER™ Mammalian Protein Extraction Reagent (ThermoFisher Cat# 78501) for total 750 µl per dish. Ten µl of 750 µl cell

lysate was used to measure β-NAG activity using β-NAG assay kit (Sigma Cat# CS0780). The rest of the samples were added protease inhibitor (ThermoFisher Cat# 78425) and stored at -80^{o}C. Later aliquots of frozen samples were used to measure protein concentrations using Pierce BCA protein assay kit (Thermo Fisher Cat# 23227). β-NAG activity (U/ml) was normalized to protein concentration (ng/µl) for statistical analysis.

Microscopy

Confocal images of fixed cells and tissues were taken using NIKON eclipse Ti-E system and Olympus FV1000 system. Confocal and DIC images of live cells were taken using Zeiss LSM780 system. Whole brain images of LAMP1 immunostaining were taken using Zeiss ApoTome2 on AxioImager system. Super-resolution images of lysosomes were taken using Zeiss Elyra PS.1 with LSM 710 laser-scanning confocal and Airyscan system.

Western blotting

Western blot of LAMP1 were performed using forebrain samples. Thirty µg of protein were loaded on NuPAGE 4%-12% Tris-Bis gel (ThermoFisher) and ran for 90 minutes at 200V. Blot was transferred onto a BioTrace PVDF membrane (Pall life Sciences) at 25V for 2 hours. Blots were blocked in 0.1 TBST + 3% non-fat milk for 30 minutes. LAMP1 (Abcam Cat# AB25245; 1:1,000) and Actin (Millipore Cat# AB1501R; 1:5,000) primary antibodies were applied at 4°C overnight. 2nd

antibodies conjugated with AlexaFluor® 680 (Life Technologies Cat# A-21096; 1:10,000) and DyLight™ 800 (Rockland Cat# 610-145-121; 1:10,000) were applied at room temperature for 1 hour. Blots were visualized using the Licor Odyssey imaging system.

Electron micrograph

Electron-micrographic images of LAMP1-immunolabeled corpus callosum were obtained following the protocol published by Sue A. Aicher, Alla Goldberg, and Sarita Sharma in 2002 in *The Journal of Pain*. Mice were perfused at 3 weeks of age. Primary antibody was rat anti-LAMP1 (Abcam Cat# ab25245). Secondary antibody was Goat anti-Rat IgG (H&L) (Electron Microscopy Sciences Cat# 25181). Sliver Enhancer Kit was used for immunostaining (Abcam Cat# ab170733).

Psychosine measurements

OPCs were cultured in 10 cm dishes and induced differentiation. Cell pellets were collected at day 0, 2, 5, 8, 11, 14 days after differentiation. Frozen cell samples were sent to Dr. Ernesto Bongarzone's lab at University of Illinois at Chicago for psychosine analysis. The protocol of psychosine measurement was described by Dr. Ernesto Bongarzone: Separations were done on methanol-acetic acid extracts using a Shimadzu (Kyoto, Japan) Nexera UHPLC system equipped with a Waters Acquity UPLC BEH amide column (2.1 mm X 50 mm, 1.7 μm). Psychosine was eluted using a 30 second isocratic flow of 85% acetonitrile and 15% 5 mM ammonium formate and

0.2% formic acid in water at a flow rate of 0.90 mL/min. Data acquisition and integration were carried out using Shimadzu Lab Solutions software. The UHPLC system was interfaced to a Shimadzu LCMS-8050 triple quadrupole mass spectrometer equipped with positive ion electrospray. Nitrogen was used for nebulization at a flow rate of 3.0 L/min, drying gas at 10 L/min and heating gas flow at 10 L/min. Psychosine was measured using collision-induced dissociation and selected reaction monitoring (SRM). The SRM transition for psychosine was m/z 462 to 282 and the transition for the surrogate standard D-lactosyl-β1-1'-D-erythro-sphingosine was m/z 624 to 282.

RESULTS

We acquired *Twi* and *Twi-5J* mice from Jackson Laboratory on the C57BL/6J and BXD32/TyJ backgrounds, respectively. To compare *Twi* and *Twi-5J* and eliminate the strain variation, we backcrossed *Twi-5J* (BXD32) animals with C57BL/6J animals for at least six generations to attain animals with the *Twi-5J* mutation on a C57BL/6J background (*Twi-5J* (Bl6)). Unlike *Twi-5J* (BXD32), which has a life span of about 25 days, *Twi-5J* (Bl6) homozygotes have a life span of about 40-45 days, similar to that of the *Twi* homozygotes. At three weeks of age, *Twi-5J* (Bl6) mice became less active than their WT and heterozygous littermates and presented muscle weakness and hind limb twitching phenotype. The general health of the homozygotes declined progressively until the end of life.

Primary *Twi-5J* oligodendrocytes differentiated comparably to WT oligodendrocytes and accumulated psychosine during maturation.

To investigate the subcellular structures in which GALC is disrupted, we generated primary oligodendrocyte cultures from P5 to P8 cortices using an immunopanning method. PDGFRα+ cells were selected, allowed to proliferate, and passaged three times. At the last passage, PDGF and NT3 were replaced by T_3 in the medium to induce differentiation. Once differentiating, primary oligodendrocytes survived in the differentiation medium for two to three weeks. Differentiation of primary *Twi-5J*

oligodendrocytes was comparable to WT (Fig. 2.2 A, B). MBP positive cells were quantified as 8.8% ± 2.7% for WT and 8.8% ± 3.6% for *Twi-5J* (P = 0.985) at day 4 in the differentiation media (DIF 4), 41.0% ± 8.5% for WT and 46.9% ± 7.3% for *Twi-5J* at DIF 8 (P = 0.410), and 46.4% ± 5.0% for WT and 45.4% ± 8.4% for *Twi-5J* at DIF 14 (P = 0.855). Few astrocytes were present in the culture. GFAP positive cells represented 5~10% and 10~15% of total DAPI labeled nuclei after two and three passages, respectively. Because GALC^{E130K} lacks enzymatic activity, we measured the concentration of psychosine, a toxic substrate of GALC (Fig. 2.2 C). Prior to differentiation, both WT and *Twi-5J* had a low amount of psychosine: 17.42±11.35 fmol/μg for WT and 28.90 ± 19.76 fmol/μg for *Twi-5J* (P = 0.433). Two days after differentiation, *Twi-5J* cultures exhibited a significant increase in psychosine accumulation (64.14 ± 11.95 fmol/μg) compared to WT (19.23 ± 2.90 fmol/μg) (P = 0.03). Two weeks after differentiation, *Twi-5J* accumulated (345.31 ± 27.36 fmol/μg) over 30 times more psychosine than WT (10.53 ± 6.85 fmol/μg). In conclusion, primary *Twi-5J* oligodendrocytes differentiated with a timeline and efficiency similar to WT and accumulated psychosine along the time course of differentiation, thus providing a valid model to study the cellular pathologies of Krabbe disease during differentiation. These data also indicate that intracellular psychosine accumulation does not delay oligodendroyte differentiation, as previously described for *twitcher* oligodenrdocyte cultures[114].

Primary GALC^{mutant} oligodendrocytes developed LAMP1-labeled, enlarged, and tubular lysosomes.

Because GALC is a lysosomal hydrolase and its substrate GalCer is the most abundant lipid component of myelin, we asked how the dysfunction of GALC would affect the lysosomal compartment of oligodendrocytes. To answer this question, we stained a lysosomal transmembrane glycoprotein, LAMP1, to visualize lysosomes in primary oligodendrocytes. Representative images of LAMP1-labeled lysosomes of oligodendrocytes were shown in the Fig. 2.3 A. WT oligodendrocytes generally had their lysosome diameters of less than 1.2 μm but occasionally larger than 1.2 μm (Fig. 2.3 A1, A2, A3). In contrast, GALC^{mutant} oligodendrocytes often had their lysosomes larger than 1.2 μm, and even reached 2-3 μm (Fig. 2.3 A4). We quantified the size of lysosomes of *Twi-5J* (Bl6), *Twi-5J* (BXD) and *Twi* oligodendrocytes at DIF 11/12 (Fig. 2.3 B). The median diameters of WT and *Twi-5J* (Bl6) lysosomes were 0.53 μm and 0.72 μm, respectively. The median diameter of WT and Twi-5J (BXD32) lysosomes were 0.61 μm and 0.91 μm, respectively. The median diameter of WT and *Twi* lysosomes were 0.57 μm and 0.78 μm, respectively. The significant increase of lysosome diameters across all GALC^{mutant} oligodendrocytes indicates that lysosomal enlargement is an autonomous and common phenotype among GALC deficient oligodendrocytes. In addition, GALC^{mutant} oligodendrocytes sometimes also had lysosomes that appeared as short or long tubular structures, which were not observed in WT (Fig. 1 A4, A5). As many as ~70% of oligodendrocytes could have lysosomes with short or long tubular morphologies, and multiple factors could affect

the development of these tubular lysosomes. Primary oligodendrocytes passaged twice had more tubular lysosomes than those passaged three times. In the same passage, primary oligodendrocytes differentiated longer, e.g. at DIF 17 had more tubular lysosomes than those differentiated shorter, e.g. at DIF 12, or no had tubular lysosomes at all, e.g. at DIF 9. The mechanisms by which these factors affected the lysosomal tubule formation are unclear. To eliminate the possibility that the tubular lysosomes were an artifact of limited imaging resolution of confocal microscopy and were multiple vesicles aligning closely to each other, we used the superresolution structured illumination (SIM) microscopy to further confirm that both enlarged and tubular lysosomes occurred in the $GALC^{mutant}$ oligodendrocytes (Fig. 2.3 C). Both enlarged and tubular lysosomes occurred in mature oligodendrocytes that express myelin-specific proteins, e.g. PLP and MAG (Sup. Fig. 2.1, 2.2). In conclusion, we found that the $GALC^{mutant}$ oligodendrocytes developed LAMP1-labeled enlarged and tubular lysosomes.

Enlarged, tubular lysosomes of primary *Twi-5J* oligodendrocytes retained lysosomal characteristics, including LAMP2 expression, acidic pH, and NAG enzymatic activities

Because LAMP1 is only one of the lysosomal membrane proteins, we also investigated another lysosomal membrane protein, LAMP2, using immunostaining. LAMP2-labeled *Twi-5J* lysosomes revealed similar lysosomal phenotypes, i.e.

enlarged (Fig. 2.4 A left) and tubular (Fig. 2.4 A right) lysosomes. Normal lysosomes should have a pH in the range of 4.0~5.0. To investigate the pH of lysosomes of *Twi-5J* oligodendrocytes, we applied the Lysotracker Red DND-99, a membrane permeable pH sensitive dye, to the live oligodendrocytes and imaged under confocal microscopy in the live cell imaging solution. Fluorescent positive signals of Lysotracker Red DND-99 indicated that *Twi-5J* lysosomes retained an acidic pH (<6.0) (Fig. 2.4 B). NAG is a lysosomal enzyme that expresses in various tissues. To investigate if the lysosomal enlargement and tubulation affected NAG enzymatic activities in *Twi-5J* oligodendrocytes, we collected WT and *Twi-5J* primary oligodendrocytes and measured NAG enzymatic activities using commercial available kit (see method). Results showed that there was no significant difference of NAG enzymatic activities between WT and *Twi-5J* (Fig. 2.4 C). The results were (5.24 ± 0.35) x 10^{-2} Unit/ng for WT and (4.99 ± 0.72) x 10^{-2} Unit/ng for *Twi-5J*. In conclusion, we found that enlarged and tubular lysosomes of *Twi-5J* oligodendrocytes retained functional lysosomal characteristics, including LAMP2 expression, acidic pH, and unchanged NAG enzymatic activities.

Some GALC^{E130K} traffics through the ER and Golgi to lysosomes, indicating that the abnormalities of *Twi-5J* lysosomes are less likely due to the misfolded protein responses than to the lack of enzymatic activities

Because GALC^{E130K} is thought to be misfolded, we considered the possibility that the mutant enzyme is retained in the ER and Golgi complex due to impaired trafficking to the lysosomes. GALC^{E130K} trafficking was investigated by immunolabeling GALC^{E130K} alongside calreticulin, GM130 and LAMP1 as makers of ER, Golgi complex and lysosomes, respectively (Fig. 2.5). Results showed that at least some of the GALC^{E130K} proteins trafficked through ER and Golgi compartments, and reached to the lysosomes, indicating that the abnormalities described in *Twi-5J* lysosomes are probably not attributable to a misfolded protein response. Because *Twi* oligodendrocytes, which didn't express GALC, also showed similar lysosomal phenotypes to *Twi-5J*, we concluded that the lysosomal phenotype of GALC^{mutant} primary oligodendrocytes were due to the lack of enzymatic activities.

Enlarged lysosomes predominantly occurred in oligodendrocytes in *Twi-5J* neurosphere cultures that contained oligodendrocytes, neurons and astrocytes

GALC is ubiquitously expressed among all cells, but the main substrate of GALC, GalCer, is the most abundant lipid component of myelin. Enlarged lysosomes of

oligodendrocytes could potentially be due to the interruption of lipid metabolism, especially, sphingolipid regulation. To gain insight into potential mechanisms of lysosomal enlargement, we examined other cell types in the central nervous system that express lower levels of GALC substrates. To do so, *Twi-5J* neurosphere cultures containing oligodendrocytes, neurons and astrocytes were generated (Fig. 2.6 A). Cell types were identified on the basis of morphology and immunolabeling for cell-type specific markers. We first examined oligodendrocytes labeled by MAG or PLP. More than 90% of *Twi-5J* oligodendrocytes showed increased LAMP1 expression and enlarged circular lysosomes, recapitulating the phenotype described in primary oligodendrocyte cultures. Next, we assessed neurons labeled with Tuj1. Neurons had small soma volume and contained few LAMP1-labled lysosomes around the nuclei, and did not exhibit appreciable differences between Twi-5J and WT. Lastly, we looked at astrocytes stained for GFAP. Astrocytes had vesicular lysosomes and the majority of lysosomes were located in the perinuclear space, while the rest were distributed in the cytoplasm. We quantified the lysosomal diameter of astrocytes and found that *Twi-5J* lysosomes were comparable to WT using this metric (Fig. 2.6 B). Data were analyzed as normal distribution, and statistical results were $F(1,7051) = 1.64$, $P = 0.2010$, the median diameters of WT and *Twi-5J* were 0.898 μm and 0.875 μm, respectively. In conclusion, we found that the significant enlargement of lysosomes was a cell autonomous effect that occurred predominantly in the GALC deficient oligodendrocytes.

GALC^{mutant} white matter showed increased expression of LAMP1 and LAMP1-labeled enlarged lysosomes

To investigate the lysosomal phenotype *in vivo*, we first evaluated LAMP1 expression in coronal forebrain sections of WT and *Twi-5J* (Bl6) animals at 2, 3, 6 weeks of age using standard immunostaining methods (Fig. 2.7 A). Along the corpus callosum, which was abundant with oligodendrocytes and myelinated axons, WT mice showed decreased expression of LAMP1 during development. In contrast, *Twi-5J* (Bl6) mice showed increased expression of LAMP1 from 3 to 6 weeks of age (6 weeks = terminal age of *Twi-5J* (Bl6)). Other white matter tracts, such as the anterior and posterior commissures, were also examined and showed a similarly increased level of LAMP1 expression at the terminal age in *Twi-5J* (Bl6) forebrains (data not shown). We further applied protein immunoblotting to confirm this result using forebrain samples of WT and *Twi-5J* (Bl6) at the terminal age (Fig. 2.7 B). The quantification of LAMP1 immunoblots showed that there was an increase of 90 ± 13% of LAMP1 expression in the *Twi-5J* (Bl6) forebrains relative to WT controls (Fig. 2.7 C). Because the proportion of oligodendrocytes in the entire forebrain was lower than in the corpus callosum, we expect that the actual increase in LAMP1 expression within white matter tracts is greater than 90%.

High power examination of LAMP1-labled lysosomes, demonstrated the enlargement of lysosomes in *Twi-5J* (Bl6) animals at 2-week of age, i.e. we were able to capture the lysosomal enlargement in one of three sites examined (Fig. 2.7 D).

Following quantification of lysosome diameters within the corpus callosum, we found the median diameter of lysosomes from WT and *Twi-5J* (Bl6) animals were 0.72 μm and 0.87 μm, respectively (Fig. 2.7 E). There was a significant increase in the diameter of lysosomes. At 2-weeks of age 2.7% of WT lysosomes and 8.9 % of *Twi-5J* (Bl6) lysosomes were larger than 2 μm in diameter ($\chi^2(1) = 695.86$, $P = 0.000$) (Fig. 2.7 F). At 3-weeks of age, we were able to observe enlarged lysosomes in every image evaluated. Quantification demonstrated that WT lysosomes had a median diameter of 0.73 μm with 1.9% of lysosomes being larger than 2 μm, while *Twi-5J* (Bl6) had a median diameter of 0.99 μm with 16.8% of lysosomes exhibiting a diameter greater than 2 μm. At the 6-week time point, the lysosomal enlargement became pronounced in the *Twi-5J* (Bl6) and lysosomes began to form irregular morphologies. Quantification showed that WT lysosomes had a median diameter of 0.80 μm and 4.4% of lysosomes were greater than 2 μm in diameter, while *Twi-5J* (Bl6) had a median diameter of 1.04 μm and 18.5% of lysosomes were greater than 2 μm in diameter.

Because *Twi* and *Twi-5J* (Bl6) animals had similar life spans and different mutations in the GALC gene, we also examined *Twi* forebrains at the terminal age. Similar to *Twi-5J* (Bl6) animals, *Twi* forebrains showed an apparent increase in LAMP1 expression along the major white matter tracts (Fig. 2.7 G). High-resolution images were taken along the *Twi* corpus callosum and these illustrated the severe lysosomal enlargement observed in these animals (Fig. 2.7 H).

In conclusion, we found that $GALC^{mutant}$ white matter had increased LAMP1 expression and enlarged lysosomes. Particularly in *Twi* and *Twi-5J* (Bl6) animals that had life spans of approximately six weeks, the lysosomal phenotype began to appear at around two weeks of age, and developed increasing severity as development progressed, reaching maximal severity around the time of death.

Enlarged lysosomes of *Twi-5J* (Bl6) white matter retained essential lysosomal characteristics and developed non-selectively from all heterogeneous lysosomes.

In addition to LAMP1, we also examined the subcellular distribution of two other lysosomal proteins, LAMP2 and Cathepsin D within the *Twi-5J* (Bl6) corpus callosum at the terminal age. LAMP2 is a lysosomal membrane glycoprotein similar to LAMP1 and Cathepsin D is a soluble lysosomal hydrolase. Both LAMP2 and Cathepsin D were expressed at significantly higher levels in the *Twi-5J* (Bl6) white matter and revealed enlarged lysosomes (Fig. 2.8 A, B). In addition, when we co-labeled LAMP1 and Cathepsin D, we found that LAMP1-labled lysosomes also contained Cathepsin D (Fig. 2.8 B). In conclusion, the enlarged lysosomes of *Twi-5J* (Bl6) white matter expressed LAMP2 and contained Cathepsin D, indicating that at least these essential lysosomal characteristics were preserved in the GALC deficient lysosomes even until the severities of the phenotype *in vivo*.

Normal lysosomes are heterogeneous vesicles. We asked the question whether the enlarged lysosomes derived from lysosomes in a certain appearance, or not specific to one subpopulation but from heterogeneous vesicles. To do so, we labeled lysosomes by LAMP1-sliver and collected images under electronmicroscopy (EM) (Fig. 2.8 C). EM images revealed that, at 3 weeks of age when the lysosomal phenotype was apparent, both WT and enlarged *Twi-5J* (Bl6) lysosomes retained their heterogeneous contents, such as vacuoles, electron-light deposit, or electron-dense membrane-like structures. Therefore, the development of enlarged lysosomes was not limited to a certain type of lysosomes, but more likely resulted from a non-selective process among all lysosomes.

Enlarged lysosomes occurred primarily in the oligodendrocytes from *Twi-5J* (Bl6) white matter and secondarily in microglia and astrocytes

Because enlarged lysosomes primarily developed in the oligodendrocytes in the neurosphere cultures (Fig. 2.6), we hypothesized that oligodendrocytes are also the main affected cell type *in vivo*. To test this, we co-labeled *Twi-5J* (Bl6) forebrain sections with LAMP1 and various cell-type specific markers. We determined that, at 3 weeks of age, when the lysosomal phenotype was apparent, enlarged lysosomes occurred predominantly in oligodendrocytes expressing Olig2 and APC, but not in other cell types, such as GFAP-positive astrocytes, Iba1-positive microglia, or neurofilament-positive axons (Fig. 2.9 A). However, at 6 weeks of age, when the

lysosomal phenotype is the most severe, the enlarged lysosomes were found not only in oligodendrocytes, but also in astrocytes and microglia, suggesting that enlarged lysosomes eventually develop in astrocytes and microglia of the GALC deficient white matter (Fig. 2.9 B). We believed that the *in vivo* data was consistent with our *in vitro* data, in which the lysosomal phenotype predominantly affected oligodendrocytes, most likely due to perturbations in sphingolipid metabolism to which oligodendrocyte lineage cells were most susceptible. The *in vivo* data also suggested that both astrocytes and microglia were activated in the GALC deficient white matter, contributing to a gliotic environment early, and developing enlarged lysosomes near the terminal stage of the pathophysiology. It would be our future plan to address whether the lysosomal enlargement of astrocytes and microglia was cell autonomous or resulted from engulfing the debris of unhealthy oligodendrocytes.

FIGURES

Fig. 2.1

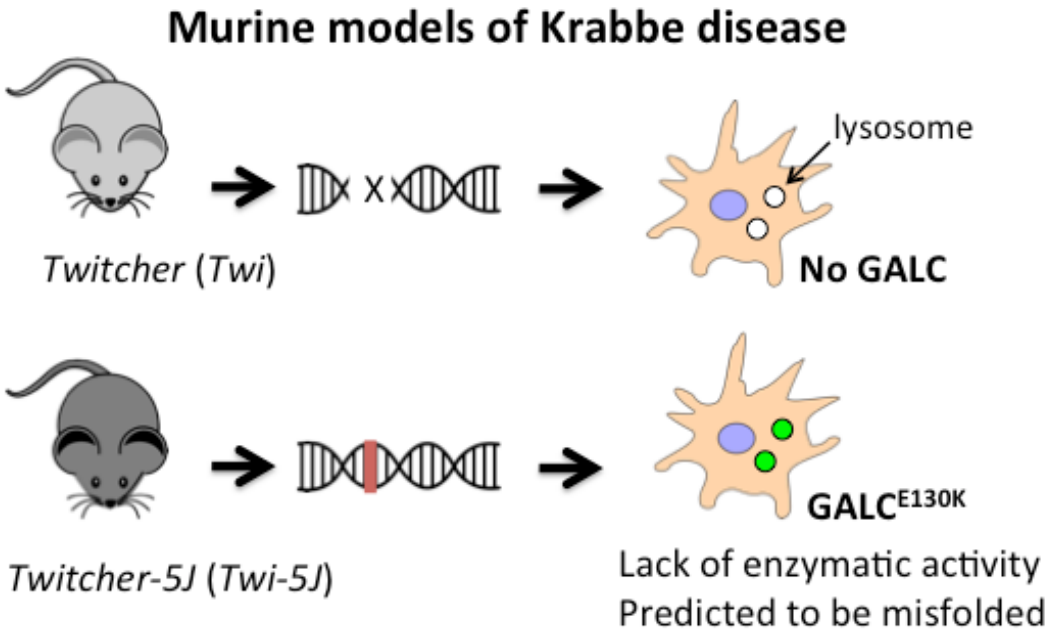

Fig. 2.1 Cartoon showing murine models of Krabbe disease.

Twitcher (*Twi*) mice didn't express GALC while *Twitcher-5J* (*Twi-5J*) expressed a mutant version of GALC, so called $GALC^{E130K}$. $GALC^{E130K}$ had been shown to be lack of enzymatic activities and predicted to be misfolded.

Fig. 2.2

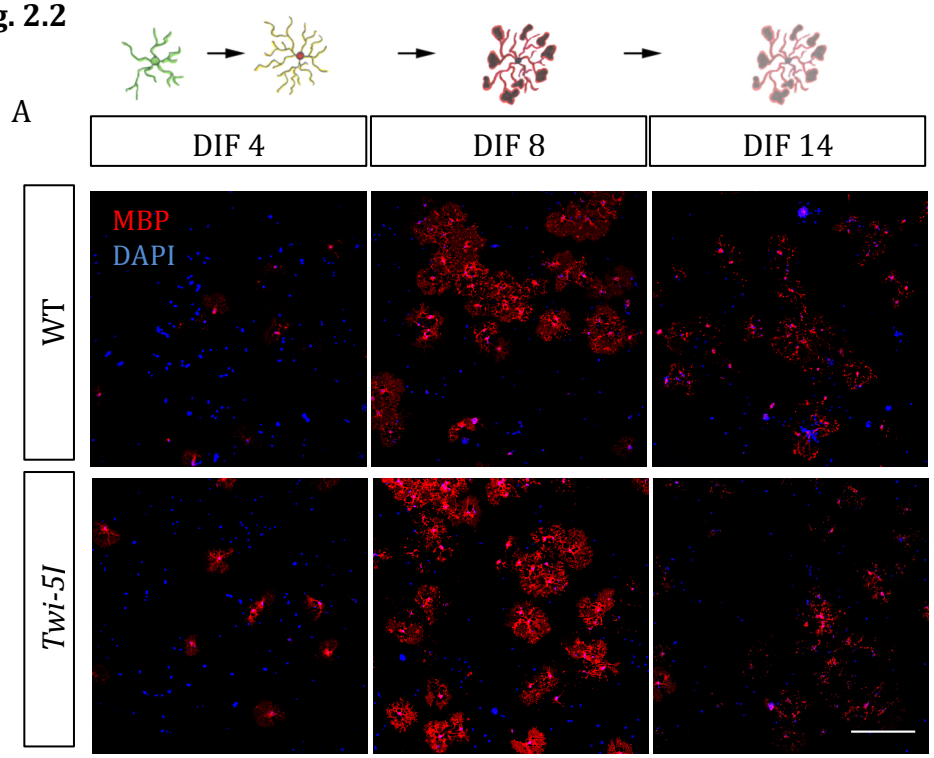
A
DIF 4
DIF 8
DIF 14
WT
Twi-5J
MBP
DAPI
B Oligodendrocyte Differentiation
% of MBP cells
60%
50%
40%
30%
20%
10%
0%
WT
Twi-5J
n.s.
n.s.
n.s.
DIF 4
DIF 8
DIF 14
C Psychosine Accumulation
400
300
200
100
0
fmol/ug
WT
Twi-5j
**
0 2 4 6 8 10 12 14
DIF

Fig. 2.2 Primary Twi-5J oligodendrocytes differentiated comparably to WT oligodendrocytes and accumulated psychosine along differentiation.

(A) Mouse primary oligodendrocytes were generated by immunopanning methods[145]. Oligodendrocytes precursor cells (OPCs) were isolated from P5-P8 cortexes, proliferated and passaged two to three times. At the last passage, PDGF and NT3 were replaced by T3 in media to induce differentiation. MBP staining of both WT and *Twi-5J* primary oligodendrocytes showed the time course of differentiation. Primary oligodendrocytes can survive for about two to three weeks in the culture condition. 300 μm scale bar.

(B) The percentage of MBP-positive cells over DAPI were quantified as an indication of oligodendrocyte differentiation. At DIF 4, 8.8% ± 2.7% of WT cells and 8.8%±3.6% of *Twi-5J* cells were MBP positive (P = 0.985). At DIF 8, 41.0% ± 8.5% of WT cells and 46.9% ± 7.3% of Twi-5J cells were MBP positive (P = 0.410). At DIF 14, 46.4% ± 5.0% of WT cells and 45.4% ± 8.4% of *Twi-5J* cells were MBP positive (P = 0.855). Statistics were done using ANOVA and shown as mean±SD.

(C) Because $GALC^{E130K}$ had been shown to be lack of enzymatic activities, the concentrations of psychosine, a toxic substrate of GALC, were measured along differentiation. Prior to the differentiation, there was no significant difference of psychosine concentration between WT (17.42 ± 11.35 fmol/μg) and *Twi-5J* (28.90 ± 19.76 fmol/μg) (P = 0.433). Two days after differentiation, Twi-5J had significant increase of psychosine concentration (64.14 ± 11.95 fmol/μg) comparing to WT (19.23 ± 2.90 fmol/μg) (P = 0.03). Two weeks after differentiation, *Twi-5J* accumulated psychosine (345.31 ± 27.36 fmol/μg) over 30 times more than WT (10.53 ± 6.85 fmol/μg). Statistics were done using ANOVA and shown as mean ± SD.

Fig. 2.3

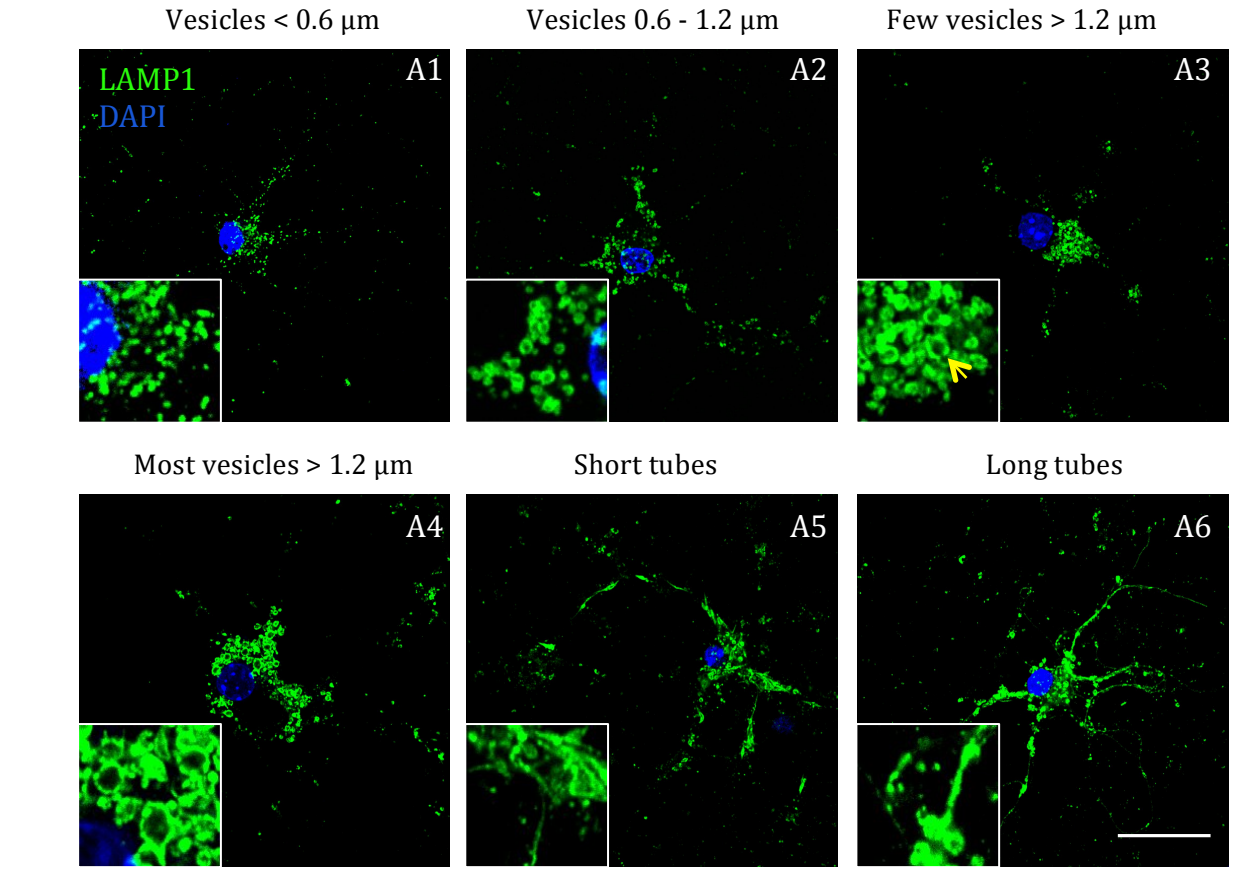
Vesicles < 0.6 µm
Vesicles 0.6 - 1.2 µm
Few vesicles > 1.2 µm
LAMP1
DAPI
A1
A2
A3
Most vesicles > 1.2 µm
Short tubes
Long tubes
A4
A5
A6

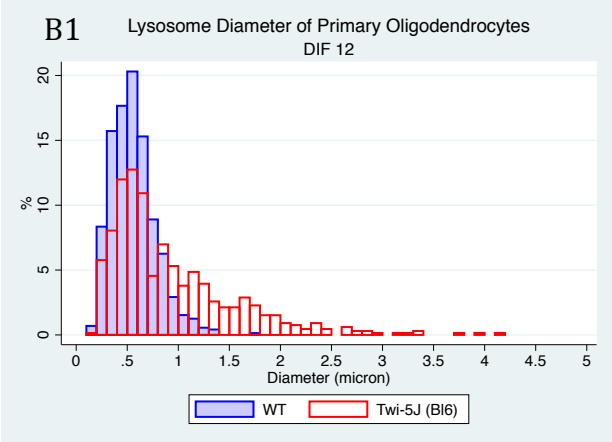
B1
Lysosome Diameter of Primary Oligodendrocytes
DIF 12
%
Diameter (micron)
WT
Twi-5J (BI6)

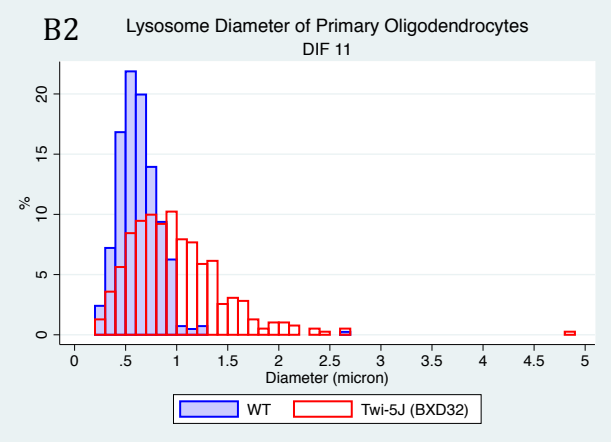
B2
Lysosome Diameter of Primary Oligodendrocytes
DIF 11
%
Diameter (micron)
WT
Twi-5J (BXD32)

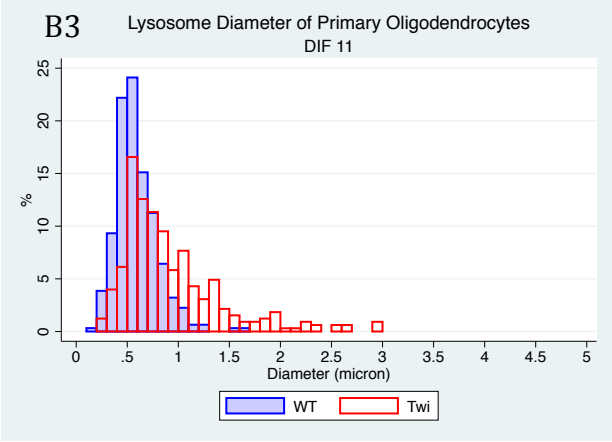
B3
Lysosome Diameter of Primary Oligodendrocytes
DIF 11
%
Diameter (micron)
WT
Twi

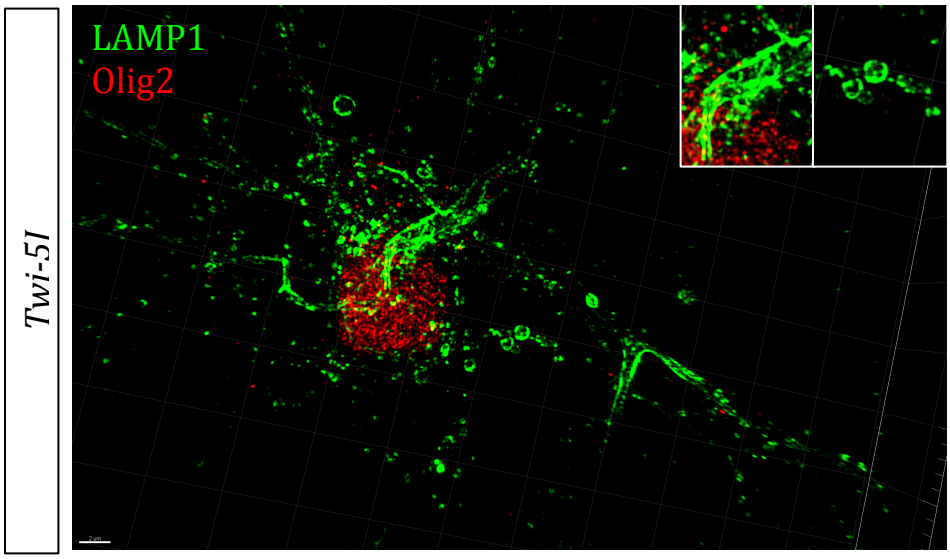

Fig. 2.3 GALC^{mutant} primary oligodendrocytes developed LAMP1-labeled, enlarged, and tubular lysosomes.

(A) Representative pictures showed normal, enlarged and tubular LAMP1-labeled lysosomes in WT and GALC^{mutant} primary oligodendrocytes. (A1) Oligodendrocytes had lysosomes of diameter less than 0.6 μm; (A2) Oligodendrocytes had lysosomes of diameter between 0.6 μm to 1.2 μm; (A3) Oligodendrocytes occasionally had lysosomes of diameter over 1.2 μm; Oligodendrocytes like (A1), (A2) and (A3) were found among both WT and GALC^{mutant} primary oligodendrocytes. (A4) Oligodendrocytes had a majority of lysosomes that were enlarged and of diameter over 1.2 μm; (A5) Oligodendrocytes had lysosomes of short tubular shapes; (A6) Oligodendrocytes had lysosomes of long tubular shapes extended from the perinuclear space to the edge of the proximal plasma. Oligodendrocytes like (A4), (A5) and (A6) were dominant among GALC^{mutant} primary oligodendrocytes. Tubular lysosomes were only found in GALC^{mutant} primary oligodendrocytes. 25 um scale bar.

(B) Diameters of LAMP1-labled lysosomes were measured. Oligodendrocytes were generated from *Twi-5J* (Bl6) mice (B1), *Twi-5J* (BXD32) mice (B2) as well as Twi mice (B3). GALC^{mutant} primary oligodendrocytes across all three strains developed enlarged lysosomes. The median diameters of WT and *Twi-5J* (Bl6) lysosomes were 0.53 μm and 0.72 μm, respectively. The median diameter of WT and *Twi-5J* (BXD32) lysosomes were 0.61 μm and 0.91 μm, respectively. The median diameter of WT and *Twi* lysosomes were 0.57 μm and 0.78 μm, respectively. Kolmogorov–Smirnov tests between genotypes were done for all three groups and all the P values are less than 0.01.

(C) To eliminate the possibility that the observation of tubular lysosomes of GALC^{mutant} primary oligodendrocytes was an artifact and due to the limited resolutions of laser-scan confocal microscopy, superresolution structured illumination (SIM) microscopy was applied and confirmed that the both enlarged and tubular lysosomes occurred in GALC^{mutant} primary oligodendrocytes. 2 μm scale bar.

Fig. 2.4

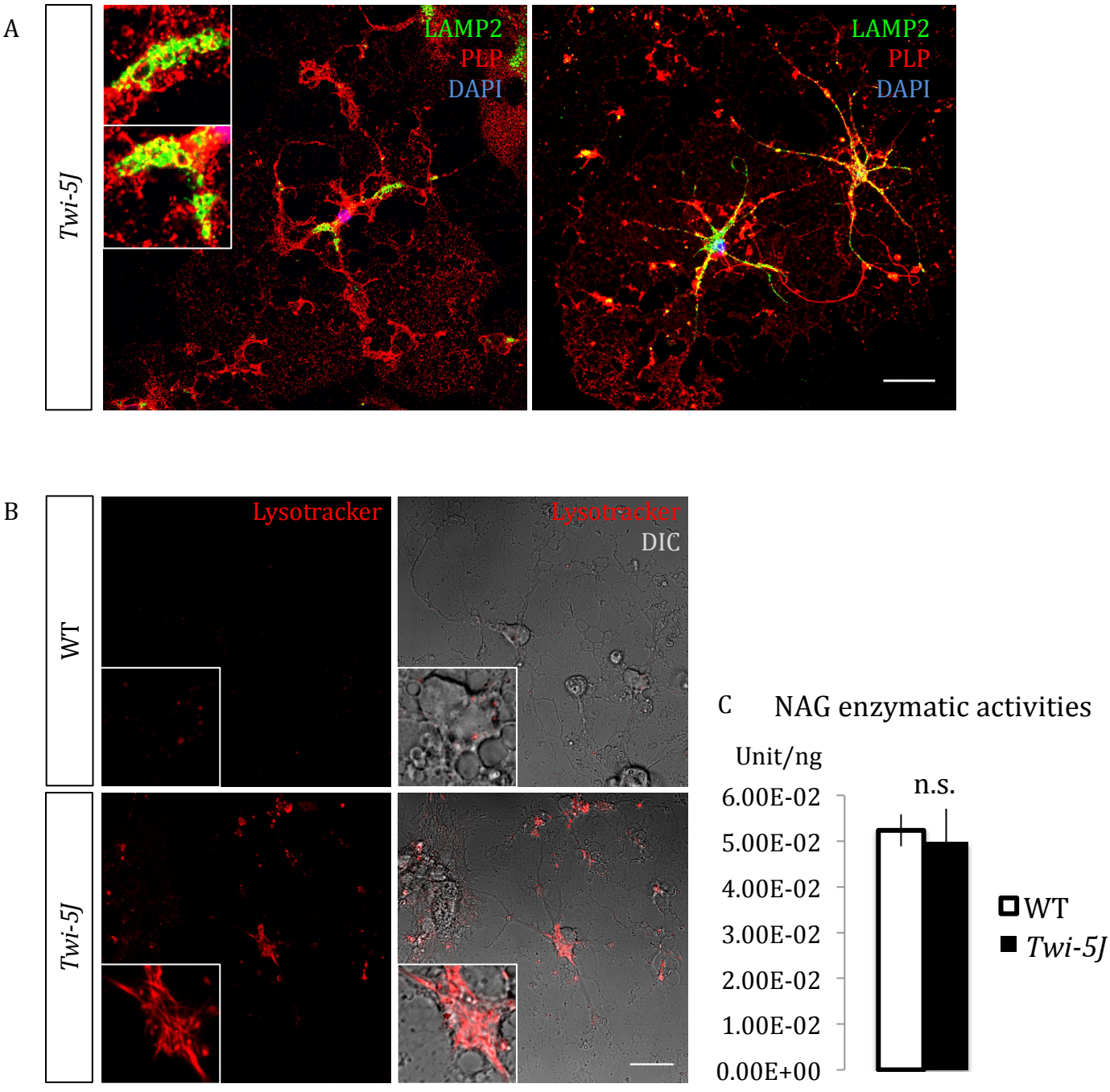
A
Twi-5J
LAMP2
PLP
DAPI
LAMP2
PLP
DAPI
B
WT
Lysotracker
Lysotracker
DIC
Twi-5J
C
NAG enzymatic activities
Unit/ng
6.00E-02
5.00E-02
4.00E-02
3.00E-02
2.00E-02
1.00E-02
0.00E+00
n.s.
WT
Twi-5J

Fig. 2.4 Enlarged, tubular lysosomes of *Twi-5J* oligodendrocytes retained lysosomal characteristics including LAMP2 expression, acidic pH and NAG enzymatic activities.

(A) The lysosomal phenotype of *Twi-5J* oligodendrocytes was investigated by staining of another lysosomal membrane protein, LAMP2. LAMP2-labeled lysosomes revealed similar lysosomal phenotypes as labeled by LAMP1. Both enlarged lysosomes (left) and tubular lysosomes (right) occurred in *Twi-5J* oligodendrocytes. 25 μm scale bar.

(B) The pH of lysosomes of *Twi-5J* oligodendrocytes was investigated by applying Lysotracker Red DND-99, a membrane permeable pH sensitive dye, to live oligodendrocytes and imaging under confocal microscopy in the live cell imaging solution. Fluorescent positive signals of Lysotracker Red DND-99 indicated that *Twi-5J* lysosomes retained the acidic pH (< 6.0). 25 μm scale bar.

(C) The enzymatic activity of NAG, a lysosomal enzyme, was measured in WT and *Twi-5J* oligodendrocytes. There was no significant difference of NAG activities between *Twi-5J* and WT. The results were (5.24 ± 0.35) x 10^{-2} Unit/ng for WT and (4.99 ± 0.72) x 10^{-2} Unit/ng for *Twi-5J*. Data was analyzed by ANOVA method and shown as mean ± SD.

Fig. 2.5

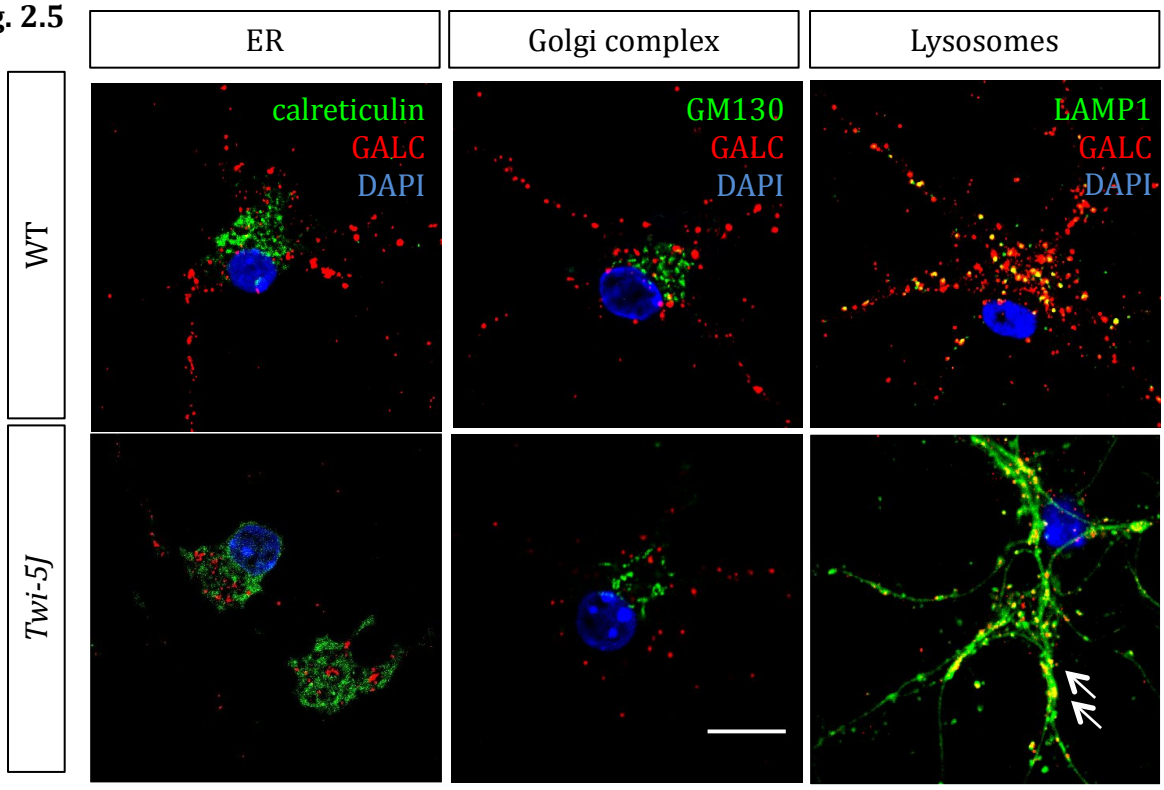

Fig. 2.5 Some GALC^{E130K} traffics through the ER and Golgi to lysosomes, indicating that the abnormalities of *Twi-5J* lysosomes are less likely due to the misfolded protein responses than to the lack of enzymatic activities.

Because GALC^{E130k} was predicted to be misfolded and could potentially be stuck in ER and Golgi complex and failed to be transported to lysosomes. GALC^{E130k} trafficking was investigated by staining GALC^{E130k} alongside calreticulin, GM130 and LAMP1 as makers of ER, Golgi complex and lysosomes respectively. Results showed that at least some of the GALC^{E130k} proteins trafficked through ER and Golgi and reached to the lysosomes (arrows), indicating that the abnormalities of *Twi-5J* lysosomes were less likely due to the misfolded protein responses. Because *Twi* oligodendrocytes which didn't express GALC also showed similar lysosomal phenotypes as Twi-5J, we concluded that the lysosomal phenotypes of GALC^{mutant} primary oligodendrocytes were due to the lack of enzymatic activities. 10 μm scale bar.

Fig. 2.6

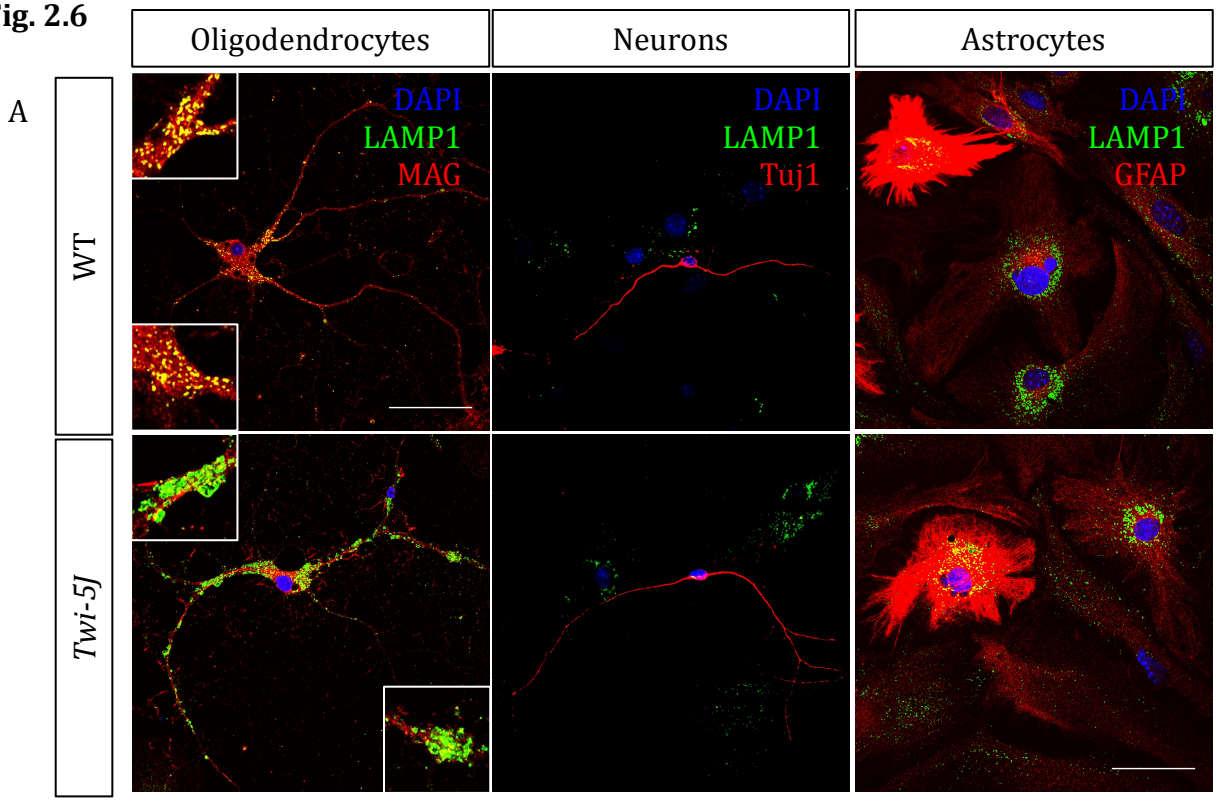
A
Oligodendrocytes
Neurons
Astrocytes
WT
Twi-5J
DAPI
LAMP1
MAG
DAPI
LAMP1
Tuj1
DAPI
LAMP1
GFAP

B

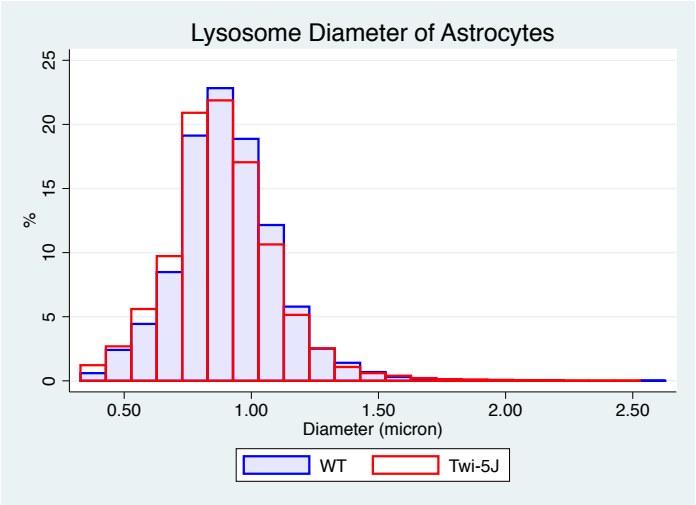
Lysosome Diameter of Astrocytes
%
0
5
10
15
20
25
0.50
1.00
1.50
2.00
2.50
Diameter (micron)
WT
Twi-5J

Fig. 2.6 Enlarged lysosomes predominantly occurred in oligodendrocytes in *Twi-5J* neurosphere culture that contained oligodendrocytes, neurons and astrocytes.

(A) Neurosphere cultures were generated from P3 or P4 forebrains. Different cell types were identified by their morphologies and cell type-specific markers: MAG for oligodendrocytes, Tuj1 for neurons, and GFAP for astrocytes. Enlarged lysosomes were found in >90% of Twi-5J oligodendrocytes shown in the representative images (left panel). Neurons contained small volume of plasma and very few LAMP1-labeled spots in the soma, and there was no appreciable difference between *Twi-5J* and WT (middle panel). Astrocytes had vesicular lysosomes, and the majority of lysosomes located in the perinuclear space and the rest of them diffusively distributed in the plasmas (right panel). There was no significant difference between *Twi-5J* and WT, and the quantification was shown in (B). 50 μm scale bar.

(B) The diameters of lysosomes of astrocytes were quantified and analyzed by ANOVA method. There was no significant difference between *Twi-5J* and WT ($P = 0.2010$). The median diameters of WT and *Twi-5J* were 0.898 μm and 0.875 μm, respectively.

Fig. 2.7

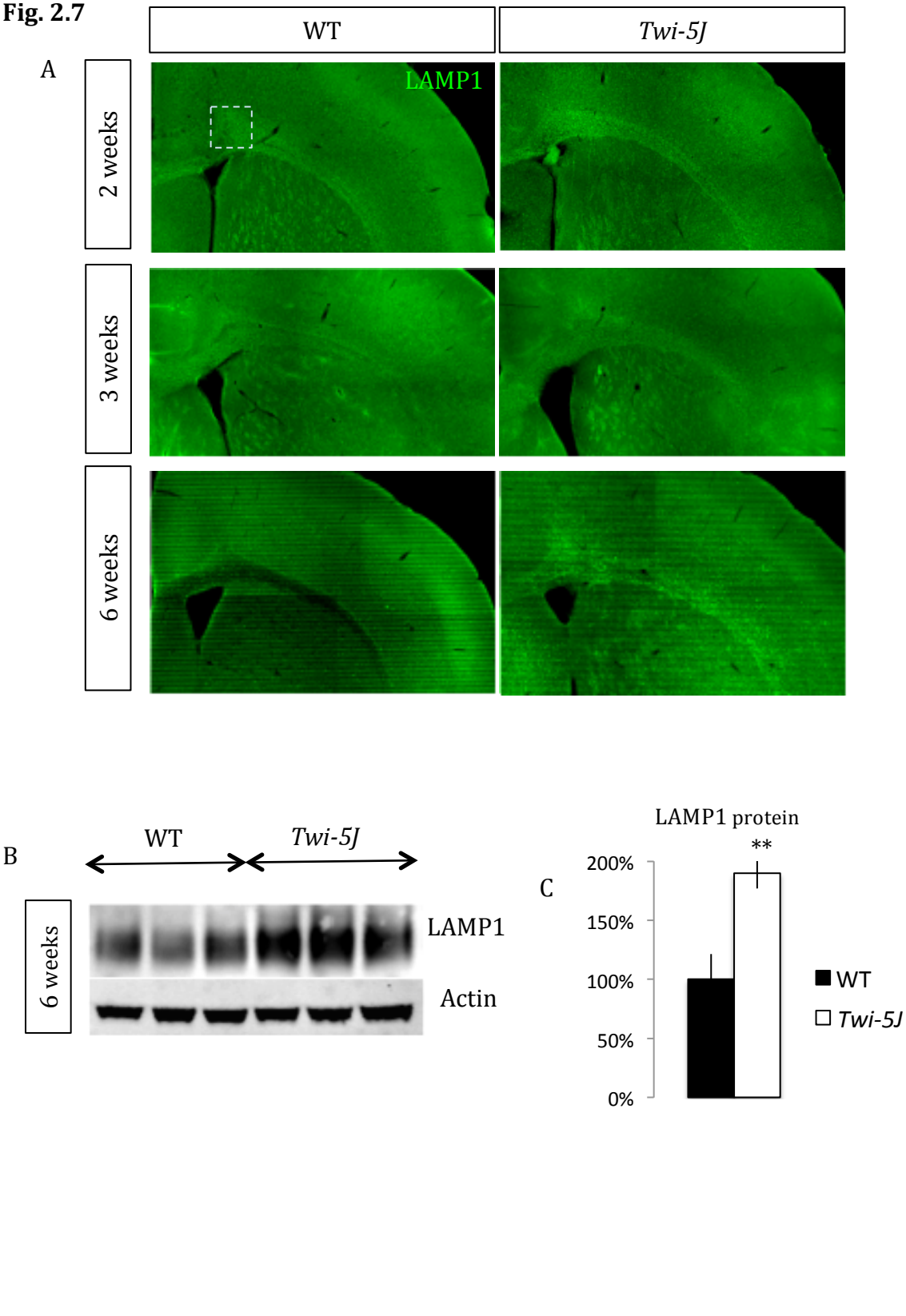
WT
Twi-5J
A
LAMP1
2 weeks
3 weeks
6 weeks
B
WT
Twi-5J
6 weeks
LAMP1
Actin
C
LAMP1 protein
**
200%
150%
100%
50%
0%
WT
Twi-5J

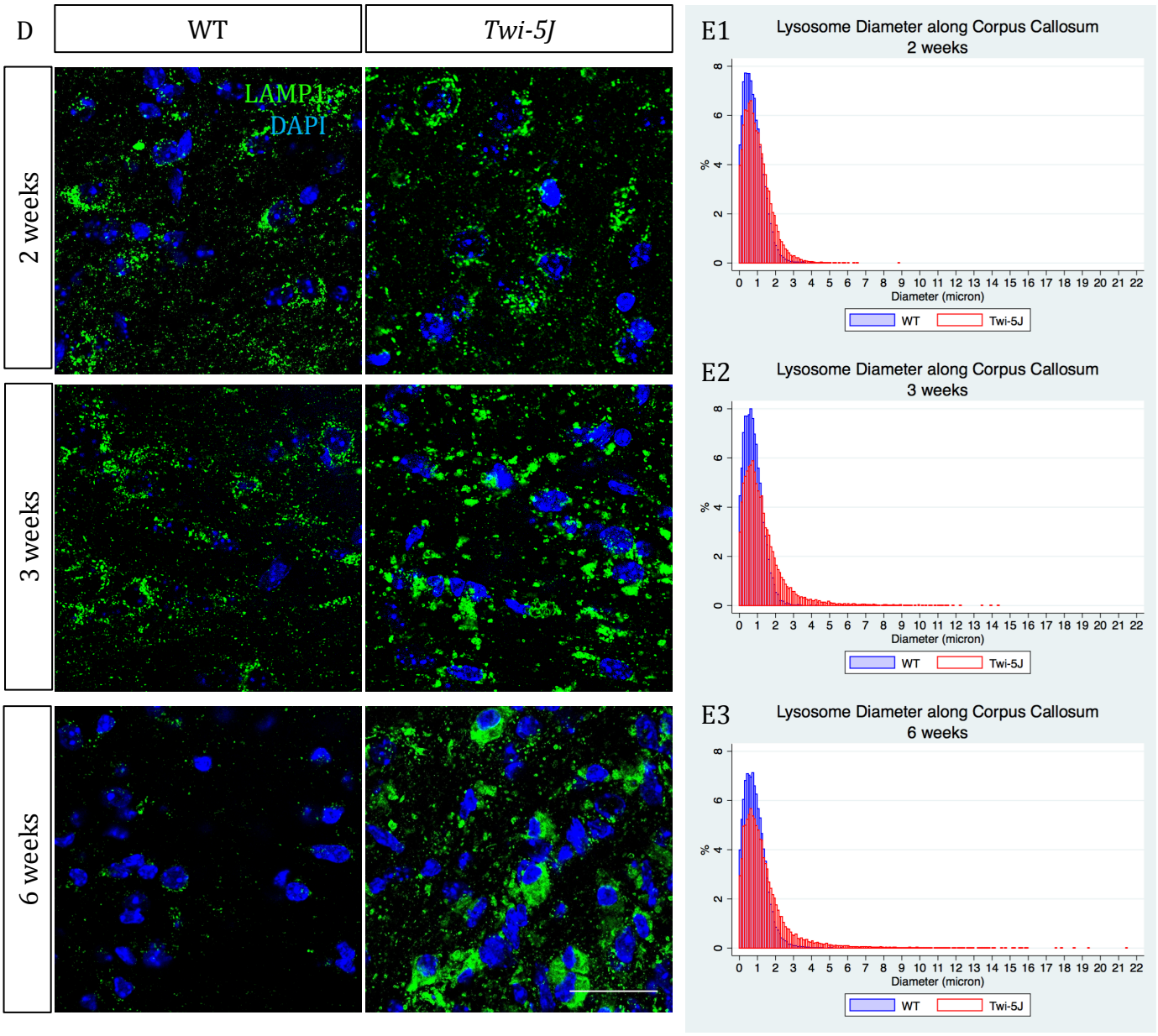

F

Lysosomes		% ≤ 2 µm	% > 2 µm	P value of χ^2 analysis
2 weeks	WT	97.3%	2.7%	< 0.01
	Mut	91.1%	8.9%	
3 weeks	WT	98.1%	1.9%	< 0.01
	Mut	83.2%	16.8%	
6 weeks	WT	95.6%	4.4%	< 0.01
	Mut	81.5%	18.5%	

H

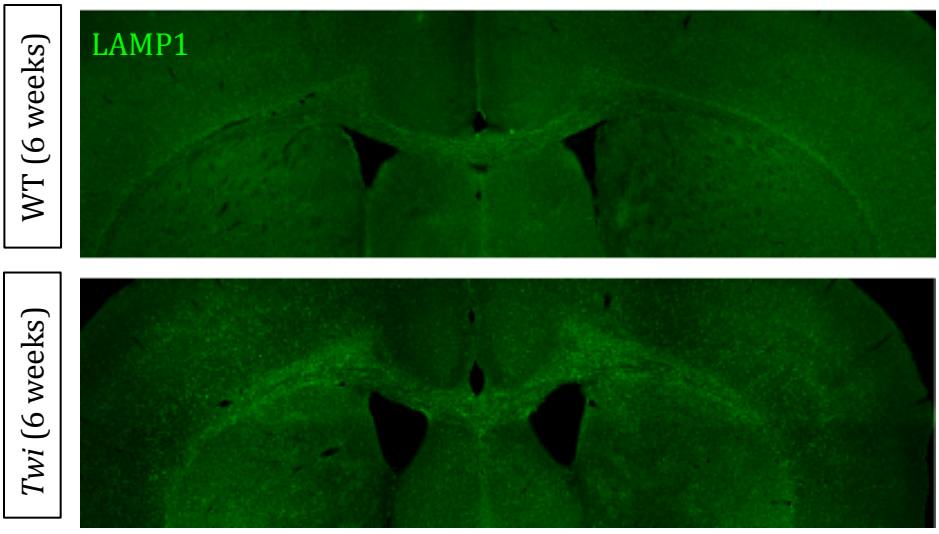

I

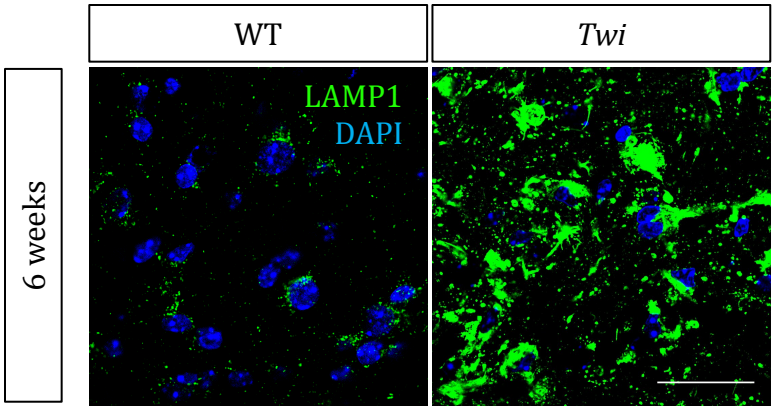

Fig. 2.7 GALC^{mutant} white matters had increased expression of LAMP1 and LAMP1-labeled enlarged lysosomes.

(A) Lysosomal phenotypes were investigated *in vivo*. WT and *Twi-5J* (Bl6) forebrain coronal sections were labeled by LAMP1 at 2, 3 and 6 weeks of age. During development, LAMP1 expression along corpus callosum was decreased in WT but increased in *Twi-5J* (Bl6). At 6 weeks of age (terminal age), LAMP1 expression of *Twi-5J* (Bl6) corpus callosum was obviously higher than WT.

(B) To compare LAMP1 expression in WT and *Twi-5J* (Bl6) at the terminal age, LAMP1 western blots were applied on forebrains samples. LAMP1 expression was significantly higher in the *Twi-5J* (Bl6) forebrain.

(C) Quantification of LAMP1 western blots. There was an increase of 90 ± 13% of LAMP1 expression in *Twi-5J* (Bl6) forebrains comparing to WT (T-Test, $P < 0.01$, statistics was shown as mean ± SD). Because the portion of oligodendrocytes in forebrains was lower than in corpus callosum, the actual increase of LAMP1 expression in the white matter tracks should be more than 90%.

(D) High-resolution images were taken in corpus callosum (location shown as the white square in (A)). *Twi-5J* (Bl6) corpus callosum developed LAMP1-labeled enlarged lysosomes that occasionally appeared at 2 weeks of age, became apparent at 3-week of age, and were severe at 6 weeks of age. 30 μm scale bar.

(E) Lysosome diameters were quantified at WT and *Twi-5J* (Bl6) corpus callosum at 2 (E1), 3 (E2) and 6 (E3) weeks of age. The median diameters of WT lysosomes at 2, 3, and 6 weeks of age were 0.72 μm, 0.73 μm and 0.80 μm, respectively. *Twi-5J* (Bl6) corpus callosum developed significant amount of enlarged lysosomes along development. The median diameters of *Twi-5J* (Bl6) lysosomes at 2, 3 and 6 weeks of age were 0.80 μm, 0.99 μm and 1.04 μm, respectively.

(F) To better characterize the enlargement of *Twi-5J* (Bl6) lysosomes, the portion of lysosomes of diameter over 2 μm was quantified. As shown in the table, there is a significant increase of lysosomes of diameter over 2 μm in *Twi-5J* (Bl6) corpus callosum. Statistics were done by χ^2 analysis. *P* values indicated the significance between genotypes at each time points.

(G) *Twi* corpus callosum that didn't express GALC was also investigated for the LAMP1 expression. Comparable to *Twi-5J* (Bl6), *Twi* white matter also showed robust increase of LAMP1 expression at 6 weeks of age (terminal age).

(H) High-resolution images were taken at *Twi* corpus callosums. Similar to *Twi-5J* (Bl6), *Twi* developed a severe lysosomal enlargement at the terminal age, indicating that the lysosomal enlargement was a common phenotype across GALC deficient white matter. 30 μm scale bar.

Fig. 2.8

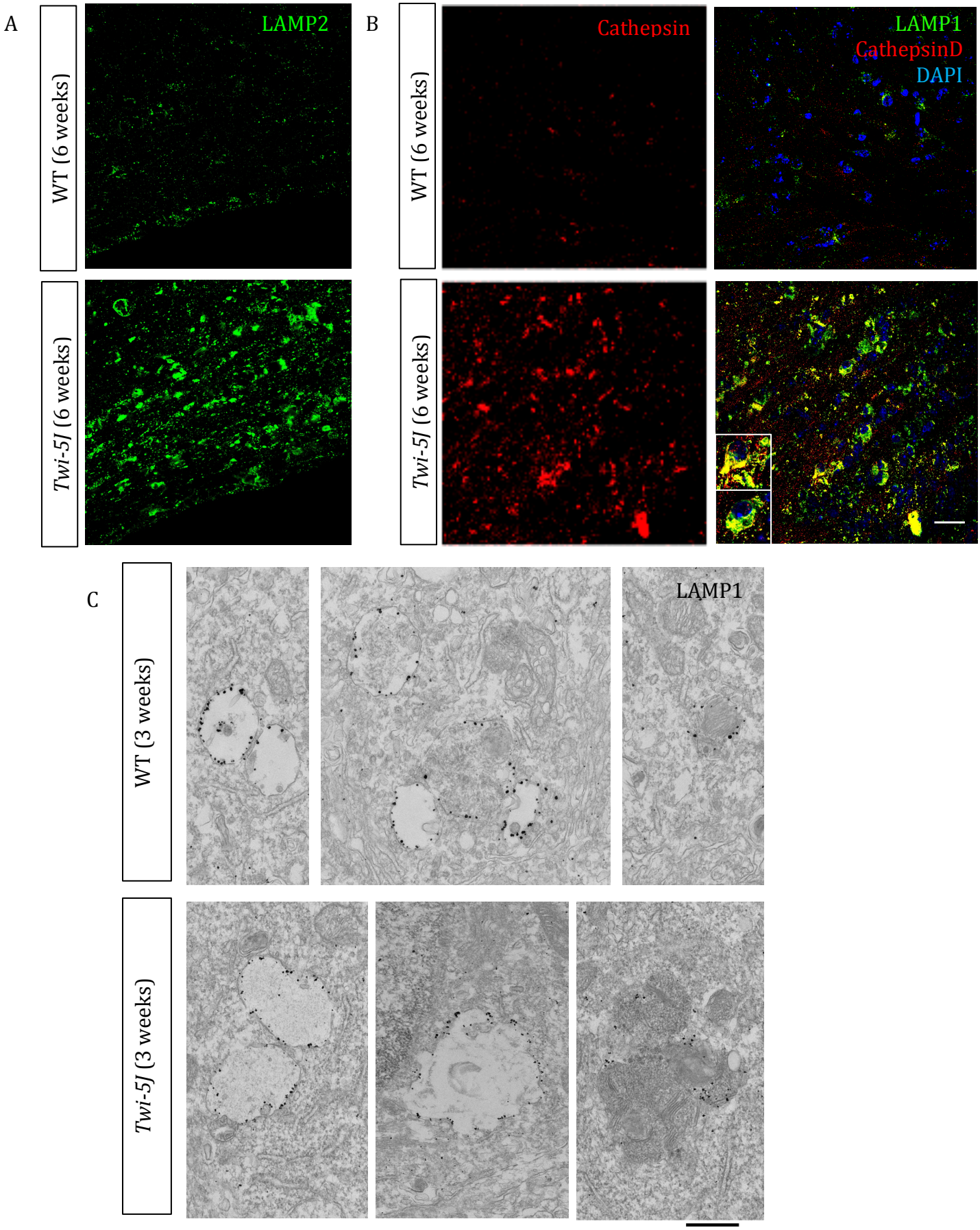
A
WT (6 weeks)
LAMP2
Twi-5J (6 weeks)
B
WT (6 weeks)
Cathepsin
LAMP1
CathepsinD
DAPI
Twi-5J (6 weeks)
C
WT (3 weeks)
LAMP1
Twi-5J (3 weeks)

Fig. 2.8 Enlarged lysosomes of *Twi-5J* (Bl6) white matter retained essential lysosomal characteristics and developed non-selectively from all heterogeneous lysosomes.

(A) The lysosomes of *Twi-5J* (Bl6) white matters were investigated by staining of another lysosomal membrane protein, LAMP2. LAMP2-labeled lysosomes revealed similar lysosomal phenotypes, i.e. increased LAMP2 expression and enlarged lysosomes as labeled by LAMP1. 25 μm scale bar.

(B) The lysosomes of *Twi-5J* (Bl6) white matters were investigated by staining of a soluble lysosomal protease, Cathepsin D. Results showed that *Twi-5J* (Bl6) had an increased expression of Cathepsin D and the enlarged LAMP1-labeled lysosomes retained the content of Cathepsin D. 25 μm scale bar.

(C) LAMP1-silver immunolabeled lysosomes from corpus callosum were investigated under electronmicroscopy (EM). Both WT and enlarged *Twi-5J* (Bl6) lysosomes retained the heterogeneities of electron densities and deposit contents, e.g. containing vacuoles, electron-light deposit, or electron-dense membrane-like structures, indicating that the development of enlarged lysosomes was not limited to a certain type of lysosomes, but more likely resulted from a non-selective process among all lysosomes. 500 nm scale bar.

Fig. 2.9

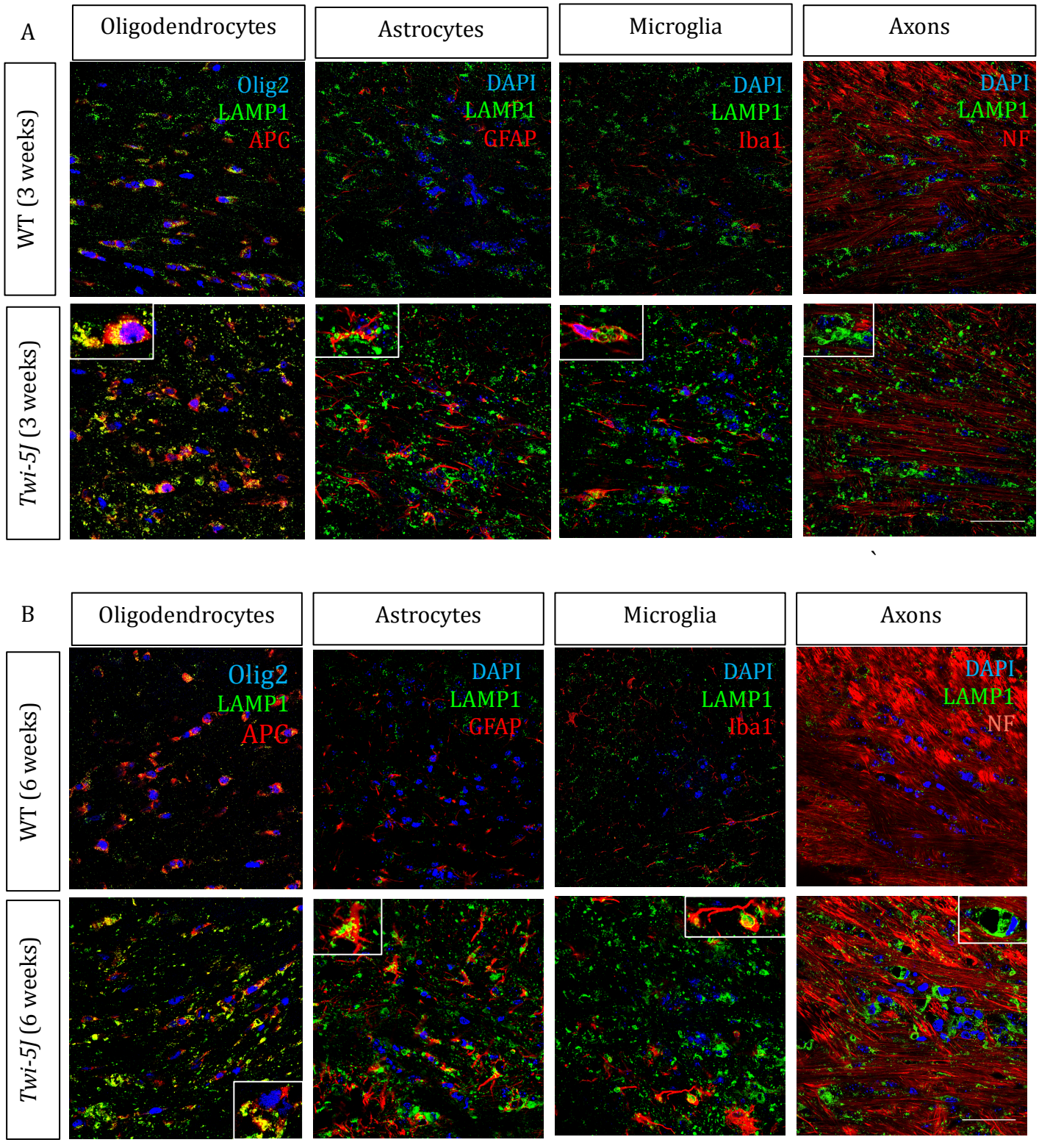
A
Oligodendrocytes
Astrocytes
Microglia
Axons
WT (3 weeks)
Twi-5J (3 weeks)
Olig2
LAMP1
APC
DAPI
LAMP1
GFAP
DAPI
LAMP1
Iba1
DAPI
LAMP1
NF
B
Oligodendrocytes
Astrocytes
Microglia
Axons
WT (6 weeks)
Twi-5J (6 weeks)
Olig2
LAMP1
APC
DAPI
LAMP1
GFAP
DAPI
LAMP1
Iba1
DAPI
LAMP1
NF

Fig. 2.9 Enlarged lysosomes occurred primarily in the oligodendrocytes from *Twi-5J* (Bl6) white matter and occurred secondarily in microglia and astrocytes.

(A) LAMP1 was co-labeled with cell-specific markers at 3-week of age when lysosomal enlargement started to become apparent. Makers used for identifying oligodendrocytes were Olig2 and APC, for identifying astrocytes was GFAP, for identifying microglia was Iba1, and for identifying axons was NF. Results showed that enlarged lysosomes primarily occurred in the oligodendrocytes from Twi-5J (Bl6) corpus callosum at the early onset of the lysosomal phenotypes. 50 μm scale bar.

(B) LAMP1 was co-labeled with cell-specific markers at the terminal age when the lysosomal phenotype became severe. Results showed that oligodendrocytes, astrocytes and microglia from *Twi-5J* (Bl6) corpus callosum all contained enlarged lysosomes, indicating that the enlarged lysosomes secondarily occurred in astrocytes and microglia. 50 μm scale bar.

SUPPLEMENTAL FIGURES

Sup. Fig. 2.1

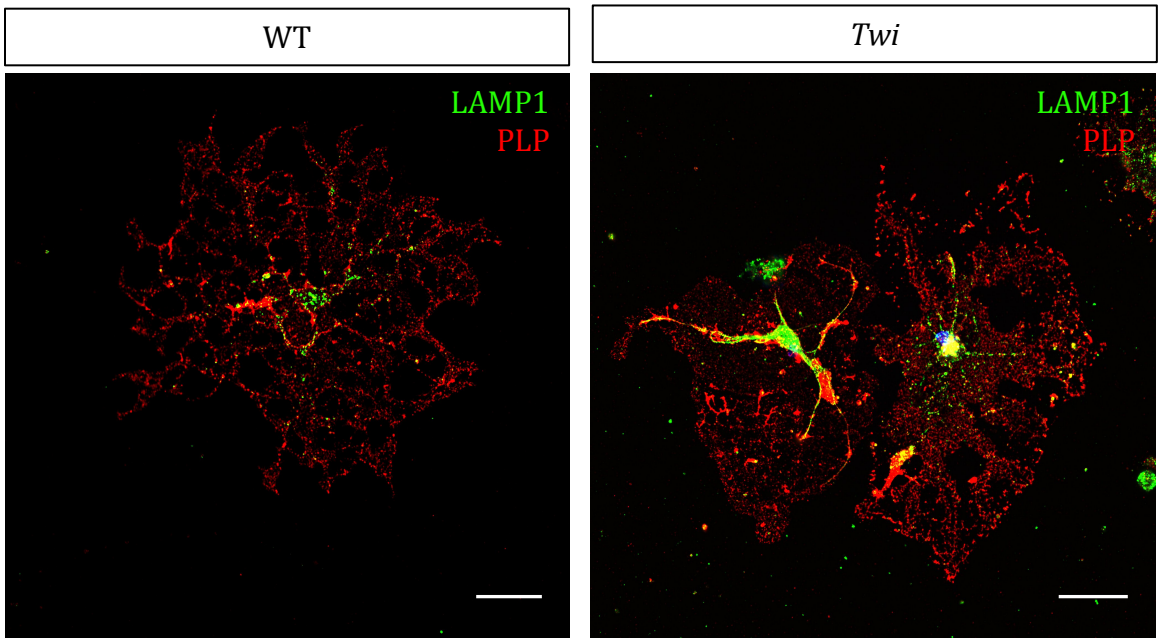

Sup. Fig. 2.1 *Twi* primary oligodendrocyte developed enlarged, tubular lysosomes

Representative images showing WT (left) and *Twi* (right) lysosomes. *Twi* primary oligodendroctyes developed tubular (left cell) and enlarged (right cell) lysososomes. 50 μm scale bar

Sup. Fig. 2.2

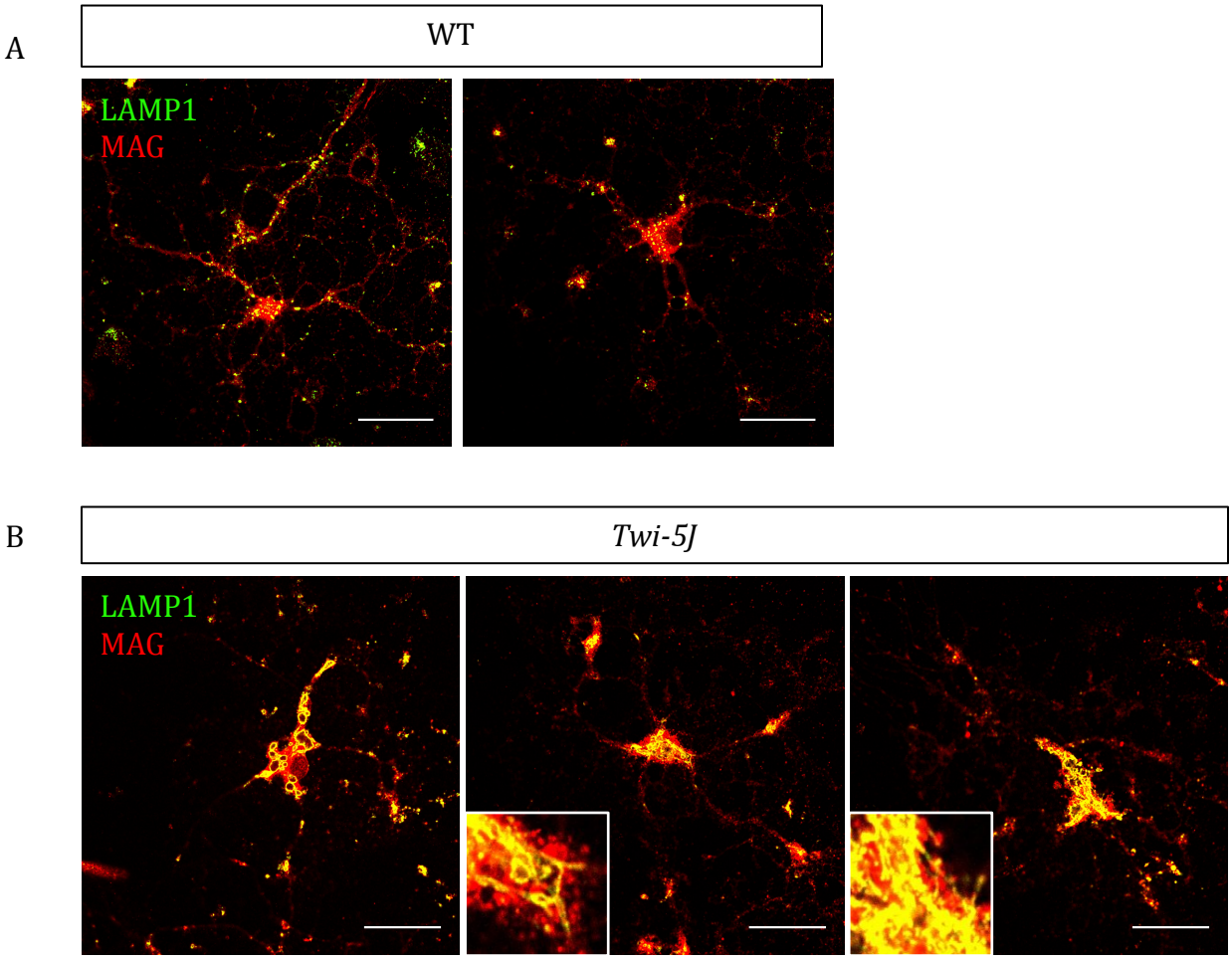

Sup. Fig. 2.2 *Twi-5J* primary oligodendrocyte developed enlarged, tubular lysosomes

(A) Representative images showing vesicular lysosomes in WT primary oligodendroctyes. 50 μm scale bar.
(B) Representative images showing enlarged (left panel) and tubular (middle and right panels) lysosomes in *Twi-5J* primary oligodendroctyes. 50 μm scale bar.

DISCUSSION

Sphingolipids are highly regulated in cells, and mutations of enzymes of the sphingolipid pathway often result in human diseases[39]. Krabbe disease is a lysosome storage disorder caused by the mutation of GALC gene, which subsequently results in the perturbation of the sphingolipid pathway, e.g. psychosine accumulation. Previous studies have largely focused on the molecular cascades induced by psychosine, and there is a lack knowledge of lysosomal pathologies caused by the GALC enzymatic deficiency. Our studies are the first to identify a common phenotype of lysosomal abnormalities in $GALC^{mutant}$ oligodendrocytes both *in vivo* and *in vitro*. The enlarged and tubular lysosomes of *Twi-5J* and *Twi* oligodendrocytes suggested disrupted lysosomal dynamics, which has been reported in other lysosome disorders[146]. Because the enlarged lysosomes primarily occurred in oligodendrocytes both in white matter and in neurosphere mixed culture, the lysosomal phenotype was suspected to result from sphingolipid perturbation in myelin, therefore leading us to investigate the relationship between lysosomal abnormalities and psychosine accumulation. In addition, the lysosomal enlargement initiated at around two weeks of age, prior to the peak of myelin generation in WT, occurring at around three weeks of age, therefore indicating an important role of the lysosomal pathophysiology in the early disease progression. Last but not least, understanding the pathological changes of $GALC^{mutant}$ lysosomes will be crucial for developing clinical treatments by which over-expressed GALC delivered by cross-

correction or viral transfection methods will fulfill its enzymatic functions in the recipient lysosomes.

Enlarged lysosomes as a result of disrupted lysosomal dynamics

Given the role of lysosomes in the endomembrane systems, there are multiple explanations for the enlarged lysosomes of GALC deficient oligodendrocytes, including enhanced homotypic lysosome fusion, reduced lysosome fission, and enhanced heterotypic lysosome fusion with late endosomes or autophagosomes,. Enhanced homotypic lysosome fusion, for example, has been reported to be triggered by elevated intracellular free Ca^{2+} concentration in NRK cells[147]. In NRK cells, microinjection of antibodies binding to cytosolic domain of lgp120, the homologue of LAMP1 in rat, induces the clustering of lysosomes[147]. Microinjection of lgp120 antibodies, as well as treating the cells with Ca^{2+} ionophore ionomycin that increased the intracellular free Ca2+ concentration, triggers the fusion of up to 15 lysosomes[147]. Furthermore, NRK cells that are permeabilized by streptolysim O and exposed to extracellular buffer containing 1 μM extracellular Ca^{2+} form large lysosomes, indicating that 1 μM Ca^{2+} is sufficient to enhance lysosome fusion[147].

Contrary to the enhanced lysosome fusion, reduced lysosome fission is found in the *beige*$_j$ bone marrow-derived macrophages of the Chediak-Higashi disorder murine model[146]. The *beige*$_j$ bone marrow-derived macrophages are absent of Chs/Lyst proteins and form enlarged lysosomes[146]. By applying Acetate Ringer's treatment, which results in lysosome fragmentation, the rate of lysosome recovery through

lysosome fusion is measured and no significant difference is found between WT and *beige*$_j$ cells[146]. However, by applying vacuolin-1, which results in lysosome enlargement, *beige*$_j$ cells show delayed lysosome recovery, indicating a deficiency of lysosome fission[146]. Interestingly, the *beige*$_j$ lysosomes also show increased tubular morphology, likely due to reduced lysosome fission[146]. In addition to homotypic lysosome fusion and fission, increased lysosome fusion with late endosome or autophagosomes could also explain enlarged lysosomes, despite that they are separate cellular processes.

Lysosome fusion with late-endosomes is a well-known process for exchanging the contents of endosomes and lysosomes, e.g. delivering endocytosed macromolecules to lysosomes for degradation. Two types of late-endosome-lysosome fusion, kiss-and-run and direct fusion, have observed by live-cell imaging and electron microscopy[125,148-150]. Both types require *trans*-SNARE complexes and Ca^{2+} release from lysosomal and endosomal lumens for efficient fusion[125,150-153]. One way to distinguish late endosome-lysosome fusion from homotypic lysosome fusion is that late endosome-lysosome-fused structures retain the mannose-6-phosphate (MPR) expression that is absent from the homotypic lysosome-fused structures[154,155]. Unlike how lysosome fuse with late endosomes to mix their endocytosed contents, lysosomes fuse with autophagosomes to degrade bulky cellular components, such as mitochondria and peroxisomes, and recycle nutrients via autophagy triggered by stress signals including several different nutrient starvation conditions [156-159]. Lysosome-autophagosome fusion to form autolysosomes requires autophagy-

related (Atg) proteins for the complete fusion[157]. One of the Atg proteins, Atg8, or LC3 in mammalian cells, can be used to distinguish autophagosomes from lysosomes fused to late-endosomes[157,160]. After autolysosomes are formed, lysosomes are regenerated via autophagic lysosome reformation (ALR), a process highly regulated by phosphatidylinositol-4,5-bisphosphate (Ptdlns(4,5)P_2) and that requires clathrin-mediated membrane budding[161,162]. During ALR, autolysosomes extrude tubes that pitched off later to form regenerated lysosomes[161]. Dysregulation of Ptdlns(4,5)P_2 by knockdown of *PIP5K1A* causes LAMP1-positive elongated tubular structures[162]. In our study, we were unclear about the causes of the enlarged lysosomes, but by investigating the late-endosome marker MPR or the autophagosome marker LC3, one should be able to distinguish heterotypic fusion from homotypic fusion. If homotypic fusion is thought to be most likely, then live cell imaging of labeled lysosomes can assess lysosome dynamics. Furthermore, lysosome *in vitro* assays also offer additional tools to look at the fusion process of isolated lysosomes[163].

Possible mechanisms of tubular lysosome formation

Besides the enlarged lysosomes, the tubular structures we observed in the $GALC^{mutant}$ primary oligodendrocytes were also interesting phenotypes along with the lysosomal enlargement. Tubular lysosomes can result from a variety of factors, including reduced lysosome fission, incomplete ALR.[146,161,162,164]. During ALR, the Ptdlns(4,5)P_2-TRPML1-ALG2-dynein signaling drives lysosomes towards the (-)-end of microtubules while kinesin-1 binds to the extruded lysosome membrane

buddings and pulls out the tubular lysosomes towards the (+)-end of microtubules[164]. Future experiments would address whether tubular lysosomes of $GALC^{mutant}$ primary oligodendrocytes is caused by reduced lysosome fission or via ALR.

Potential molecular mechanisms of lysosomal phenotype of Krabbe disease

The molecular mechanisms of lysosome enlargement in GALC-deficient oligodendrocytes are unclear, though an accumulation of psychosine could be the cause. This study showed that psychosine accumulates in *Twi-5J* primary oligodendrocytes, consistent with previous studies in which psychosine was observed to accumulate in Krabbe disease patients' brains, *Twi* mice and *Twi-5J* mice brains, GALC knock-down MO3.13 human OPC like cells, and GALC knock-down rat primary oligodendrocytes[7,61,68,114,165]. Psychosine accumulation is found to be toxic and is considered to be one of the main causes of Krabbe disease cellular pathologies[8,32]. Exogenous and endogenous psychosine accumulation results in cell death, activation of $sPLA_2$ and release of AA and PLC, etc. in oligodendrocyte-like cells and primary oligodendrocytes[46,50,54,71,114,166]. Interestingly, psychosine is found to highly accumulate in the membrane lipid rafts of *Twi* brain and sciatic nerves along with an increase of cholesterol concentration of the lipid rafts as well as inhibition of PKC activities[44]. Psychosine accumulation in lipid rafts is ultimately shown to be an inhibitory factor of the raft-mediated endocytosis of *Twi* neural cells and is responsible for the perturbation of the membrane architectures by lipid-lipid interaction between psychosine and other membrane lipid components[47,57]. Lipid

rafts serve important roles in membrane trafficking and fusion by regulating SNARE activities and attachment[167]. SNARE complexes are required for both homotypic and heterotypic lysosome fusions[125]. It is reasonable to speculate that the accumulation of psychosine would affect lysosome fusion and dynamics by interrupting lipid rafts and SNARE complexes, thereby resulting in enlarged lysosomes. Of course, we cannot exclude other possible mechanisms that cause lysosome enlargement through either psychosine-mediated signals or psychosine-independent signals. For example, lysosome swelling has been reported in Hela cells when the cation-independent mannose 6-phosphate receptors (CI-MPR) failed to return back to the trans-Golgi networks (TGN) from endosomes by RNA interference of the subunit hVps26 of the retromer[168].

Another example of lysosome enlargement is caused by the depletion of LYST protein in mice fibroblasts and Hela cells with unchanged lysosome pH, autophagy, and endocytic degradation[169]. Besides the accumulation of psychosine, other perturbations of the sphingolipid pathway caused by GALC deficiency should also be considered. For example, ceramide, the product of GALC hydrolyzation of galactosylceramide, is reduced in the *Twi* brains[54]. Ceramide serves important roles in triggering the raft-dependent vesicle trafficking from exosomes to endosomes[170]. Whether the lack of ceramide affects lysosome trafficking is unclear. Future experiments will probe the link between GALC deficiency and lysosome enlargement.

Chapter 3 Thesis Summary

CONCLUSIONS

Summary of the thesis project

Krabbe disease, also called globoid cell leukodystrophy, is a lysosomal disorder. Affected infants show both motor and cognitive degenerations and live no longer than 2 years[17]. Unfortunately, there is a lack of effective clinical therapies. The histopathology of Krabbe disease includes demyelination, axonal degeneration and neuroinflammation[17,19]. Krabbe disease is caused by recessive mutations of the GALC gene. GALC is a lysosomal hydrolase, and its deficiency induces an accumulation of the neurotoxin psychosine[17,19,39]. Recent studies of Krabbe disease pathophysiology have mainly focused on the molecular cascades triggered by psychosine accumulation. However, little is known about the effect of GALC-deficiency on lysosomes.

The motivation of my thesis was to answer the question: what is the lysosomal pathology in Krabbe disease? To do so, I used the Krabbe disease murine models, *Twi* and *Twi-5J* mice. Both mice represent the genetic deficiencies found in human patients. *Twi* mice have a nonsense mutation and do not express GALC, whereas *Twi-5J* mice have a missense mutation and express a mutant version, $GALC^{E130K}$. Both models provide the advantage of looking at common mechanisms across different genotypes.

I discovered an abnormal enlargement of lysosomes in *Twi* and *Twi-5J* oligodendrocytes both *in vitro* and *in vivo,* which may suggest enhanced lysosomal fusion or reduced lysosomal fission caused by GALC deficiency. In primary oligodendrocytes, tubular lysosomes also occurred as well as lysosomal enlargement, supporting the idea of disrupted lysosomal dynamics. Further experiments showed that the abnormal lysosomes retained an acid pH, electron micrographic heterogeneities, unchanged β-NAG activities, and an expression of lysosomal proteins (e.g. LAMP1, LAMP2, cathepsinD, and $GALC^{E130K}$), indicating at least partially retained lysosomal functions. In GALC deficient white matter, the lysosomal enlargement was an early-onset phenotype apparent by two weeks of age, prior to the peak of myelin generation that occurs in WT mice at approximately three weeks of age. Enlarged lysosomes primarily occurred in oligodendrocytes in both white matter and neurosphere mixed culture, corresponding to the disruption of sphingolipid metabolism, e.g. psychosine accumulation, in myelin caused by the GALC enzymatic deficiency. Therefore, our results provided the first evidence for lysosomal pathophysiology in Krabbe disease, which not only advances our knowledge of the cellular mechanisms of the disease progression, but also enables the phenotype of early onset abnormality as a potential target for developing clinical treatments.

Due to a limited time frame, this thesis work hasn't yet fully characterized the lysosomal functions of GALC deficient oligodendrocytes. Lysosomal enzymes have their highest activities in an acidic environment, i.e. pH 4.5~5.0. By applying

LysoTracker, a pH sensitive dye, the lysosomes of *Twi-5J* oligodendrocytes were found to retain the acidity. However, these experiments were qualitative, not quantitative. LysoTracker has a fluorescent signal when the pH is lower than 6.0. Therefore, the exact pH of *-5J* lysosomes can not be measured by LysoTracker. Another way to evaluate lysosomal functions is to measure the activities of lysosomal enzymes. In my thesis project, the activity of NAG was β-NAG measured in primary WT and *Twi-5J* oligodendrocytes. No significant difference was found between WT and *Twi-5J* lysosomes. Other lysosomal enzymes, e.g. cathepsin D, L, S and β-hexosaminidase, have not been analyzed. These lysosomal enzymes can be measured using commercial available kits, and the analysis of these enzymes will shed light on how the abnormal lysosomes affect the cellular functions of *Twi-5J* oligodendrocytes. Another important question about the lysosome function is whether the delivery of macromolecules from endosomes to lysosomes is affected in *Twi-5J* oligodendrocytes. Lysosomes receive and digest the endocytosed macromolecules from endosomes. One way to observe the trafficking and delivery process is to use live cell imaging methods. By applying pHrodo Green Dextran (Life Tech, Cat# P35368), molecules that only have their fluorescent signals after being endocytosed, combined with LysoTracker Red, the time course and efficiency of the trafficking from matrix to lysosomes can be analyzed. Pioneer experiments have been done to show that after 12 hours, the majority of the pHrodo Green Dextran have been trafficked into lysosomes in WT oligodendrocytes, as measured by the co-localization of pHrodo Green Dextran and LysoTracker Red (data not shown). More experiments need to be done to quantitatively compare the cargo trafficking in WT

and *Twi-5J* lysosomes. In summary, my thesis project offered strong evidences for and detailed characterization of the morphological changes of GALC deficient lysosomes. Future functional studies of the enlarged, tubular lysosomes will greatly expand our knowledge of the lysopathophysiology of Krabbe disease.

Summary of additional experiments in Krabbe disease

Besides the thesis project, I also conducted experiments that contributed to other projects to better understand Krabbe disease pathology. In brief, for the purpose of generating HeLa cell lines that express either human GALC (h-GALC) or human $GALC^{E130K}$ (h-$GALC^{E130K}$), I cloned the construct carrying h-GALC or h-$GALC^{E130K}$ in the pTRE3G vector. To genotype mouse lines that carried uncertain copies of target genes, I performed quantitative PCR and the $2^{-\Delta\Delta C_T}$ analysis methods and measured the copy numbers of Cre in the Sox10 Cre; RFP mouse – that analysis revealed that the homozygous mouse carried about 20 copies of Cre. To investigate the effects of exogenous psychosine in neonatal brain development, I injected the white matter of P1 WT mice with psychosine at 0.15 μM, 1.5 μM and 15 μM. At 3 weeks of age, the injection tracks were visible, but there were no significant differences in the number of astrocytes and microglia activation labeled by GFAP and Iba, respectively. The lack of neuroinflammation might reflect that either (a) that the exogenous psychosine at this concentration did not evoke inflammation or (b) that the exogenous psychosine was degraded by GALC enzyme expressed in WT brain. To investigate the roles of *Twi* primary mouse oligodendrocytes in the neuroinflammation effects, I transplanted WT and *Twi* oligodendrocyte precursor

cells (OPCs) into recipient WT white matter (data shown in Thesis Appendix) and found that transplanted OPCs survived, developed the oligodendrocyte-like morphology, and did not induce local neuroinflammation.

FUTURE DIRECTIONS

The discovery of the lysosomal abnormalities in Krabbe disease leads to the question: what are the cellular structures that derive the enlarged lysosomes with apparently normal acidic pH? Answering this question may provide a clue to the underlying molecular mechanisms. The lysosomal enlargement could result from several changes: (a) lysosome swelling, (b) enhanced lysosomal fusion, (c) reduced lysosomal fission, (d) enhanced lysosomal fusion with late endosomes, or (e) enhanced lysosomal fusion with autolysosomes during autophagy. To examine each possibility, a first step could be to distinguish whether lysosomal enlargement is homotypic or heterotypic by co-labeling with lysosomal markers and late endosomes- or autolysosomes-specific markers, e.g. MPR or LC3, respectively. If the enlarged lysosomes express neither late-endosomal markers nor autolysosomal markers, then the underlying mechanisms are likely due to the lysosomal swelling or an imbalance between lysosomal fusion and fission. Hence, the homotypic lysosomal dynamics can be accessed using live cell imaging methods, e.g. by labeling lysosomes by LAMP1-GFP (Addgene, Cat# 16290) via transfection. Anther way to track down the homotypic lysosomal fusion is an *in vitro* assay developed by J. Kaplan's group, in which the purified lysosomes were labeled by either b-HRP or avidin, and the fusion of the lysosomes were examined by measuring the formation of avidin-HRP complexes[163]. On the other hand, if the enlarged lysosomes are positive for the late-endosomal markers, then mistrafficking between endosomes and lysosomes should be further investigated. Similar to this idea, if the enlarged

lysosomes are positive for the autolysosomal markers, then autophagy is likely the mechanism underlying lysosomal enlargement.

Another interesting question is what molecular mechanisms cause the large and tubular lysosomes? Understanding the molecular cascades will guide us to rescue the phenotype and determine how it impacts the disease. It is reasonable to speculate that psychosine accumulation, which has been shown in previous studies to disrupt membrane architectures via lipid-lipid interaction, is a possible cause of the lysosomal enlargement through changing the properties and the dynamics of lysosomal membranes[44,47,57]. One way to investigate this hypothesis would be to apply exogenous psychosine to primary oligodendrocytes and examine lysosome development. However, this method, as with all Krabbe disease studies using exogenous psychosine, has the caveat that exogenous psychosine might not function in the same manner as endogenous psychosine. But given the technical difficulties to manipulate endogenous psychosine, applying exogenous psychosine may be useful for preliminary experiments. It is also possible that changes in lysosomal morphology are independent of psychosine-induced cascades, e.g. the phosphatidylinositide-dependent pathway that serves important roles in the autophagic lysosome reformation[161,162]. Knowing what cellular structures contribute to the enlarged lysosomes should provide insights into candidate pathways.

The ultimate goal for any lysosomal disorder is a cure. Developing clinical treatments progresses alongside our understanding of the pathological mechanisms. Therefore, investigating methods to rescue or prevent the lysosomal abnormalities, an early-onset phenotype *in vivo*, is an important goal for the future. Delivering WT GALC into GALC deficient oligodendrocytes by either viral transfection or cross correction is one strategy[17,20]. However, it is unclear whether WT GALC will retain enzymatic activity in abnormally enlarged lysosomes. Hence, the timing of GALC delivering may be crucial. For example, delivery of GALC at the pre-symptomatic status might produce higher efficiencies. The development of clinical treatments will also benefit from our knowledge of the molecular mechanisms of the phenotype. The more we know about the mechanism, the more targets we have to investigate to develop correcting methods.

Fig 3.1 Future Directions

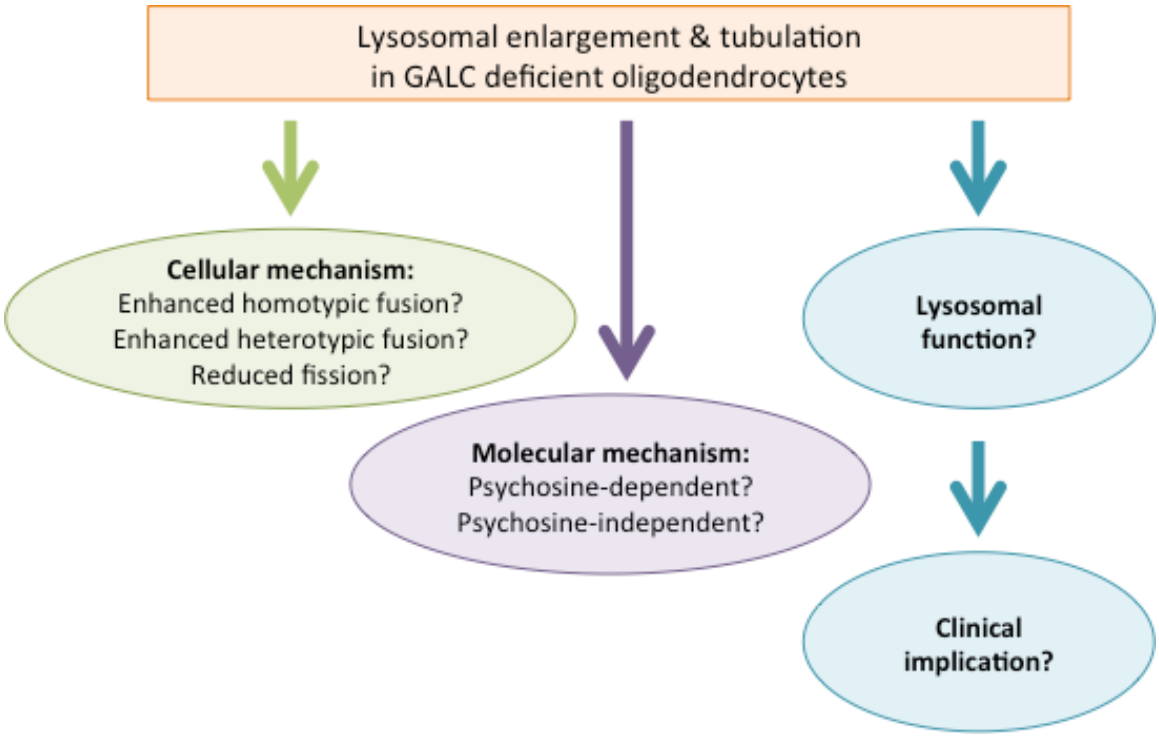

APPENDIX

Rationale:

The pathology of Krabbe disease in human patients and murine models includes demyelination, axonal degeneration, and neuroinflammation. Neuroinflammation, e.g. astrocytes activation and microglia recruitment, occurs generally concomitant with myelin degeneration. However, the molecular mechanisms of the induction of neuroinflammation remain unclear. One possibility is that GALC deficient oligodendrocytes are sufficient to induce gliosis responses. To test this hypothesis, we plan to transplant *Twi* primary oligodendrocytes precursor cells (OPCs) into WT forebrains and compare the neuroinflammationary effects to the control. This experiment can be technical demanding. Therefore, I conducted the following experiments to build up a platform for transplanting primary mouse OPCs.

Aims:

These experiments aim to investigate the following questions: (a) Can primary OPCs generated from WT and *Twi* mice be transplanted into WT mouse white matter? (b) Can transplanted OPCs survive and be detected in the recipient mouse brains? (c) Can transplanted OPCs trigger local neuroinflammation responses?

Procedures:

WT and *Twi* OPCs generated by the immunopanning protocol (Ben Emery and Jason C. Dugas, *CSHL*, 2013) were maintained in the proliferation media containing PDGFα and NT3. At the night before transplantation, BacMam 2.0 baculovirus system

nuclear-GFP (Life Tech.) was added into OPC cultures and incubated over night. On the day of transplantation, transfected OPCs were harvested and resuspended in the Leibovitz's L-15 medium (ThermoFisher Cat# 11415114) containing DNAse at 90,000~100,000 cells/μl concentration. Recipient animals were postnatal day 1 (P1) WT mice in the C57BL/6J background, the same background as the mice for generating OPCs. WT mice were anesthetized by putting the animals on an icy pad throughout the surgery. Approximately 3.4 x 10^4 to 3.7 x 10^4 cells were injected at both sides of the cortexes using pulled and tip-grinded calibrated glass micropipettes (Drummond Scientific Cat# 2-000-001, 1-5 μl). Injection was operated by using a micromanipulator and targeted at the corpus callosum. Five WT mice and eight *Twi* mice were injected and all survived after the surgery. Mice were lived in their original cages until being perfused. Both WT and twticher mice were perfused at P22, P24, and P30 using 4% paraformaldehyde. Brains were sectioned at 50 μm thickness on the vibrotome (Leica VT1000S). To visualize the transplanted OPCs, immunohistochemistry (IHC) and immunofluorescence (IF) were applied using anti-GFP antibodies. GFP primary antibodies were: (i) chicken anti-GFP (Abcam Cat# ab13970), used for IHC, and (ii) rabbit anti-GFP (LifeTech Cat#11122), used for IF. Other primary antibodies used for labeling myelin, microglia and astrocytes were rat anti-MBP (Millipore Cat# MAB386), rabbit anti-Iba1 (Wako Cat# 019-19741) and rabbit anti-GFAP (Millipore Cat# AB5804), respectively.

Results:

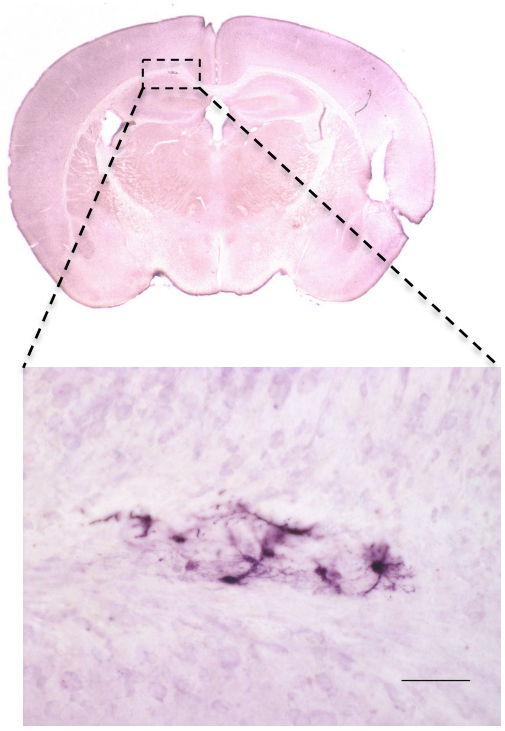

Fig. 4.1 Transplanted WT OPCs survived in the recipient white matter.

WT primary mouse OPCs labeled by BacMam nuclear-GFP were transplanted into WT mouse forebrains. Recipient mice were perfused at P22. Transplanted OPCs were detected by IHC using anti-GFP primary antibody. 50 μm scale bar.

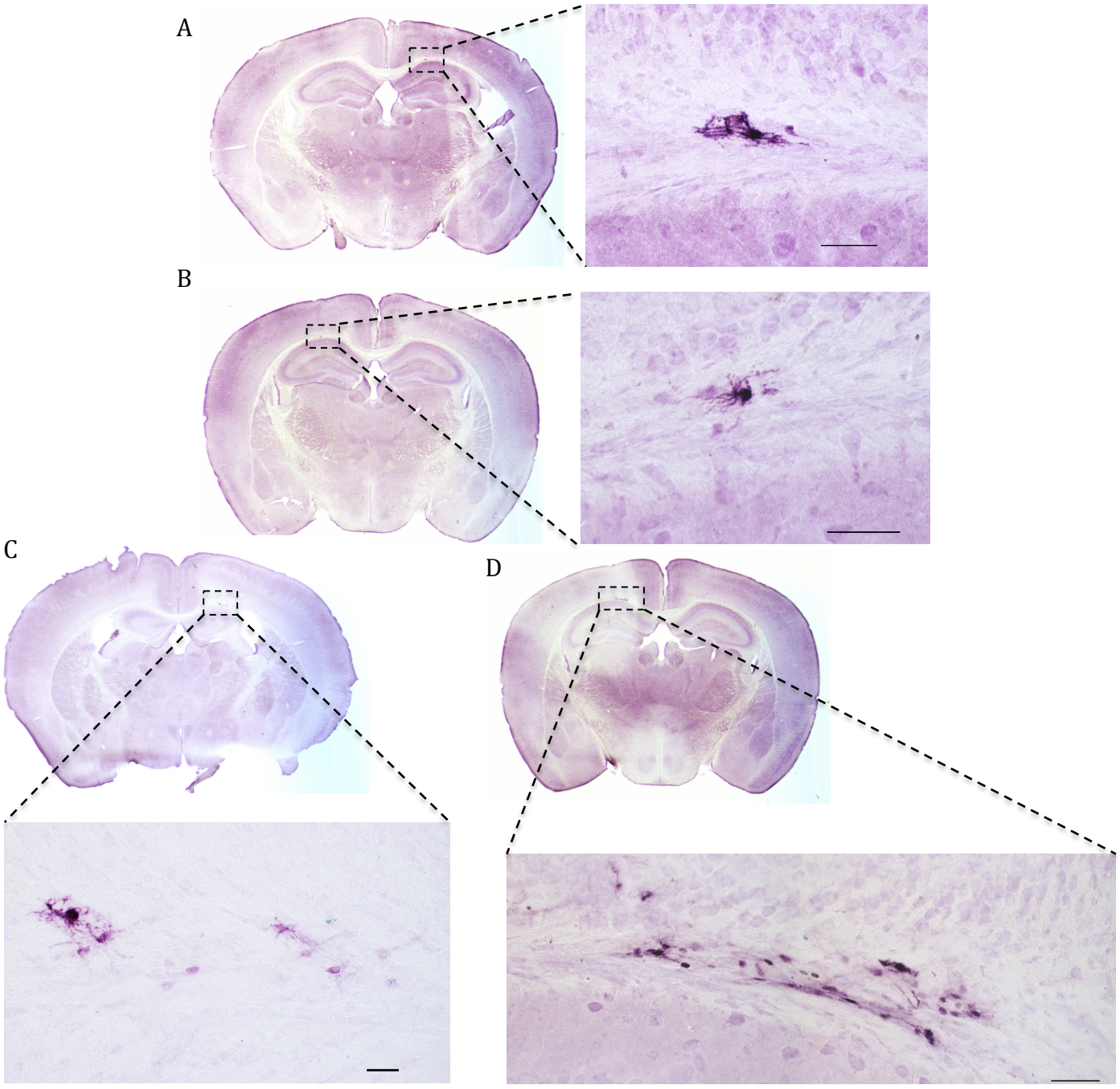

Fig. 4.2 Transplanted *Twi* OPCs survived in the recipient white matter.

(A)-(D) *Twi* primary mouse OPCs labeled by BacMam nuclear-GFP were transplanted into WT mouse forebrains. Recipient mice were perfused at P22 or P24. Transplanted OPCs were detected by IHC using anti-GFP primary antibody. 50 μm scale bar.

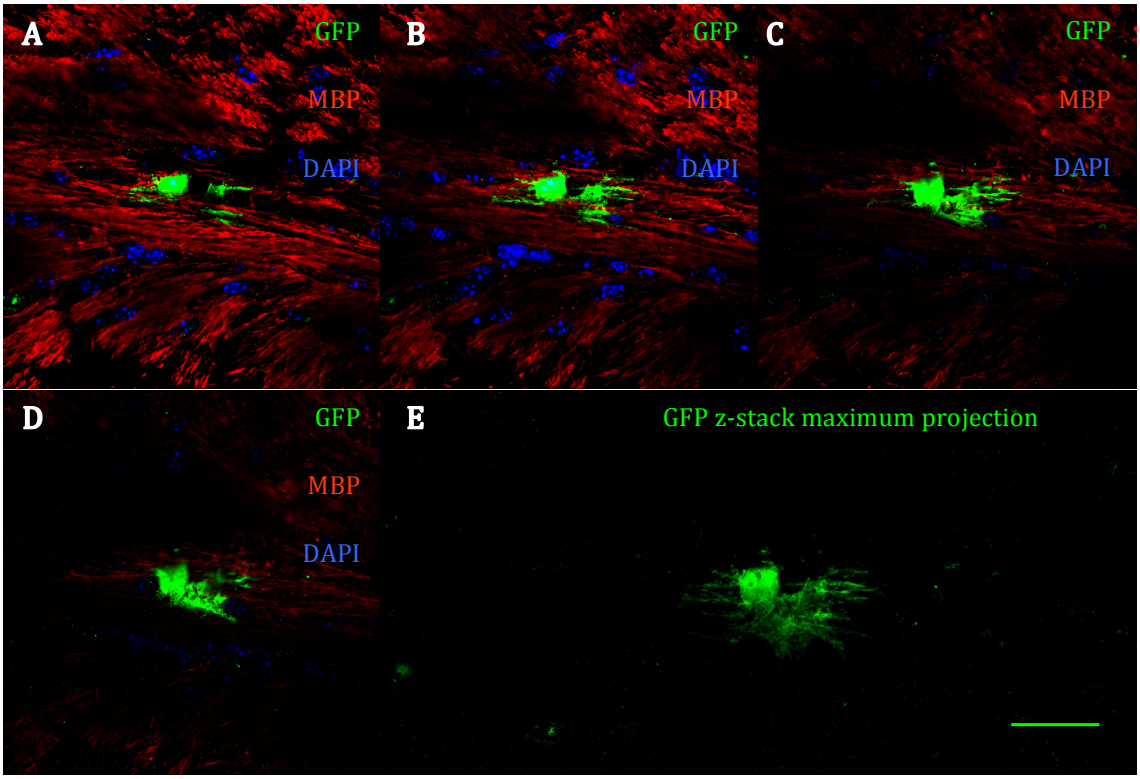

Fig. 4.3 Transplanted WT OPCs developed oligodendrocyte-like morphologies.

(A)-(D) Z-stack series images of one transplanted cell in the corpus callosum. WT primary mouse OPCs labeled by BacMam nuclear-GFP were transplanted into WT mouse forebrains. Recipient mice were perfused at P30. Transplanted OPCs were detected by IF using anti-GFP primary antibody. Myelin was co-labeled using anti-MBP primary antibody. (E) Z-stack maximum projection of the GFP-labeled WT oligodendrocytes. 50 μm scale bar.

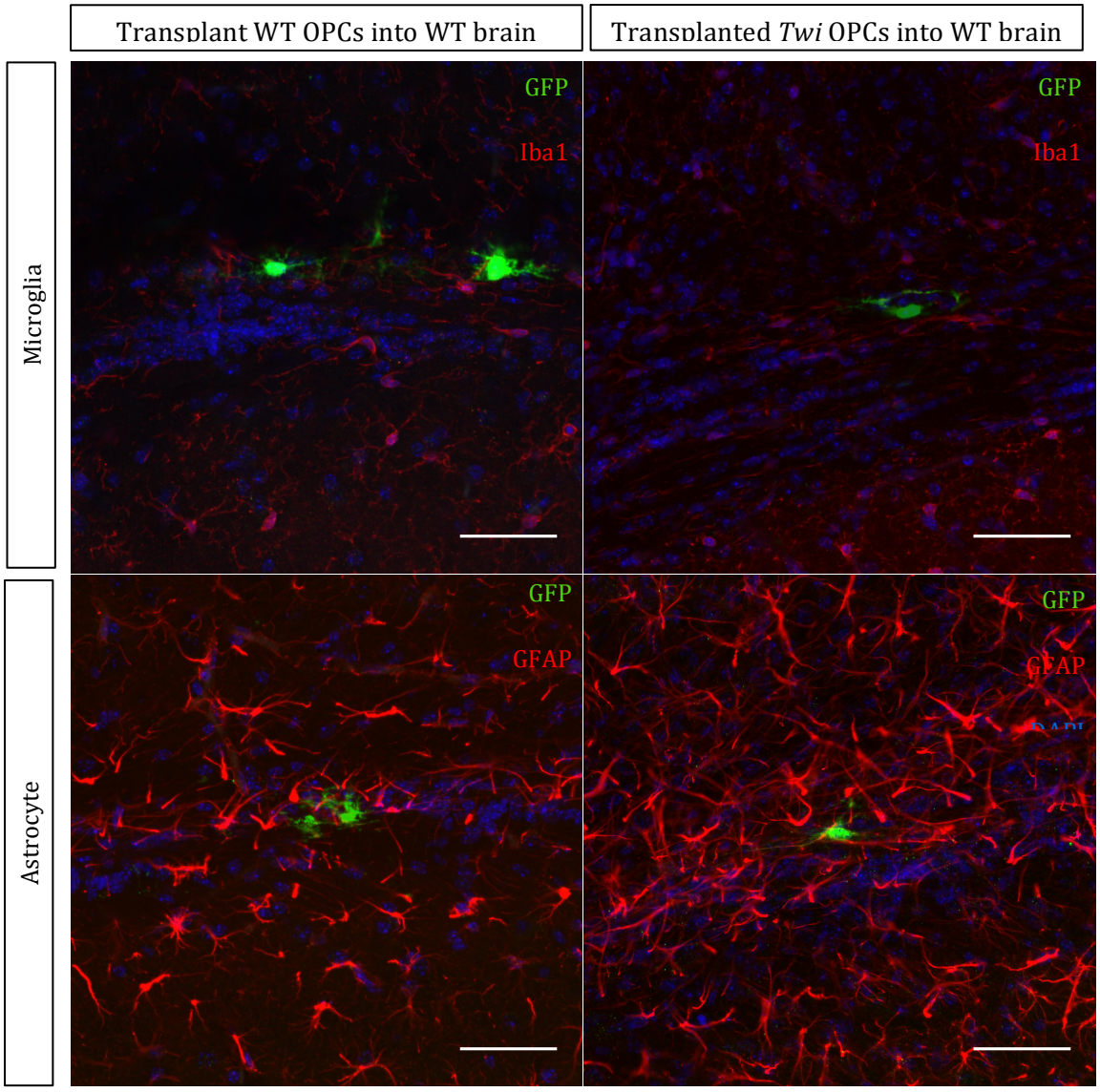

Fig. 4.4 Single transplanted WT or *Twi* OPC did not trigger local neuroinflammation responses.

WT or *Twi* primary mouse OPCs labeled by BacMam nuclear-GFP were transplanted into WT mouse forebrains. Recipient mice were perfused at P22, P24 or P30. Transplanted OPCs were detected by IF using anti-GFP primary antibody. Microglia or astrocytes were co-labeled using anti-GFAP or anit-Iba primary antibody, respectively. 50 μm scale bar.

Conclusion:

Primary OPCs generated from WT and *Twi* mice were successfully labeled by BacMam nuclear-GFP *in vitro*, transplanted into neonatal WT white matter, and detected by IHC and IF methods. Transplanted WT and *Twi* OPCs survived at least 4-weeks *in vivo* and developed oligodendrocyte-like morphologies. Single transplanted WT or *Twi* OPC didn't trigger local neuroinflammation responses. However, the yield of transplanted OPCs was very low. One possible explanation of this is due to the induction of cell differentiation by the BacMam 2.0 baculovirus system. In another set of experiment, BacMam nuclear-GFP induced the differentiation of OPCs 3 days after transfection (data not shown). Therefore, OPCs differentiation induced by the BacMam system could possibly reduce the cell proliferation *in vivo* after the transplantation, thus lowing the yield of GFP-positive oligodendrocytes. One-way to resolve this problem is to generate GFP-positive OPCs using a transgenic approach, i.e. by crossing *Twi* mice and GFP-carriers.

REFERENCES

1. Compston, A. A new familial infantile form of diffuse brain-sclerosis. *Brain* **136,** 2649–2651 (2013).
2. Suzuki, K. & Suzuki, Y. Globoid cell leucodystrophy (Krabbe's disease): deficiency of galactocerebroside beta-galactosidase. *Proc. Natl. Acad. Sci. U.S.A.* **66,** 302–309 (1970).
3. Suzuki, Y. & Suzuki, K. Krabbe's globoid cell leukodystrophy: deficiency of glactocerebrosidase in serum, leukocytes, and fibroblasts. *Science* **171,** 73–75 (1971).
4. Miyatake, T. & Suzuki, K. Additional deficiency of psychosine galactosidase in globoid cell leukodystrophy: an implication to enzyme replacement therapy. *Birth Defects Orig. Artic. Ser.* **9,** 136–140 (1973).
5. Wenger, D. A., Satter, M. & Markey, J. P. Deficiency of monogalactosyl diglycerid beta-B-galactosidase activity in krabbe's disease. *Biochem. Biophys. Res. Commun.* **53,** 680–685 (1973).
6. Wenger, D. A., Sattler, M. & Hiatt, W. Globoid cell leukodystrophy: deficiency of lactosyl ceramide beta-galactosidase. *Proc. Natl. Acad. Sci. U.S.A.* **71,** 854–857 (1974).
7. Svennerholm, L., Vanier, M. T. & Månsson, J. E. Krabbe disease: a galactosylsphingosine (psychosine) lipidosis. *J. Lipid Res.* **21,** 53–64 (1980).
8. Tanaka, H. & Suzuki, K. Studies on the pathogenesis of Krabbe's

leukodystrophy: cellular reaction of the brain to exogenous galactosylsphingosine, monogalactosyl diglyceride, and lactosylceramide. *Adv. Exp. Med. Biol.* **68,** 99–114 (1976).

9. Kobayashi, T., Yamanaka, T., Jacobs, J. M., Teixeira, F. & Suzuki, K. The Twitcher mouse: an enzymatically authentic model of human globoid cell leukodystrophy (Krabbe disease). *Brain Res.* **202,** 479–483 (1980).

10. Chen, Y. Q. & Wenger, D. A. Galactocerebrosidase from human urine: purification and partial characterization. *Biochim. Biophys. Acta* **1170,** 53–61 (1993).

11. Sakai, N. *et al.* Krabbe disease: isolation and characterization of a full-length cDNA for human galactocerebrosidase. *Biochem. Biophys. Res. Commun.* **198,** 485–491 (1994).

12. Chen, Y. Q., Rafi, M. A., de Gala, G. & Wenger, D. A. Cloning and expression of cDNA encoding human galactocerebrosidase, the enzyme deficient in globoid cell leukodystrophy. *Hum. Mol. Genet.* **2,** 1841–1845 (1993).

13. Meikle, P. J., Hopwood, J. J., Clague, A. E. & Carey, W. F. Prevalence of lysosomal storage disorders. *JAMA* **281,** 249–254 (1999).

14. Poorthuis, B. J. *et al.* The frequency of lysosomal storage diseases in The Netherlands. *Hum. Genet.* **105,** 151–156 (1999).

15. Wenger, D. A., Rafi, M. A. & Luzi, P. Molecular genetics of Krabbe disease (globoid cell leukodystrophy): diagnostic and clinical implications. *Hum. Mutat.* **10,** 268–279 (1997).

16. Zlotogora, J., Regev, R., Zeigler, M., Iancu, T. C. & Bach, G. Krabbe disease:

increased incidence in a highly inbred community. *Am. J. Med. Genet.* **21,** 765–770 (1985).

17. Graziano, A. C. E. & Cardile, V. History, genetic, and recent advances on Krabbe disease. *Gene* **555,** 2–13 (2015).

18. HAGBERG, B., SOURANDER, P. & Svennerholm, L. Diagnosis of Krabbe's infantile leucodystrophy. *J. Neurol. Neurosurg. Psychiatr.* **26,** 195–198 (1963).

19. Suzuki, K. Globoid cell leukodystrophy (Krabbe's disease): update. *J. Child Neurol.* **18,** 595–603 (2003).

20. Wenger, D. A., Rafi, M. A., Luzi, P., Datto, J. & Costantino-Ceccarini, E. Krabbe disease: genetic aspects and progress toward therapy. *Mol. Genet. Metab.* **70,** 1–9 (2000).

21. Bajaj, N. P. S., Waldman, A., Orrell, R., Wood, N. W. & Bhatia, K. P. Familial adult onset of Krabbe's disease resembling hereditary spastic paraplegia with normal neuroimaging. *J. Neurol. Neurosurg. Psychiatr.* **72,** 635–638 (2002).

22. Jacob, J. C., Kutty, K. M., Islam, M., Dominic, R. G. & Dawson, G. Krabbe's disease: globoid cell leukodystrophy. *Can Med Assoc J* **108,** 1398–1400 (1973).

23. Yunis, E. J. & Lee, R. E. The ultrastructure of globoid (Krabbe) leukodystrophy. *Lab. Invest.* **21,** 415–419 (1969).

24. Jatana, M., Giri, S. & Singh, A. K. Apoptotic positive cells in Krabbe brain and induction of apoptosis in rat C6 glial cells by psychosine. *Neurosci. Lett.* **330,**

183–187 (2002).

25. Hill, C. H., Graham, S. C., Read, R. J. & Deane, J. E. Structural snapshots illustrate the catalytic cycle of β-galactocerebrosidase, the defective enzyme in Krabbe disease. *PNAS* **110,** 20479–20484 (2013).

26. Luzi, P., Rafi, M. A., Victoria, T., Baskin, G. B. & Wenger, D. A. Characterization of the rhesus monkey galactocerebrosidase (GALC) cDNA and gene and identification of the mutation causing globoid cell leukodystrophy (Krabbe disease) in this primate. *Genomics* **42,** 319–324 (1997).

27. Victoria, T., Rafi, M. A. & Wenger, D. A. Cloning of the canine GALC cDNA and identification of the mutation causing globoid cell leukodystrophy in West Highland White and Cairn terriers. *Genomics* **33,** 457–462 (1996).

28. Cannizzaro, L. A., Chen, Y. Q., Rafi, M. A. & Wenger, D. A. Regional mapping of the human galactocerebrosidase gene (GALC) to 14q31 by in situ hybridization. *Cytogenet. Cell Genet.* **66,** 244–245 (1994).

29. Luzi, P., Rafi, M. A. & Wenger, D. A. Structure and organization of the human galactocerebrosidase (GALC) gene. *Genomics* **26,** 407–409 (1995).

30. Nagano, S. *et al.* Expression and processing of recombinant human galactosylceramidase. *Clin. Chim. Acta* **276,** 53–61 (1998).

31. Deane, J. E. *et al.* Insights into Krabbe disease from structures of galactocerebrosidase. *PNAS* **108,** 15169–15173 (2011).

32. Spratley, S. J. *et al.* Molecular Mechanisms of Disease Pathogenesis Differ in Krabbe Disease Variants. *Traffic* (2016). doi:10.1111/tra.12404

33. Shin, D., Feltri, M. L. & Wrabetz, L. Altered Trafficking and Processing of

GALC Mutants Correlates with Globoid Cell Leukodystrophy Severity. *J. Neurosci.* **36,** 1858–1870 (2016).

34. Morimoto, S. *et al.* Saposin A: second cerebrosidase activator protein. *Proc. Natl. Acad. Sci. U.S.A.* **86,** 3389–3393 (1989).

35. Harzer, K. *et al.* Saposins (sap) A and C activate the degradation of galactosylceramide in living cells. *FEBS Lett.* **417,** 270–274 (1997).

36. Harzer, K., Hiraiwa, M. & Paton, B. C. Saposins (sap) A and C activate the degradation of galactosylsphingosine. *FEBS Lett.* **508,** 107–110 (2001).

37. Matsuda, J., Yoneshige, A. & Suzuki, K. The function of sphingolipids in the nervous system: lessons learnt from mouse models of specific sphingolipid activator protein deficiencies. *J. Neurochem.* **103 Suppl 1,** 32–38 (2007).

38. Matsuda, J., Vanier, M. T., Saito, Y., Tohyama, J. & Suzuki, K. A mutation in the saposin A domain of the sphingolipid activator protein (prosaposin) gene results in a late-onset, chronic form of globoid cell leukodystrophy in the mouse. *Hum. Mol. Genet.* **10,** 1191–1199 (2001).

39. Platt, F. M. Sphingolipid lysosomal storage disorders. *Nature* **510,** 68–75 (2014).

40. van Rappard, D. F., Boelens, J. J. & Wolf, N. I. Metachromatic leukodystrophy: Disease spectrum and approaches for treatment. *Best Pract. Res. Clin. Endocrinol. Metab.* **29,** 261–273 (2015).

41. Vanier, M. T. & Svennerholm, L. Chemical pathology of Krabbe's disease. III. Ceramide-hexosides and gangliosides of brain. *Acta Paediatr Scand* **64,** 641–648 (1975).

42. Kobayashi, T., Shinnoh, N., Goto, I. & Kuroiwa, Y. Hydrolysis of galactosylceramide is catalyzed by two genetically distinct acid beta-galactosidases. *J. Biol. Chem.* **260,** 14982–14987 (1985).

43. CLELAND, W. W. & KENNEDY, E. P. The enzymatic synthesis of psychosine. *J. Biol. Chem.* **235,** 45–51 (1960).

44. White, A. B. *et al.* Psychosine accumulates in membrane microdomains in the brain of krabbe patients, disrupting the raft architecture. *J. Neurosci.* **29,** 6068–6077 (2009).

45. Formichi, P. *et al.* Psychosine-induced apoptosis and cytokine activation in immune peripheral cells of Krabbe patients. *J. Cell. Physiol.* **212,** 737–743 (2007).

46. Zaka, M. & Wenger, D. A. Psychosine-induced apoptosis in a mouse oligodendrocyte progenitor cell line is mediated by caspase activation. *Neurosci. Lett.* **358,** 205–209 (2004).

47. Hawkins-Salsbury, J. A. *et al.* Psychosine, the cytotoxic sphingolipid that accumulates in globoid cell leukodystrophy, alters membrane architecture. *J. Lipid Res.* **54,** 3303–3311 (2013).

48. Tanaka, K. & Webster, H. D. Effects of psychosine (galactosylsphingosine) on the survival and the fine structure of cultured Schwann cells. *J. Neuropathol. Exp. Neurol.* **52,** 490–498 (1993).

49. Giri, S. *et al.* Galactosylsphingosine (psychosine)-induced expression of cytokine-mediated inducible nitric oxide synthases via AP-1 and C/EBP: implications for Krabbe disease. *FASEB J.* **16,** 661–672 (2002).

50. Haq, E., Giri, S., Singh, I. & Singh, A. K. Molecular mechanism of psychosine-induced cell death in human oligodendrocyte cell line. *J. Neurochem.* **86,** 1428–1440 (2003).

51. Maghazachi, A. A., Knudsen, E., Jin, Y., Jenstad, M. & Chaudhry, F. A. D-galactosyl-beta1-1‘-sphingosine and D-glucosyl-beta1-1’-sphingosine induce human natural killer cell apoptosis. *Biochem. Biophys. Res. Commun.* **320,** 810–815 (2004).

52. Rawji, K. S. & Yong, V. W. The benefits and detriments of macrophages/microglia in models of multiple sclerosis. *Clin. Dev. Immunol.* **2013,** 948976–13 (2013).

53. Jennings, K. H., Ghabriel, M. N. & Allt, G. Lysophosphatidylcholine-induced incipient demyelination: involvement of a new tubular structure. *J. Neurol. Sci.* **93,** 253–261 (1989).

54. Khan, M., Haq, E., Giri, S., Singh, I. & Singh, A. K. Peroxisomal participation in psychosine-mediated toxicity: implications for Krabbe's disease. *J. Neurosci. Res.* **80,** 845–854 (2005).

55. Haq, E., Contreras, M. A., Giri, S., Singh, I. & Singh, A. K. Dysfunction of peroxisomes in twitcher mice brain: a possible mechanism of psychosine-induced disease. *Biochem. Biophys. Res. Commun.* **343,** 229–238 (2006).

56. Cantuti Castelvetri, L. *et al.* The sphingolipid psychosine inhibits fast axonal transport in Krabbe disease by activation of GSK3β and deregulation of molecular motors. *J. Neurosci.* **33,** 10048–10056 (2013).

57. White, A. B. *et al.* Persistence of psychosine in brain lipid rafts is a limiting

factor in the therapeutic recovery of a mouse model for Krabbe disease. *J. Neurosci. Res.* **89,** 352–364 (2011).

58. Duchen, L. W., Eicher, E. M., Jacobs, J. M., Scaravilli, F. & Teixeira, F. Hereditary leucodystrophy in the mouse: the new mutant twitcher. *Brain* **103,** 695–710 (1980).

59. Olmstead, C. E. Neurological and neurobehavioral development of the mutant 'twitcher' mouse. *Behav. Brain Res.* **25,** 143–153 (1987).

60. Sakai, N. *et al.* Molecular cloning and expression of cDNA for murine galactocerebrosidase and mutation analysis of the twitcher mouse, a model of Krabbe's disease. *J. Neurochem.* **66,** 1118–1124 (1996).

61. Potter, G. B. *et al.* Missense mutation in mouse GALC mimics human gene defect and offers new insights into Krabbe disease. *Hum. Mol. Genet.* **22,** 3397–3414 (2013).

62. Jacobs, J. M., Scaravilli, F. & De Aranda, F. T. The pathogenesis of globoid cell leucodystrophy in peripheral nerve of the mouse mutant twitcher. *J. Neurol. Sci.* **55,** 285–304 (1982).

63. Nagara, H., Kobayashi, T. & Suzuki, K. The twitcher mouse: normal pattern of early myelination in the spinal cord. *Brain Res.* **244,** 289–294 (1982).

64. Castelvetri, L. C. *et al.* Axonopathy is a compounding factor in the pathogenesis of Krabbe disease. *Acta Neuropathol.* **122,** 35–48 (2011).

65. Takahashi, H. & Suzuki, K. Demyelination in the spinal cord of murine globoid cell leukodystrophy (the twitcher mouse). *Acta Neuropathol.* **62,** 298–308 (1984).

66. Taniike, M. & Suzuki, K. Spacio-temporal progression of demyelination in twitcher mouse: with clinico-pathological correlation. *Acta Neuropathol.* **88,** 228–236 (1994).

67. LeVine, S. M., Wetzel, D. L. & Eilert, A. J. Neuropathology of twitcher mice: examination by histochemistry, immunohistochemistry, lectin histochemistry and Fourier transform infrared microspectroscopy. *Int. J. Dev. Neurosci.* **12,** 275–288 (1994).

68. Esch, S. W., Williams, T. D., Biswas, S., Chakrabarty, A. & LeVine, S. M. Sphingolipid profile in the CNS of the twitcher (globoid cell leukodystrophy) mouse: a lipidomics approach. *Cell. Mol. Biol. (Noisy-le-grand)* **49,** 779–787 (2003).

69. Tanaka, K., Nagara, H., Kobayashi, T. & Goto, I. The twitcher mouse: accumulation of galactosylsphingosine and pathology of the sciatic nerve. *Brain Res.* **454,** 340–346 (1988).

70. Baskin, G. B. *et al.* Genetic galactocerebrosidase deficiency (globoid cell leukodystrophy, Krabbe disease) in rhesus monkeys (Macaca mulatta). *Lab. Anim. Sci.* **48,** 476–482 (1998).

71. Giri, S., Khan, M., Rattan, R., Singh, I. & Singh, A. K. Krabbe disease: psychosine-mediated activation of phospholipase A2 in oligodendrocyte cell death. *J. Lipid Res.* **47,** 1478–1492 (2006).

72. Desnick, R. J. & Schuchman, E. H. Enzyme replacement and enhancement therapies: lessons from lysosomal disorders. *Nat. Rev. Genet.* **3,** 954–966 (2002).

73. McGowan, J. C., Haskins, M., Wenger, D. A. & Vite, C. Investigating demyelination in the brain in a canine model of globoid cell leukodystrophy (Krabbe disease) using magnetization transfer contrast: preliminary results. *J Comput Assist Tomogr* **24,** 316–321 (2000).

74. Ichioka, T., Kishimoto, Y., Brennan, S., Santos, G. W. & Yeager, A. M. Hematopoietic cell transplantation in murine globoid cell leukodystrophy (the twitcher mouse): effects on levels of galactosylceramidase, psychosine, and galactocerebrosides. *Proc. Natl. Acad. Sci. U.S.A.* **84,** 4259–4263 (1987).

75. Krivit, W. *et al.* Hematopoietic stem-cell transplantation in globoid-cell leukodystrophy. *N. Engl. J. Med.* **338,** 1119–1126 (1998).

76. Krivit, W., Aubourg, P., Shapiro, E. & Peters, C. Bone marrow transplantation for globoid cell leukodystrophy, adrenoleukodystrophy, metachromatic leukodystrophy, and Hurler syndrome. *Curr. Opin. Hematol.* **6,** 377–382 (1999).

77. Luzi, P. *et al.* Biochemical and pathological evaluation of long-lived mice with globoid cell leukodystrophy after bone marrow transplantation. *Mol. Genet. Metab.* **86,** 150–159 (2005).

78. Lee, W. C. *et al.* Single-dose intracerebroventricular administration of galactocerebrosidase improves survival in a mouse model of globoid cell leukodystrophy. *FASEB J.* **21,** 2520–2527 (2007).

79. Costantino-Ceccarini, E. *et al.* Transduction of cultured oligodendrocytes from normal and twitcher mice by a retroviral vector containing human galactocerebrosidase (GALC) cDNA. *Neurochem. Res.* **24,** 287–293 (1999).

80. Gama Sosa, M. A. *et al.* Correction of the galactocerebrosidase deficiency in globoid cell leukodystrophy-cultured cells by SL3-3 retroviral-mediated gene transfer. *Biochem. Biophys. Res. Commun.* **218,** 766–771 (1996).

81. Lattanzi, A. *et al.* Therapeutic benefit of lentiviral-mediated neonatal intracerebral gene therapy in a mouse model of globoid cell leukodystrophy. *Hum. Mol. Genet.* **23,** 3250–3268 (2014).

82. Lin, D. *et al.* AAV2/5 vector expressing galactocerebrosidase ameliorates CNS disease in the murine model of globoid-cell leukodystrophy more efficiently than AAV2. *Mol. Ther.* **12,** 422–430 (2005).

83. Luddi, A. *et al.* Retrovirus-mediated gene transfer and galactocerebrosidase uptake into twitcher glial cells results in appropriate localization and phenotype correction. *Neurobiol. Dis.* **8,** 600–610 (2001).

84. Rafi, M. A. *et al.* Retroviral vector-mediated transfer of the galactocerebrosidase (GALC) cDNA leads to overexpression and transfer of GALC activity to neighboring cells. *Biochem. Mol. Med.* **58,** 142–150 (1996).

85. Rafi, M. A. *et al.* AAV-mediated expression of galactocerebrosidase in brain results in attenuated symptoms and extended life span in murine models of globoid cell leukodystrophy. *Mol. Ther.* **11,** 734–744 (2005).

86. Rafi, M. A., Rao, H. Z., Luzi, P., Curtis, M. T. & Wenger, D. A. Extended normal life after AAVrh10-mediated gene therapy in the mouse model of Krabbe disease. *Mol. Ther.* **20,** 2031–2042 (2012).

87. Shen, J. S., Watabe, K., Ohashi, T. & Eto, Y. Intraventricular administration of recombinant adenovirus to neonatal twitcher mouse leads to

clinicopathological improvements. *Gene Ther.* **8,** 1081–1087 (2001).

88. LeVine, S. M., Pedchenko, T. V., Bronshteyn, I. G. & Pinson, D. M. L-cycloserine slows the clinical and pathological course in mice with globoid cell leukodystrophy (twitcher mice). *J. Neurosci. Res.* **60,** 231–236 (2000).

89. Sundaram, K. S. & Lev, M. The long-term administration of L-cycloserine to mice: specific reduction of cerebroside level. *Neurochem. Res.* **14,** 245–248 (1989).

90. Biswas, S., Biesiada, H., Williams, T. D. & LeVine, S. M. Substrate reduction intervention by L-cycloserine in twitcher mice (globoid cell leukodystrophy) on a B6;CAST/Ei background. *Neurosci. Lett.* **347,** 33–36 (2003).

91. Mohri, I. *et al.* Prostaglandin D2-mediated microglia/astrocyte interaction enhances astrogliosis and demyelination in twitcher. *J. Neurosci.* **26,** 4383–4393 (2006).

92. Parenti, G. Treating lysosomal storage diseases with pharmacological chaperones: from concept to clinics. *EMBO Mol Med* **1,** 268–279 (2009).

93. Hill, C. H. *et al.* Azasugar inhibitors as pharmacological chaperones for Krabbe disease. *Chem Sci* **6,** 3075–3086 (2015).

94. Berardi, A. S. *et al.* Pharmacological chaperones increase residual β-galactocerebrosidase activity in fibroblasts from Krabbe patients. *Mol. Genet. Metab.* **112,** 294–301 (2014).

95. Lantos, J. D. Dangerous and expensive screening and treatment for rare childhood diseases: the case of Krabbe disease. *Dev Disabil Res Rev* **17,** 15–18 (2011).

96. Dimmock, D. P. Should states adopt newborn screening for early infantile Krabbe disease? *Genet. Med.* **18,** 217–220 (2016).

97. Orsini, J. J. *et al.* Newborn screening for Krabbe disease in New York State: the first eight years' experience. *Genet. Med.* **18,** 239–248 (2016).

98. Wasserstein, M. P. *et al.* Clinical outcomes of children with abnormal newborn screening results for Krabbe disease in New York State. *Genet. Med.* (2016). doi:10.1038/gim.2016.35

99. Duffner, P. K. *et al.* Later onset phenotypes of Krabbe disease: results of the world-wide registry. *Pediatr. Neurol.* **46,** 298–306 (2012).

100. Rafi, M. A., Luzi, P., Chen, Y. Q. & Wenger, D. A. A large deletion together with a point mutation in the GALC gene is a common mutant allele in patients with infantile Krabbe disease. *Hum. Mol. Genet.* **4,** 1285–1289 (1995).

101. O'Rourke, M., Gasperini, R. & Young, K. M. Adult myelination: wrapping up neuronal plasticity. *Neural Regen Res* **9,** 1261–1264 (2014).

102. Nave, K.-A. Myelination and support of axonal integrity by glia. *Nature* **468,** 244–252 (2010).

103. Nave, K.-A. & Werner, H. B. Myelination of the nervous system: mechanisms and functions. *Annu. Rev. Cell Dev. Biol.* **30,** 503–533 (2014).

104. Richardson, W. D., Kessaris, N. & Pringle, N. Oligodendrocyte wars. *Nat. Rev. Neurosci.* **7,** 11–18 (2006).

105. Bergles, D. E. & Richardson, W. D. Oligodendrocyte Development and Plasticity. *Cold Spring Harb Perspect Biol* **8,** a020453 (2016).

106. Takebayashi, H. & Ikenaka, K. Oligodendrocyte generation during mouse

development. *Glia* **63,** 1350–1356 (2015).

107. Schumacher, M. *et al.* Progesterone synthesis in the nervous system: implications for myelination and myelin repair. *Front Neurosci* **6,** 10 (2012).

108. Silbereis, J. C., Huang, E. J., Back, S. A. & Rowitch, D. H. Towards improved animal models of neonatal white matter injury associated with cerebral palsy. *Dis Model Mech* **3,** 678–688 (2010).

109. Semple, B. D., Blomgren, K., Gimlin, K., Ferriero, D. M. & Noble-Haeusslein, L. J. Brain development in rodents and humans: Identifying benchmarks of maturation and vulnerability to injury across species. *Prog. Neurobiol.* **106-107,** 1–16 (2013).

110. Galabova-Kovacs, G. *et al.* Essential role of B-Raf in oligodendrocyte maturation and myelination during postnatal central nervous system development. *J. Cell Biol.* **180,** 947–955 (2008).

111. Pereira, G. B., Dobretsova, A., Hamdan, H. & Wight, P. A. Expression of myelin genes: comparative analysis of Oli-neu and N20.1 oligodendroglial cell lines. *J. Neurosci. Res.* **89,** 1070–1078 (2011).

112. Buntinx, M. *et al.* Characterization of three human oligodendroglial cell lines as a model to study oligodendrocyte injury: morphology and oligodendrocyte-specific gene expression. *J. Neurocytol.* **32,** 25–38 (2003).

113. McLaurin, J., Trudel, G. C., Shaw, I. T., Antel, J. P. & Cashman, N. R. A human glial hybrid cell line differentially expressing genes subserving oligodendrocyte and astrocyte phenotype. *J. Neurobiol.* **26,** 283–293 (1995).

114. Won, J.-S., Kim, J., Paintlia, M. K., Singh, I. & Singh, A. K. Role of endogenous

psychosine accumulation in oligodendrocyte differentiation and survival: implication for Krabbe disease. *Brain Res.* **1508,** 44–52 (2013).

115. Graziano, A. C. E., Parenti, R., Avola, R. & Cardile, V. Krabbe disease: involvement of connexin43 in the apoptotic effects of sphingolipid psychosine on mouse oligodendrocyte precursors. *Apoptosis* **21,** 25–35 (2016).

116. Strazza, M. *et al.* Activation of cell cycle regulatory proteins in the apoptosis of terminally differentiated oligodendrocytes. *Neurochem. Res.* **29,** 923–931 (2004).

117. Emery, B. & Dugas, J. C. Purification of oligodendrocyte lineage cells from mouse cortices by immunopanning. *Cold Spring Harb Protoc* **2013,** 854–868 (2013).

118. Bujalka, H. *et al.* MYRF is a membrane-associated transcription factor that autoproteolytically cleaves to directly activate myelin genes. *PLoS Biol* **11,** e1001625 (2013).

119. LeVine, S. M. & Torres, M. V. Morphological features of degenerating oligodendrocytes in twitcher mice. *Brain Res.* **587,** 348–352 (1992).

120. Taniike, M. *et al.* An apoptotic depletion of oligodendrocytes in the twitcher, a murine model of globoid cell leukodystrophy. *J. Neuropathol. Exp. Neurol.* **58,** 644–653 (1999).

121. de Duve, C. The lysosome turns fifty. *Nat. Cell Biol.* **7,** 847–849 (2005).

122. Ballabio, A. & Gieselmann, V. Lysosomal disorders: from storage to cellular damage. *Biochim. Biophys. Acta* **1793,** 684–696 (2009).

123. Samie, M. A. & Xu, H. Lysosomal exocytosis and lipid storage disorders. *J. Lipid Res.* **55,** 995–1009 (2014).

124. Schröder, B. A., Wrocklage, C., Hasilik, A. & Saftig, P. The proteome of lysosomes. *Proteomics* **10,** 4053–4076 (2010).

125. Luzio, J. P., Pryor, P. R. & Bright, N. A. Lysosomes: fusion and function. *Nat. Rev. Mol. Cell Biol.* **8,** 622–632 (2007).

126. Schwake, M., Schröder, B. & Saftig, P. Lysosomal membrane proteins and their central role in physiology. *Traffic* **14,** 739–748 (2013).

127. Di Paolo, G. & De Camilli, P. Phosphoinositides in cell regulation and membrane dynamics. *Nature* **443,** 651–657 (2006).

128. Mayinger, P. Phosphoinositides and vesicular membrane traffic. *Biochim. Biophys. Acta* **1821,** 1104–1113 (2012).

129. APPELMANS, F., WATTIAUX, R. & DE DUVE, C. Tissue fractionation studies. 5. The association of acid phosphatase with a special class of cytoplasmic granules in rat liver. *Biochem. J.* **59,** 438–445 (1955).

130. Mistry, P. K., Belmatoug, N., Dahl, vom, S. & Giugliani, R. Understanding the natural history of Gaucher disease. *Am. J. Hematol.* **90 Suppl 1,** S6–11 (2015).

131. Huang, W. J., Zhang, X. & Chen, W. W. Gaucher disease: a lysosomal neurodegenerative disorder. *Eur Rev Med Pharmacol Sci* **19,** 1219–1226 (2015).

132. Li, Y. & Sands, M. S. Experimental therapies in the murine model of globoid cell leukodystrophy. *Pediatr. Neurol.* **51,** 600–606 (2014).

133. Suzuki, K. *Twenty five years of the 'psychosine hypothesis': a personal perspective of its history and present status. Neurochemical research* **23,** 251–259 (1998).

134. Tappino, B. *et al.* Identification and characterization of 15 novel GALC gene mutations causing Krabbe disease. *Hum. Mutat.* **31,** E1894–914 (2010).

135. Miyatake, T. & Suzuki, K. Globoid cell leukodystrophy: additional deficiency of psychosine galactosidase. *Biochem. Biophys. Res. Commun.* **48,** 539–543 (1972).

136. Kelly, B. M., Waheed, A., Van Etten, R. & Chang, P. L. Heterogeneity of lysosomes in human fibroblasts. *Mol. Cell. Biochem.* **87,** 171–183 (1989).

137. Mellman, I., Fuchs, R. & Helenius, A. Acidification of the endocytic and exocytic pathways. *Annu. Rev. Biochem.* **55,** 663–700 (1986).

138. Eskelinen, E.-L. Roles of LAMP-1 and LAMP-2 in lysosome biogenesis and autophagy. *Mol. Aspects Med.* **27,** 495–502 (2006).

139. Andrejewski, N. *et al.* Normal lysosomal morphology and function in LAMP-1-deficient mice. *J. Biol. Chem.* **274,** 12692–12701 (1999).

140. Boucek, D., Jirikowic, J. & Taylor, M. Natural history of Danon disease. *Genet. Med.* **13,** 563–568 (2011).

141. Saftig, P. & Klumperman, J. Lysosome biogenesis and lysosomal membrane proteins: trafficking meets function. *Nat. Rev. Mol. Cell Biol.* **10,** 623–635 (2009).

142. Kolter, T. & Sandhoff, K. Principles of lysosomal membrane digestion: stimulation of sphingolipid degradation by sphingolipid activator proteins

and anionic lysosomal lipids. *Annu. Rev. Cell Dev. Biol.* **21,** 81–103 (2005).

143. Lee, W. C. *et al.* Suppression of galactosylceramidase (GALC) expression in the twitcher mouse model of globoid cell leukodystrophy (GLD) is caused by nonsense-mediated mRNA decay (NMD). *Neurobiol. Dis.* **23,** 273–280 (2006).

144. Lissens, W. *et al.* A single mutation in the GALC gene is responsible for the majority of late onset Krabbe disease patients in the Catania (Sicily, Italy) region. *Hum. Mutat.* **28,** 742–742 (2007).

145. Emery, B. & Dugas, J. C. Purification of oligodendrocyte lineage cells from mouse cortices by immunopanning. *Cold Spring Harb Protoc* **2013,** 854–868 (2013).

146. Durchfort, N. *et al.* The enlarged lysosomes in beige j cells result from decreased lysosome fission and not increased lysosome fusion. *Traffic* **13,** 108–119 (2012).

147. Bakker, A. C., Webster, P., Jacob, W. A. & Andrews, N. W. Homotypic fusion between aggregated lysosomes triggered by elevated [Ca2+]i in fibroblasts. *J. Cell. Sci.* **110 (Pt 18),** 2227–2238 (1997).

148. Bright, N. A., Gratian, M. J. & Luzio, J. P. Endocytic delivery to lysosomes mediated by concurrent fusion and kissing events in living cells. *Curr. Biol.* **15,** 360–365 (2005).

149. Storrie, B. & Desjardins, M. The biogenesis of lysosomes: is it a kiss and run, continuous fusion and fission process? *Bioessays* **18,** 895–903 (1996).

150. Mullock, B. M., Bright, N. A., Fearon, C. W., Gray, S. R. & Luzio, J. P. Fusion of

lysosomes with late endosomes produces a hybrid organelle of intermediate density and is NSF dependent. *J. Cell Biol.* **140,** 591–601 (1998).

151. Luzio, J. P., Hackmann, Y., Dieckmann, N. M. G. & Griffiths, G. M. The biogenesis of lysosomes and lysosome-related organelles. *Cold Spring Harb Perspect Biol* **6,** a016840–a016840 (2014).

152. Ward, D. M., Pevsner, J., Scullion, M. A., Vaughn, M. & Kaplan, J. Syntaxin 7 and VAMP-7 are soluble N-ethylmaleimide-sensitive factor attachment protein receptors required for late endosome-lysosome and homotypic lysosome fusion in alveolar macrophages. *Mol. Biol. Cell* **11,** 2327–2333 (2000).

153. Pryor, P. R., Mullock, B. M., Bright, N. A., Gray, S. R. & Luzio, J. P. The role of intraorganellar Ca(2+) in late endosome-lysosome heterotypic fusion and in the reformation of lysosomes from hybrid organelles. *J. Cell Biol.* **149,** 1053–1062 (2000).

154. Brown, W. J., Goodhouse, J. & Farquhar, M. G. Mannose-6-phosphate receptors for lysosomal enzymes cycle between the Golgi complex and endosomes. *J. Cell Biol.* **103,** 1235–1247 (1986).

155. Griffiths, G., Hoflack, B., Simons, K., Mellman, I. & Kornfeld, S. The mannose 6-phosphate receptor and the biogenesis of lysosomes. *Cell* **52,** 329–341 (1988).

156. Menzies, F. M., Fleming, A. & Rubinsztein, D. C. Compromised autophagy and neurodegenerative diseases. *Nat. Rev. Neurosci.* **16,** 345–357 (2015).

157. Hurley, J. H. & Schulman, B. A. Atomistic autophagy: the structures of cellular

self-digestion. *Cell* **157,** 300–311 (2014).

158. Thorburn, A. Apoptosis and autophagy: regulatory connections between two supposedly different processes. *Apoptosis* **13,** 1–9 (2008).

159. Mizushima, N. Autophagy: process and function. *Genes Dev.* **21,** 2861–2873 (2007).

160. Wild, P., McEwan, D. G. & Dikic, I. The LC3 interactome at a glance. *J. Cell. Sci.* **127,** 3–9 (2014).

161. Yu, L. *et al.* Termination of autophagy and reformation of lysosomes regulated by mTOR. *Nature* **465,** 942–946 (2010).

162. Rong, Y. *et al.* Clathrin and phosphatidylinositol-4,5-bisphosphate regulate autophagic lysosome reformation. *Nat. Cell Biol.* **14,** 924–934 (2012).

163. Ward, D. M., Leslie, J. D. & Kaplan, J. Homotypic lysosome fusion in macrophages: analysis using an in vitro assay. *J. Cell Biol.* **139,** 665–673 (1997).

164. Li, X. *et al.* A molecular mechanism to regulate lysosome motility for lysosome positioning and tubulation. *Nat. Cell Biol.* **18,** 404–417 (2016).

165. Igisu, H. & Suzuki, K. Progressive accumulation of toxic metabolite in a genetic leukodystrophy. *Science* **224,** 753–755 (1984).

166. Giri, S., Khan, M., Nath, N., Singh, I. & Singh, A. K. The role of AMPK in psychosine mediated effects on oligodendrocytes and astrocytes: implication for Krabbe disease. *J. Neurochem.* **105,** 1820–1833 (2008).

167. Salaün, C., James, D. J. & Chamberlain, L. H. Lipid rafts and the regulation of exocytosis. *Traffic* **5,** 255–264 (2004).

168. Arighi, C. N., Hartnell, L. M., Aguilar, R. C., Haft, C. R. & Bonifacino, J. S. Role of the mammalian retromer in sorting of the cation-independent mannose 6-phosphate receptor. *J. Cell Biol.* **165,** 123–133 (2004).

169. Holland, P., Torgersen, M. L., Sandvig, K. & Simonsen, A. LYST affects lysosome size and quantity, but not trafficking or degradation through autophagy or endocytosis. *Traffic* **15,** 1390–1405 (2014).

170. Trajkovic, K. *et al.* Ceramide triggers budding of exosome vesicles into multivesicular endosomes. *Science* **319,** 1244–1247 (2008).